For Reference

NOT TO BE TAKEN FROM THIS ROOM

Ex libris
universitatis
albertaensis

QUAECUMQUE VERA

Digitized by the Internet Archive
in 2022 with funding from
University of Alberta Library

https://archive.org/details/Yuen1978

THE UNIVERSITY OF ALBERTA

ATOMIC SPECTROCHEMICAL MEASUREMENTS WITH A FOURIER TRANSFORM SPECTROMETER

by

© WO KAI YUEN

A THESIS
SUBMITTED TO THE FACULTY OF GRADUATE STUDIES AND RESEARCH
IN PARTIAL FULFILMENT OF THE REQUIREMENTS FOR THE DEGREE
OF DOCTOR OF PHILOSOPHY

DEPARTMENT OF CHEMISTRY

EDMONTON, ALBERTA

SPRING, 1978

ABSTRACT

Atomic spectrochemical data is most commonly measured with a dispersive instrument. The dominant types of dispersive instrumentation are: the monochromator photomultiplier tube combination, the spectrograph and the direct reader. The desired characteristics of a simultaneous multielement measurement system are present in the above types, but not one single type has all of them. The desirable characteristics are: fast, linear,wide dynamic range response; high sensitivity; wide simultaneous spectral coverage with good resolution; and direct conversion of the light intensity to an electronic signal.

Attempts to achieve these characteristics have been based mainly on variations of the dispersive theme. A totally different approach is to multiplex the information with a Michelson interferometer.

This is the Fourier transform spectroscopy technique which has been very successful in the mid and far-IR. To extend its use to the shorter wavelengths of the UV-visible region, the sampling of the interferogram must be considered because the clock signal (derived from a He-Ne laser) does not provide a high enough rate to prevent aliasing. The effects of apodization are examined because the fundamental line shape imposed by the

ACKNOWLEDGEMENT

I would like to acknowledge the guidance and assistance given by Dr. Gary Horlick.

I should also thank my wife, Naomi, for her help in copying, proof-reading, and even a little typing of this thesis.

TABLE OF CONTENTS

CHAPTER PAGE

I. SPECTROCHEMICAL MEASUREMENTS 1

II. FOURIER TRANSFORM SPECTROSCOPY 11

- A. Reasons for Using Fourier Transform Spectroscopy 11
- B. The Michelson Interferometer 19
- C. The Fourier Transformation 24

III. SAMPLING THE INTERFEROGRAM AND THE CONSEQUENCES OF ALIASING 28

IV. APODIZATION AND ITS EFFECTS 48

V. PHASE PROBLEMS IN FOURIER TRANSFORM SPECTROSCOPY 62

VI. THE MICHELSON INTERFEROMETER SYSTEM 76

- A. Description of the Michelson Interferometer 76
  - 1) Central Mounting Cube 78
  - 2) Beamsplitter Assembly 84
  - 3) Fixed Mirror Assembly 86
  - 4) Moving Mirror Assembly 86
  - 5) White Light Reference System . . . 87
  - 6) He-Ne Laser Reference System . . . 87
  - 7) Detector Assembly 88
  - 8) Input Optics 91
- B. Consequence of Using Only One Interferometer 92
- C. Interferometer Electronics 95
  - 1) Moving Mirror Drive 95
  - 2) Laser Channel 100
  - 3) White Light Channel 103
  - 4) Detector Electronics 106
  - 5) Sampling Rates 109
  - 6) Electronics With the PDP-8/e Computer 111
- D. Computer Processing 115
  - 1) The Computer Systems 115
  - 2) Computer Programming 118

CHAPTER PAGE

VII. SPECTRAL MEASUREMENTS WITH THE FOURIER TRANSFORM SPECTROMETER 123
  A. Near Infrared Measurements 124
  B. Measurements in the Visible Spectral Region 134
    1) Atomic Flame Emission 135
    2) Hollow Cathode Lamp Spectra . . . 138
    3) Effect of Large Spectral Features on Small Peaks 154
  C. Measurements in the Ultraviolet 165
  D. Infrared Measurements 171

VIII. SUMMARY 175

BIBLIOGRAPHY 178

APPENDIX 183

LIST OF TABLES

Table	Description	Page
I	Major Emission Lines of Na, Li, K, Rb, and Cs in the Near-IR	33
II	Aliasing Table for ÷4, ÷2, Direct, X2, and X4 Sampling Rates	40
III	Resolution with a Triangularly Apodized Double-Sided Interferogram	46
IV	Wavelengths Calculated From the Alkali Metals Spectrum Shown in Figure 44	129
V	Wavelengths Calculated From the Spectrum Shown in Figure 49	139
VI	Wavelengths Calculated From the Spectrum of the Multielement Steel HCL	148
VII	Wavelengths Calculated From Spectra of the Ca-Al-Mg HCL	151
VIII	Wavelengths Calculated From the Spectrum of the Chromium HCL	153
IX	Wavelengths of Magnesium Spectral Lines Shown in Figure 67	168

LIST OF FIGURES

Figure	Description	Page
1.	Spectrochemical measurement block diagram.	2
2.	Common frequency decoding instrumentation.	4
3.	Schematic diagram of a multiplex technique (Fourier transform spectroscopy).	7
4.	Block diagram of a Fourier transform spectrometer.	9
5.	Schematic diagram of a Michelson interferometer.	20
6.	Example of an interferogram of a broadband source (tungsten bulb).	23
7.	Illustration of aliasing.	30
8.	Schematic spectrum of Li, K, Rb, and Cs and the aliased schematic spectrum for a 0.6328 um sampling interval (um=micrometer).	34
9.	Schematic spectrum of Li, K, Rb, Cs, and Na and the aliased schematic spectrum.	37
10.	Schematic spectrum of Cr and the aliased schematic spectra.	38
11.	He-Ne laser 0.6328 um line, X4 sampling rate.	42
12.	Spectra of Li, K, Rb, and Cs using different sampling rates.	44
13.	The relationship between convolution and apodization.	49
14.	Boxcar and triangular apodization functions.	51
15.	Peak shapes resulting from boxcar and triangular apodization.	52

Figure	Description	Page
16.	Gaussian apodization functions.	56
17.	Peak shapes resulting from Gaussian apodization.	57
18.	Interferogram of Na 589 nm doublet.	58
19.	Interferogram of Na 589 nm doublet after Gaussian apodization.	59
20.	Na 589 nm doublet spectral peak shape with and without Gaussian apodization.	61
21.	Potassium spectrum from a single-sided interferogram with and without phase correction.	64
22.	Real and imaginary output peak shapes with various phase errors.	66
23.	Phase corrected spectra of Li, K, Rb, and Cs.	67
24.	Analog interferograms of Li, K, Rb, and Cs.	68
25.	Digitized interferograms of the analog signals shown in Figure 24.	69
26.	Multielement spectrum of Li, K, Rb, and Cs not phase corrected.	71
27.	Hollow cathode lamp spectrum resulting from single-sided and double-sided interferogram.	73
28.	Block diagram of the Michelson interferometer system.	77
29.	Schematic diagram of the Michelson interferometer.	79
30.	Lens detector assembly and white light reference assembly schematic.	80
31.	Photographs of the interferometer front and top views.	81

Figure	Description	Page
32.	Photographs of the interferometer, a) mounting cube partially disassembled, b) and beamsplitter and white light assembly. c) totally disassembled.	 82 83
33.	Transmission spectra of the quartz and NaCl substrate beamsplitters	85
34.	Interferometer electronics with the PDP-11 computer	96
35.	Schematic diagram of the control signals	97
36.	Scope photographs: white light analog, laser analog, white light digital.	98
37.	Scope photographs: laser analog without and with PLL control, white light analog and laser digital.	99
38.	PMT schematic circuit for DC and AC operation.	108
39.	Interferometer electronics with the PDP-8 computer.	112
40.	Schematic diagram of the control signals for the circuit in Figure 39.	113
41.	Minicomputer data acquisition and processing system based on the PDP-8.	116
42.	Minicomputer data acquisition and processing system based on the PDP-11	117
43.	Program sequence for data acquisition and processing of the interferogram.	119
44.	Flame emission spectrum of the alkali metals.	126
45.	Digitized interferogram for spectrum in Figure 44.	127
46.	Analytical curve for Li flame emission.	130
47.	Spectrum of a 5 ppm Li solution.	131

Figure	Description	Page
48.	Spectrum of a 0.5 ppm Li solution.	132
49.	Flame emission spectrum of Li, Na, Ba, Sr, and Ca.	136
50.	Digitized interferogram for spectrum in Figure 49.	137
51.	Spectrum of a multielement steel HCL.	140
52.	Spectrum of Mn 403 nm triplet using a scanning monochromator system.	142
53.	Expanded portion of steel spectrum around Mn 403 nm triplet.	144
54.	Expanded portion of steel spectrum around Fe 372 nm line.	145
55.	Expanded portion of steel spectrum around Cr 360 nm triplet.	146
56.	Expanded portion of steel spectrum around Ni 352 nm line.	147
57.	Spectrum of Ca-Al-Mg hollow cathode lamp.	150
58.	Spectrum of Cr hollow cathode lamp.	152
59.	Flame emission spectrum of a solution of Sr 10 ppm and Ca 1000 ppm.	155
60.	Expanded portion of Sr 10/Ca 1000 ppm spectrum around Sr peak.	156
61.	Flame emission spectrum of a solution of 10 ppm Sr by itself.	157
62.	Flame emission spectrum of Sr 10/Na 10 ppm.	158
63.	Expanded portion of Sr 10/Na 10 spectrum around Sr peak.	159
64.	Flame emission spectrum of Sr 10/Na 100 ppm.	160
65.	Expanded portion of Sr10/Na100 ppm spectrum around Sr peak.	161

Figure	Description	Page
66.	Spectrum of a Mg HCL with a 0.6328 um and a 2.5312 um sampling interval.	166
67.	The spectrum of Mg in Figure 66(b) interpolated using the zero-filling technique.	167
68.	Spectrum of Mg HCL using 0.6328 um sampling interval and 4096 points.	170
69.	Background and polystyrene spectra in the mid-IR.	172
70.	Digitized interferogram of the background spectrum.	173
71.	Digitized interferogram of the polystyrene spectrum.	174

CHAPTER I

SPECTROCHEMICAL MEASUREMENTS

The measurement of atomic spectrochemical data is one of the major techniques for acquiring qualitative and quantitative information about a sample. In an endeavour to obtain this information as accurately and as quickly as possible, there has been a continuing long range effort in many laboratories towards the development of effective simultaneous multielement analyses. A key aspect in this development is the design of spectrochemical measurement systems capable of simultaneously measuring spectral information over a wide range of wavelengths. This study is directed to that goal by investigating the feasibility of a Michelson interferometer Fourier transform spectroscopy approach.

Some background is needed to put this technique in perspective. The spectrochemical measurement process is shown in general terms in Figure 1. Spectrochemical information about a sample is encoded by various processes such as emission, absorption, fluorescence, scattering and reflection into electromagnetic radiation with the information represented by the parameters of frequency, intensity, time, and space. This must be decoded to get useful analytical data about the sample.

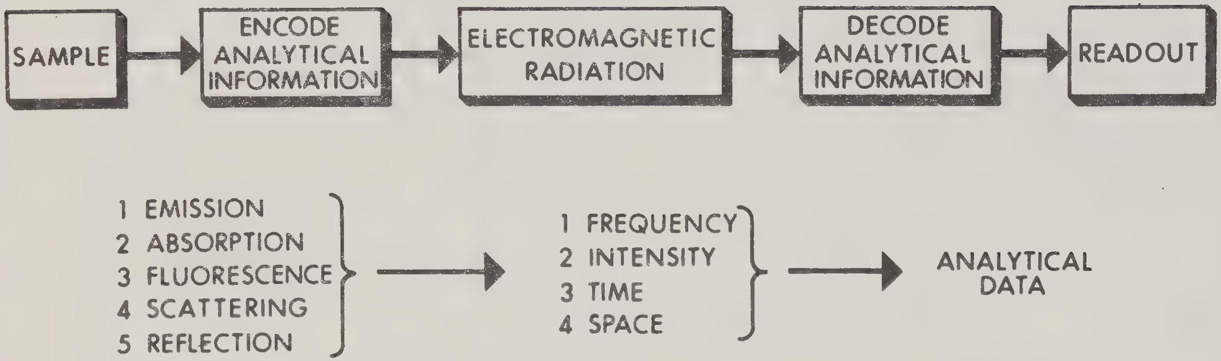

Figure 1. Spectrochemical measurement block diagram.

By far the dominant technique for the measurement of spectra is the dispersive system based on the diffraction grating combined with a photomultiplier tube (PMT) or photographic plate detector. The main types of instrumentation for decoding the information, shown schematically in Figure 2, are the monochromator with a PMT, the spectrograph and the direct reader.

The spectrograph has a photographic plate placed at the focal plane as the detector. Although the photographic plate is capable of recording thousands of lines in a single exposure as a permanent record, it has a nonlinear intensity response, limited dynamic range and very tedious readout.

In the monochromator PMT combination, the spectral information is dispersed along a focal plane where an exit slit allows one resolution element to reach the photomultiplier tube. The spectrum is obtained by scanning the dispersive element so that the frequencies reach the PMT sequentially. This can be very slow if high resolution and/or wide spectral coverage is needed. However, the PMT has the advantages of having very good linearity, wide dynamic range, high sensitivity and electronic output (light intensity is directly transduced into an electronic signal).

The direct reader is an attempt to retain the advantages of the PMT and also achieve simultaneous spectrochemical measurements. Here an exit slit-PMT combination

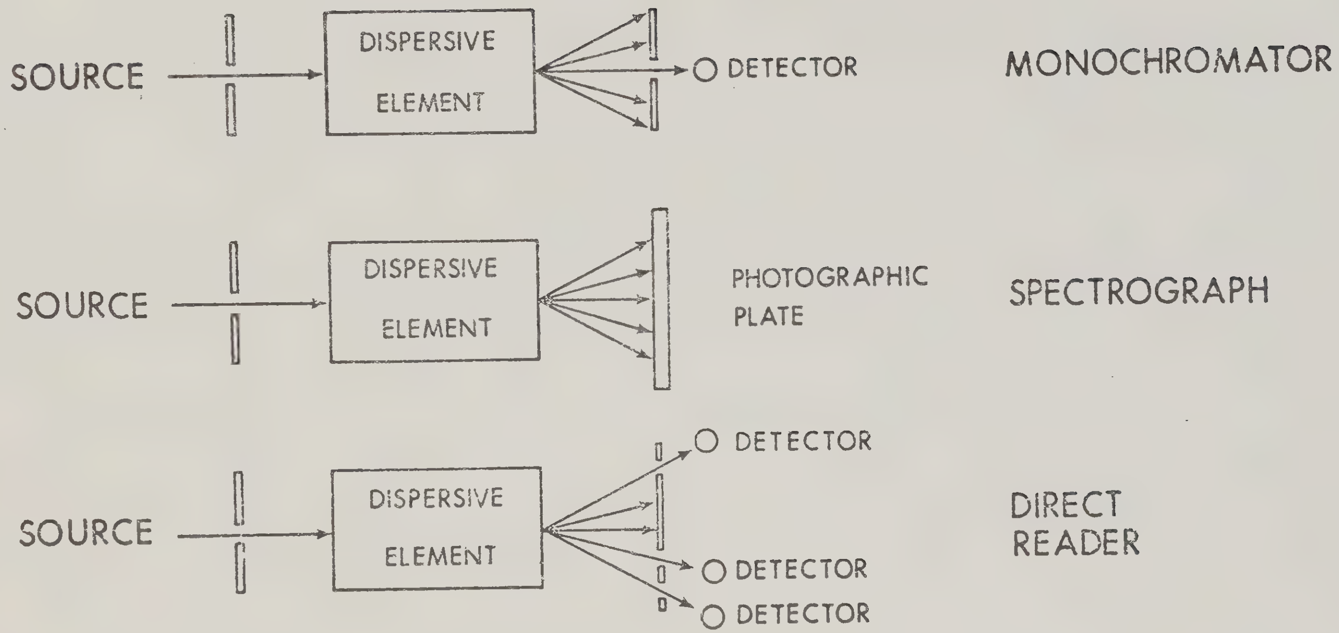

Figure 2. Common frequency decoding instrumentation.

is mounted at each point in the exit focal plane of a dispersive instrument at which measurements are to be made. But even at best, only a small fraction of the spectral information available in the spectrum can be measured. Physical size and cost considerations limit the direct reader to about 60 channels.

Over the last few years much effort has gone into the development of instrumentation that has the best characteristics of the above types. Desirable characteristics are: fast, linear, wide dynamic range response; high sensitivity; wide simultaneous spectral coverage with good resolution; and direct transduction of the light intensity to an electronic signal.

The recent technological advances in solid state electronics have produced electronic image sensors as detectors (1,2) which over a moderate wavelength region provide a continuous multichannel measurement system. Such devices, which include silicon vidicons (3-6), secondary electron conduction vidicons (7), and silicon photodiode arrays (8,9), have recently been applied to a variety of multichannel spectrochemical measurements. At present these devices cannot match the photomultiplier tube performance in sensitivity and wide dynamic range.

In addition to these multichannel systems, rapid scanning sequential systems have also proved useful for multielement analysis. Both a mechanical slew scan system

based on a programmable monochromator (10), and what amounts to an electronic slew scan system on an image dissector PMT (11) have been developed.

Another potential approach to the overall problem is to dispense with the dispersive system completely and use a multiplex technique. Here the spectral information is encoded so that a single detector can be used to simultaneously measure a wide wavelength range (Figure 3). The most common examples of multiplex techniques are Fourier transform spectroscopy and Hadamard transform spectroscopy (12). In the latter technique, a dispersive element is still necessary but the spectral information is encoded in a binary code based on Hadamard matrices (13). In Fourier transform spectroscopy, the information is encoded in sine and cosine oscillations. This encoding is accomplished by a Michelson interferometer. The encoded signal, which is measured with a single detector, is called an interferogram. It is necessary to take the Fourier transform of the interferogram to decode it and obtain the spectrum. Although Fourier transform spectroscopy has been associated with infrared measurements, there is no fundamental reason why it cannot be used for atomic spectrochemical measurements.

An introduction to Fourier transform spectroscopy will discuss some advantages of the technique over conventional methods. Also, the basics of how the Michelson

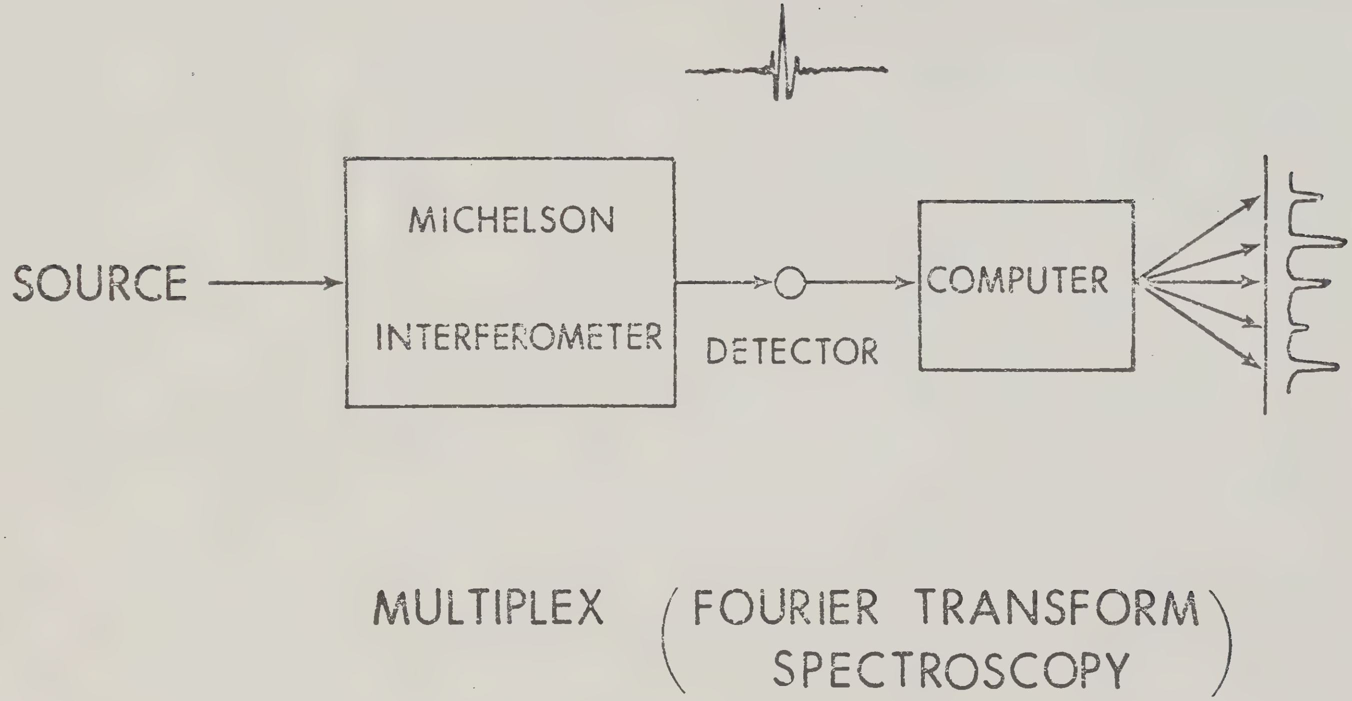

Figure 3. Schematic diagram of a multiplex technique (Fourier transform spectroscopy).

interferometer operates and the method to obtain the final spectrum from the interferometer output will be explained. It is important to understand the additional factors which need to be considered when extending the use of Fourier spectroscopy to measuring atomic emission spectra in the UV-visible spectral region. The sampling of the interferogram signal is an important consideration. Since the information in the UV-visible is at a higher spectral frequency than in the IR, a problem arises because the clock signal (derived from a He-Ne laser) does not sample the interferogram at a high enough rate to prevent aliasing. The output spectrum may not have the desired instrumental line shape. The process of apodization affects the line shape; therefore, apodization and its effects will be discussed. A major problem in Fourier spectroscopy is the phase error in the interferogram. The standard procedures for phase correction in FT-NMR and IR do not work effectively for line emission spectra. This problem and its solution will be discussed.

A Michelson interferometer system has been built to study its use as a spectrometer. A block diagram is shown in Figure 4. The philosophy behind the design was to make a general purpose spectrometer that can be used in a variety of instrumental setups. Thus, the Michelson interferometer Fourier transform spectrometer can be used to take measurements in the ultraviolet, visible or

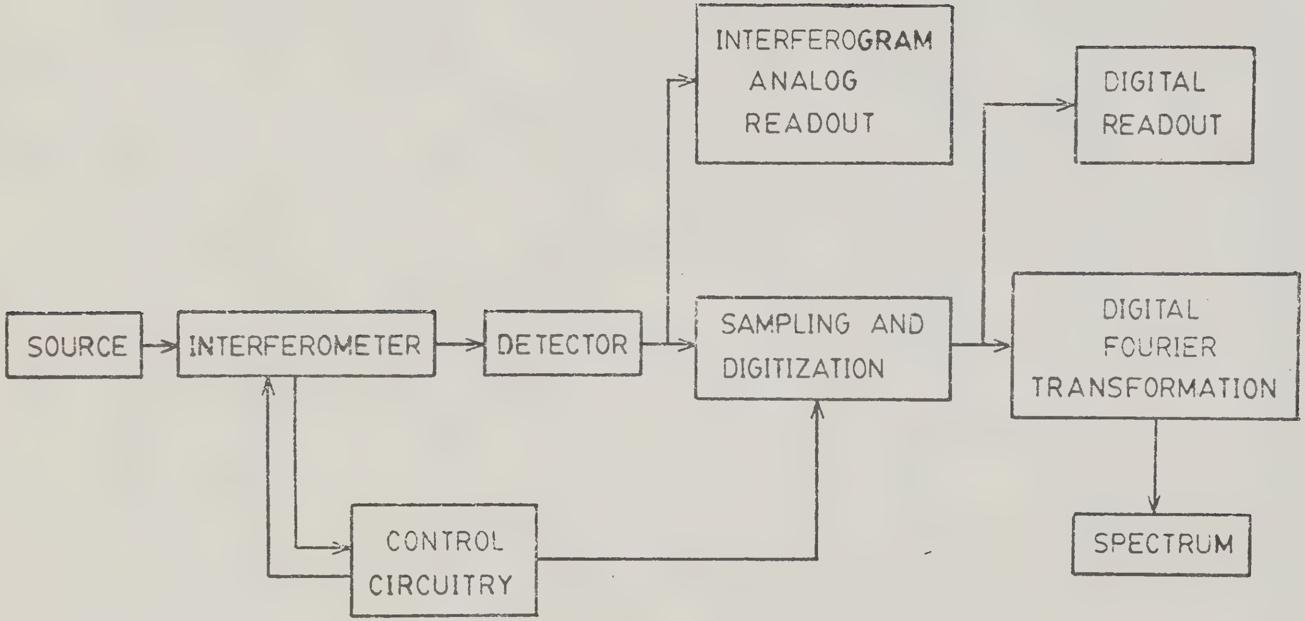
SOURCE
INTERFEROMETER
DETECTOR
INTERFEROGRAM ANALOG READOUT
SAMPLING AND DIGITIZATION
DIGITAL READOUT
DIGITAL FOURIER TRANSFORMATION
SPECTRUM
CONTROL CIRCUITRY

Figure 4. Block diagram of a Fourier transform spectrometer.

infrared regions. A variety of sources and detectors can be accomodated to suit the measurement. The mechanical design of the interferometer will be described along with the control circuitry and the measurement electronics. The software necessary to acquire and process the interferogram will be described. A complete listing of the computer programs along with a detailed description is given in the Appendix.

Finally some measurements taken with the Fourier transform spectrometer will be given to show the performance of the system. Spectra in the visible region were obtained with a 1P28 photomultiplier tube of hollow cathode lamps of several elements including Cr, Al, Mg, Ca, and a multielement lamp of Fe, Cr, Ni, Mn, Co, Cu. Flame emission spectra were also measured for Li, Na, Ba, Sr, and Ca. The Mg spectrum was measured in the UV with a solar blind PMT. Near-IR measurements were taken with a silicon photodiode detector of the flame emission of the alkali metals: Li, Na, K, Rb, Cs. Quantitative aspects of the system were studied with Li flame emission. Mid-IR measurements were taken with a TGS detector and a globar source and polystyrene film sample.

CHAPTER II

FOURIER TRANSFORM SPECTROSCOPY

A. Reasons for Using Fourier Transform Spectroscopy

The question immediately arises as to what advantages the Fourier transform approach offers over the standard instrumentation and then what are some of its disadvantages.

Fourier transform spectroscopy has been extensively used for spectral measurements in the infrared regions, but so far it has found little application for atomic spectrochemical measurements in the UV-visible spectral regions. Much of the incentive for the development of infrared Fourier spectroscopy came from the promise of achieving two advantages brought to attention by P. Jacquinot and P. Fellgett: the throughput and the multiplex advantages which carry, respectively, their names in honour of their contributions to this field. These advantages result in the Fourier transform spectrometer making more efficient use of the light available from the source.

The Jacquinot or throughput advantage (14) for the interferometer arises because the energy throughput, I, for a given resolution, R, is greater for an interferometer than a grating spectrometer. The reason is the larger acceptance angle for the interferometer without

degrading the resolution. The throughput for a grating instrument is limited by the necessity for an entrance slit. The derivation (15) gives the advantage as:

$$\frac{R \cdot I_{\text{interferometer}}}{R \cdot I_{\text{grating}}} = \frac{2\pi}{(l/f)} \qquad (1)$$

where l equals the slit height and f the focal length of the collimator of the grating instrument. A typical value for (l/f) is 1/50 (slit height of 1 cm and a 0.5 m collimating focal length). Thus the interferometer, in theory, has over two orders of magnitude more energy throughput. The Jacquinot advantage is applicable to both infrared and the UV-visible regions.

The multiplex (Fellgett's) advantage arises from the fact that the interferometer is observing all the spectral elements simultaneously whereas the scanning monochromator observes each spectral element sequentially. Suppose the spectral region of interest is between v_1 and v_2 with a resolution of δv. The number of resolution elements M is then:

$$M = (v_2 - v_1)/\delta v \quad . \qquad (2)$$

In a grating instrument each resolution element δv is observed for a time T/M, where T is the required time to scan between v_1 and v_2. The signal received is proportional to T/M. Assuming that the noise is random and independent of the signal intensity, the signal noise is proportional to $(T/M)^{1/2}$. Thus, the signal-to-noise (S/N) ratio

would be:

$$S/N \propto (T/M)^{1/2} \quad . \tag{3}$$

For the interferometer each resolution element is observed for a time T so that the signal received is proportional to T/2 (the factor of 2 arises because in a Michelson interferometer half the light is reflected back to the source). The signal noise, assuming that noise is random and signal independent, is proportional to $T^{1/2}$. Thus, for an interferometer the

$$S/N \propto T^{1/2}/2 \quad . \tag{4}$$

Comparing equations (3) and (4), the S/N for the interferometer is better than for the monochromator by $M^{1/2}/2$.

This is the case in the infrared region where the detectors are the major source of noise, and thus the noise is signal independent. However, in the UV-visible region the detectors are much more sensitive and the noise is determined by the fluctuations in the number of photons arriving at the detector. There can be several sources of this fluctuation in the number of photons (16,17). One source is the statistical nature of light. The noise level due to this is proportional to the square root of the source intensity. An even larger source of noise, especially when the source is a flame, may be source flicker. Noise due to source flicker is directly proportional to the source intensity so that this may be the dominant noise source at high signal intensities. Therefore, the benefit of

increased signal level for a resolution element due to the observation for the entire time T is cancelled because the noise level now increases as well. Hence, in the UV-visible region, the multiplex advantage is not realized.

But the situation is not quite so clear cut. Both the nature of the spectrum and the distribution of the noise in the spectrum can affect the existence of a multiplex advantage in signal noise limited measurement situations. There can be a multiplex advantage with spectra of low density, such as atomic spectra. The advantage is realized if there is little or no broadband background radiation present or if the spectrum does not contain large numbers of much more powerful lines. This has been discussed by Filler (18), Hirschfeld (19), and Winefordner (20) and essentially the same conclusion has been reached for Hadamard transform spectroscopy (21).

Another factor that must be considered is the possibility of a so-called multiplex disadvantage (18-21). This arised primarily because the distribution of photon noise in a spectrum measured with a scanning instrument is different from that in one measured with a Fourier spectrometer. In the scanning case, the rms (root mean square) noise is greatest where the signal is greatest (that is, at the top of the spectral peaks). In the Fourier case, the noise tends to be spread out more or less uniformly throughout the entire spectrum. Thus, the S/N ratio of strong peaks

should improve, but weak spectral lines may be obscured by the noise from strong lines that ends up distributed along the baseline of the spectrum. Therefore, if the spectral peaks of interest are small compared to peaks that are not of interest or background radiation, there is a decrease in the S/N ratio compared to the scanning instrument. This problem also exists in Hadamard transform spectroscopy (21), and some experimental verification of this multiplex disadvantage has been reported (22).

Thus, at this time no definitive conclusions can be reached about the existence and importance of multiplex advantage and/or disadvantages in photon noise limited multiplex spectrochemical measurements. More experimental work is necessary to clear up the situation. What the above discussion does mean, however, is that the promise of any substantial multiplex advantage cannot be a driving force in extending Fourier transform techniques into the UV-visible region. In fact, some disadvantages may exist with respect to S/N in certain measurement situations.

However, signal-to-noise ratio is not always the only and overriding consideration when carrying out a spectrochemical measurement. It becomes important only when nearing the limits of detection and many measurements are made well above this limit. The impressive success and capabilities of the Fourier transform technique in

the infrared have shown that some important advantages result from the nature of the instrumentation used to implement Fourier transform spectroscopy. These advantages are not dependent on the existence or realization of the multiplex advantages.

Some of these advantages are: spectra can be measured with a very accurate and precise wavenumber axis which is predetermined by the sampling interval (no calibration necessary), a wide range of frequencies can be simultaneously covered with proper utilization of aliasing, high resolution can be achieved in a relatively compact system along with speed of operation, the resolution function is easily controlled and manipulated as an inherent step in data reduction by use of apodization techniques, and computerization of the spectrometer is facilitated.

The digitization of the interferogram in a Fourier transform spectrometer is normally controlled with a clock signal derived from a He-Ne reference laser. This provides a final spectrum which has a very accurate wavenumber axis with the values along the axis easily calculated from the wavenumber of the laser line (no external calibration needed). This inherent accuracy of the axis greatly facilitates intercomparison of digitized spectra for small peak shifts and peak shape perturbations. Also, the accurate axis makes

identification of spectral peaks easier.

The spectra are in a digitized form as an inherent part of the data reduction, that is, the spectra are stored in the computer as part of the data processing. Hence, further processing such as ratio, peak subtraction, and correlation of spectra is easily accomplished by software. A benefit of having the interferogram stored in a computer is that, if the resultant spectrum does not have the desired resolution function, it is a simple matter to process the interferogram again with a different apodization function (23). Another possibility is to apply some form of digital filtering to smooth the spectrum or enhance resolution (24,25).

A Fourier transform spectrometer is capable of very high resolution (26-28) while maintaining relatively high throughput and with a relatively compact system. A grating instrument for high resolution can be quite bulky. For example, a 2 meter spectrograph is rather large and heavy. On the other hand, an interferometer with 8 cm mirror movement (16 cm optical retardation) can achieve nominal resolution of 0.0625 cm^{-1} (0.00225 nm at 600 nm) and still easily be placed on a tabletop.

With proper aliasing, a Fourier transform spectrometer can simultaneously cover a wide range of wavelengths while maintaining relatively high resolution. This aliasing advantage will be considered in Chapter III.

Considered in the context of capability, both the cost and basic simplicity of Fourier transform spectroscopy can be considered advantages. Present commercial instruments have not supported the cost advantage since they are very expensive, but without question, effective systems can be made at considerably lower costs. The simplicity is present in the fact that there is but one moving part in the spectrometer, the moving interferometer mirror.

As a result of these additional considerations, it seems that a Fourier transform approach is feasible in the UV-visible region (29,30) as well as in the infrared where it has without doubt shown very fine performance. The types of instrumentation and many applications of the Fourier transform approach has been discussed in the literature (31-37). One major area where Fourier transform spectroscopy has been used is in astronomy where much of the development for high resolution work has taken place (26,27,38-42). The basis of the Fourier transform technique is summarized in the next section.

B. The Michelson Interferometer

The main optical component of most Fourier transform spectrometers is the Michelson interferometer. A simplified diagram is shown in Figure 5. The interferometer encodes the spectral information from the source via two beam interference. The output signal at the detector is called an interferogram.

The most common arrangement of the Michelson interferometer is with a beamsplitter at 45° to the source. In the visible and infrared regions the beamsplitter material is too thin to be self-supporting, thus, it is coated onto a support material. A second equal thickness of the support material, called the compensator, is placed in one arm of the interferometer to equalize the optical path length in both arms. The beamsplitter ideally reflects 50% of the light and transmits the remaining 50%. The two divided beams of light reflect off plane mirrors at right angles to one another and are recombined by the beamsplitter. Half of the recombined light goes to the detector and the other half is returned to the source. One of the plane mirrors is fixed and the other mirror can be moved in a direction perpendicular to the mirror surface.

To see how the interferometer encodes the incident radiation, assume for simplicity that there is monochromatic

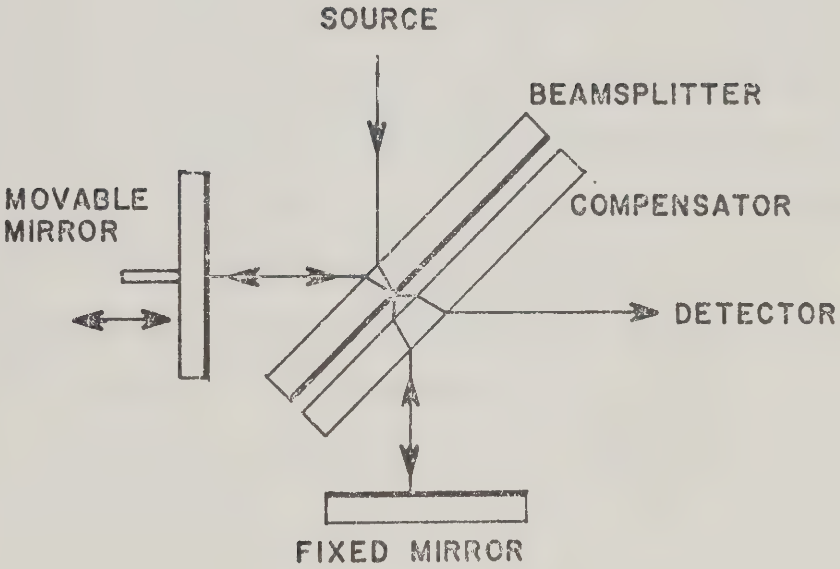

Figure 5. Schematic diagram of a Michelson interferometer.

light from the source. When the optical path lengths of the two arms are equal, the two beams of light are in phase when they return to the beamsplitter and thus interfere constructively. If the movable mirror is offset ¼ of the wavelength of the incident light, the optical path lengths will differ by ½ a wavelength. When the two beams are recombined at the beamsplitter, they are now 180° out of phase and will interfere destructively. As the mirror is continuously moved, the recombined beams of light will alternately interfere constructively and destructively, resulting in a cosinusoidally changing output at the detector. The maxima of the output (constructive interference) occurs for every ½ of a wavelength movement in the movable mirror, or, in other words, for every one wavelength difference in optical path length of the two arms. An example of a monochromatic source is a He-Ne laser and its interferometer output is shown in Figure 36(a) (lower trace).

The frequency of the output cosine wave depends on the wavelength of the incident radiation and the velocity of the movable mirror. Thus a very high optical frequency (for example 600 nm is 5×10^{14} Hz) is uniquely encoded in the form of a low frequency oscillation. In the case of the interferometer used in this study, the 632.8 nm He-Ne laser line is modulated to around 4 kHz.

If the incident radiation is broadband, there are

many wavelengths of light. Each wavelength is modulated to a different frequency. The output of the detector is then the summation of all the frequencies present. The output with a white light source (tungsten bulb) is shown in Figure 6. At zero path difference, ZPD, (optical path lengths equal in the two arms of the interferometer) all the frequencies are in phase giving a large output signal. As the mirror is moved away from the zero position, the frequencies rapidly sum out to a steady average value. In Figure 6 the white light interferogram was digitized at optical path difference intervals equal to one wavelength of the He-Ne laser 632.8 nm line. The ZPD position occurs at about point 2048 since the 4096 point interferogram was sampled on both sides of the ZPD position.

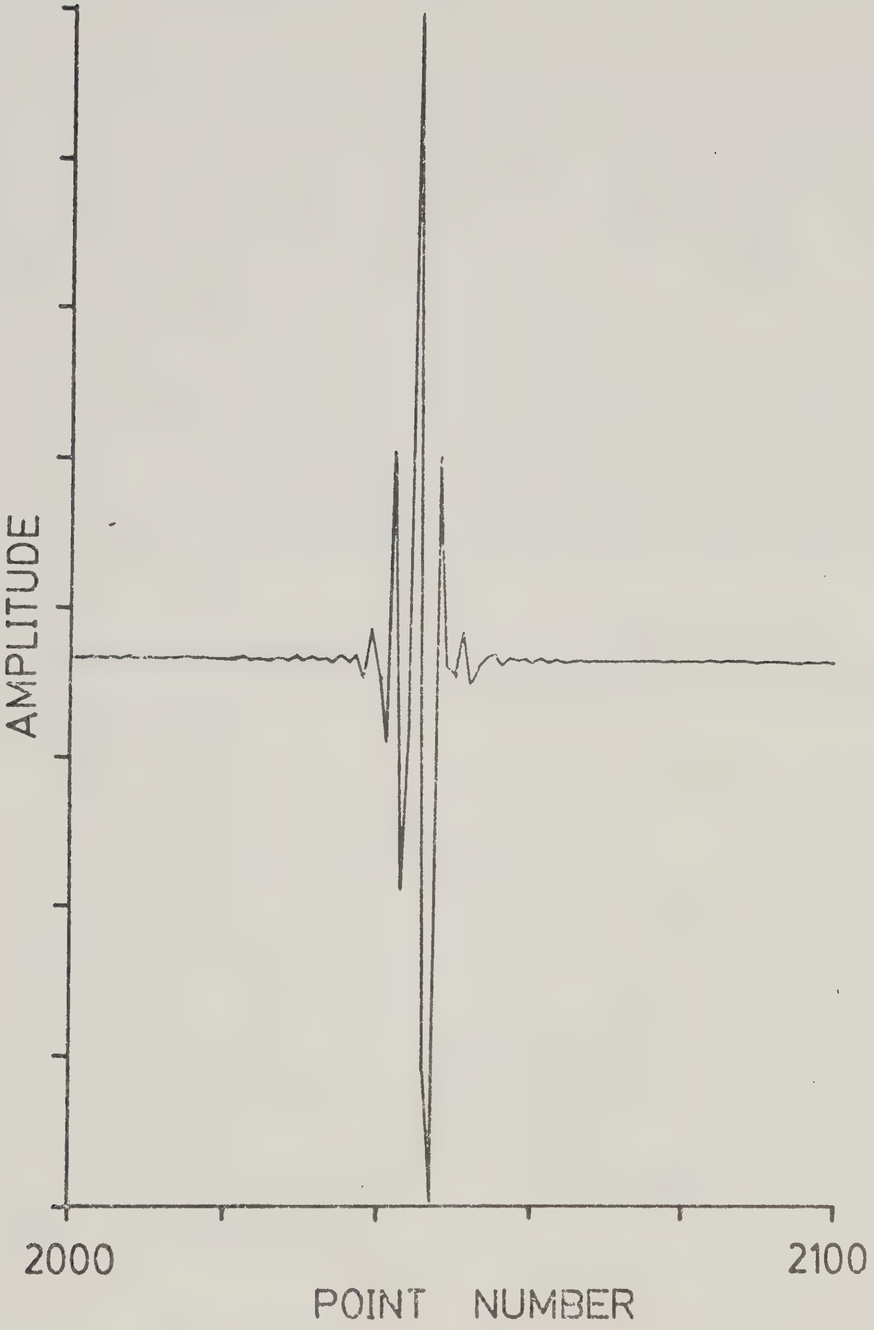

Figure 6. Example of an interferogram of a broadband source (tungsten bulb).

C. The Fourier Transformation

The basic process for decoding the interferometer output is to convert the amplitude--path difference information represented in the interferogram to the amplitude--frequency domain of a spectrum. This process is called the Fourier transformation.

The detailed theory and mathematics of the Fourier transform has been extensively documented in the literature (15,31,32,34,43-48) and will not be reproduced here except in summary.

Mathematically the ac signal called the interferogram can be expressed as

$$I(x) = \int_{-\infty}^{+\infty} B(v) \cos(2\pi xv)\, dv \qquad (5)$$

where I(x) is the intensity of the output as a function of mirror movement x; B(v) is the intensity of the source as a function of wavenumber v, that is, the spectrum. Equation (5) is one-half of a cosine Fourier transform pair (45). The other half is

$$B(v) = \int_{-\infty}^{+\infty} I(x) \cos(2\pi xv)\, dx \quad . \qquad (6)$$

Equations (5) and (6) provides the relationship between the interferogram, I(x), and the spectrum, B(v). The

spectrum can be obtained by taking the Fourier transform of the interferogram.

If all the optical components were ideal, the interferogram in Figure 6 would be perfectly symmetrical. This is not the case, therefore, there are sine components in the interferogram. Thus, in general, the interferogram and spectrum must be related by the complex Fourier transform pair,

$$I(x) = \int_{-\infty}^{+\infty} B(v) \exp(2\pi ixv)\, dv \tag{7}$$

$$B(v) = \int_{-\infty}^{+\infty} I(x) \exp(-2\pi ixv)\, dx \quad . \tag{8}$$

The exponential term contains both cosine and sine contributions (45).

In practice, the interferogram cannot be measured to infinite path difference, but only to a maximum path difference x_{max}. Also, the interferogram is measured at certain intervals of position; that is, the function I(x) is not continuous. The integral is then replaced by a summation. Equation (8) is then replaced by

$$B(v) = \sum_{k=0}^{N-1} I_{kh} \exp(2\pi ivkh) \tag{9}$$

where h is the sampling interval and $N=x_{max} / h$, N being the number of interferogram sample points from x_0 to x_{max}.

The calculation of the spectrum by direct application of equation (9) is the classical method. However, it requires long computation times even by large computers, especially as N increases, because the time needed is proportional to N^2. But since the development of the fast Fourier transform (FFT) algorithm by Cooley and Tukey (49), the most common method to calculate the spectrum is with the FFT routine. A very good description of the algorithm is given by J. Connes (50) and by others (44,51).

In this study the FFT was considered as a "black box" to convert from the time to frequency domains. The actual routine used is the same as used by Horlick (52) and is written in floating point FORTRAN. The size of the input data array must be an integral power of 2, for example, $2^9=512$, $2^{12}=4096$. If the real data is not an integral power of 2, it can be filled with zeroes to the next power of 2. It should be mentioned that the speed of the program allows a 4096 point FFT to be performed in about two minutes on the PDP-11/10 minicomputer. A single precision machine language FFT routine available for this computer requires less than 10 seconds to transform the same number of data points.

In the routine used, the odd numbered points of the input array, length N, are placed in the real input array and the even numbered points are placed in the imaginary

input array. The real and imaginary input arrays are also of length N; therefore, since only the first N/2 points have been filled so far, the remainder of the arrays are filled with zeroes. This produces a smoother spectral plot because two output points are generated per resolution element. Of course, the spectral resolution, which is determined by the maximum optical retardation in the interferogram and the apodization (discussed in Chapter IV), is not altered by filling the arrays with zeroes.

The output of the FFT routine consists of two series, X(J) and Y(J), which are the real and imaginary intensity components and J is the index of the frequency components (from 1 to N). The amplitude spectrum of these frequencies, A(J), is calculated by taking the root sum of squares of these two series:

$$A(J) = ((X(J))^2 + (Y(J))^2)^{1/2} \quad . \tag{10}$$

Normally only the amplitude spectrum is calculated. The phase spectrum can be calculated from the real and imaginary series (23).

The wavenumber of a peak in a spectrum is calculated using the J index corresponding to the point having the largest value in that peak. The calculation is based on the He-Ne laser wavelength of 632.8 nm. The precision in the peak location is shown experimentally to be within one point (Table VII) or 0.03 nm in the vicinity of 400 nm.

CHAPTER III

SAMPLING THE INTERFEROGRAM AND THE CONSEQUENCES OF ALIASING

In order to perform the digital Fourier transform of the interferogram, the analog signal must be sampled and digitized at appropriate intervals of time. The sampled interferogram should be an accurate representation of the continuous analog interferogram; that is, no information should be lost. The importance of accurate digitizing is obvious. A data point must be acquired at equal intervals of optical retardation. A missed or extra data point can have adverse effects on the spectrum (53). Also, the analog-to-digital converter must be accurate and have enough resolution. At least a 12-bit converter is necessary. For broadband type signals, even more bit resolution may be needed to accurately digitize the small fringes at large optical retardation.

Not so obvious is the importance of the sampling interval. Information theory gives the answer to what should be the appropriate sampling time interval (45). The frequency content of an analog signal is zero above a certain frequency, f_{max}. To sample the analog signal properly, the time interval between samples must not exceed $1/2f_{max}$. Another way of saying this is that the sampling frequency must be two times the highest frequency present in the signal. If the sampling rate

is too low, high frequencies will be improperly sampled and will show up as spurious low frequencies. This is termed aliasing. At near-IR and shorter wavelengths, aliasing is an important consideration; therefore a thorough understanding is necessary to interpret the spectrum. A simple illustration may explain aliasing more clearly.

In Figure 7(a), spectrum A resulted from the Fourier transform of a synthetic interferogram which contained three frequencies, each of different amplitude. The interferogram was sampled at a rate such that all frequencies, up to X were properly sampled. For example, if X=200 Hz, then the sampling rate must be at least 400 Hz (a sampling interval of 2.5 msec). Then every other sampling point was dropped, the spectrum was calculated again, resulting in spectrum B. Since the sampling interval is now twice as long, 5 msec, only those frequencies up to Y (100 Hz) are properly sampled. Peaks 2 and 3 now appear as spurious low frequencies and their position can be predicted as a folding over about the central point of the original frequency axis. The 175 Hz signal (peak 3) appears as a signal of 25 Hz; that is, it has an alias of 25 Hz. The 125 Hz signal (peak 2) has an alias of 75 Hz. Peak 1 remains at its proper position because it is still properly sampled. Figure 7(b) illustrates how a frequency becomes aliased.

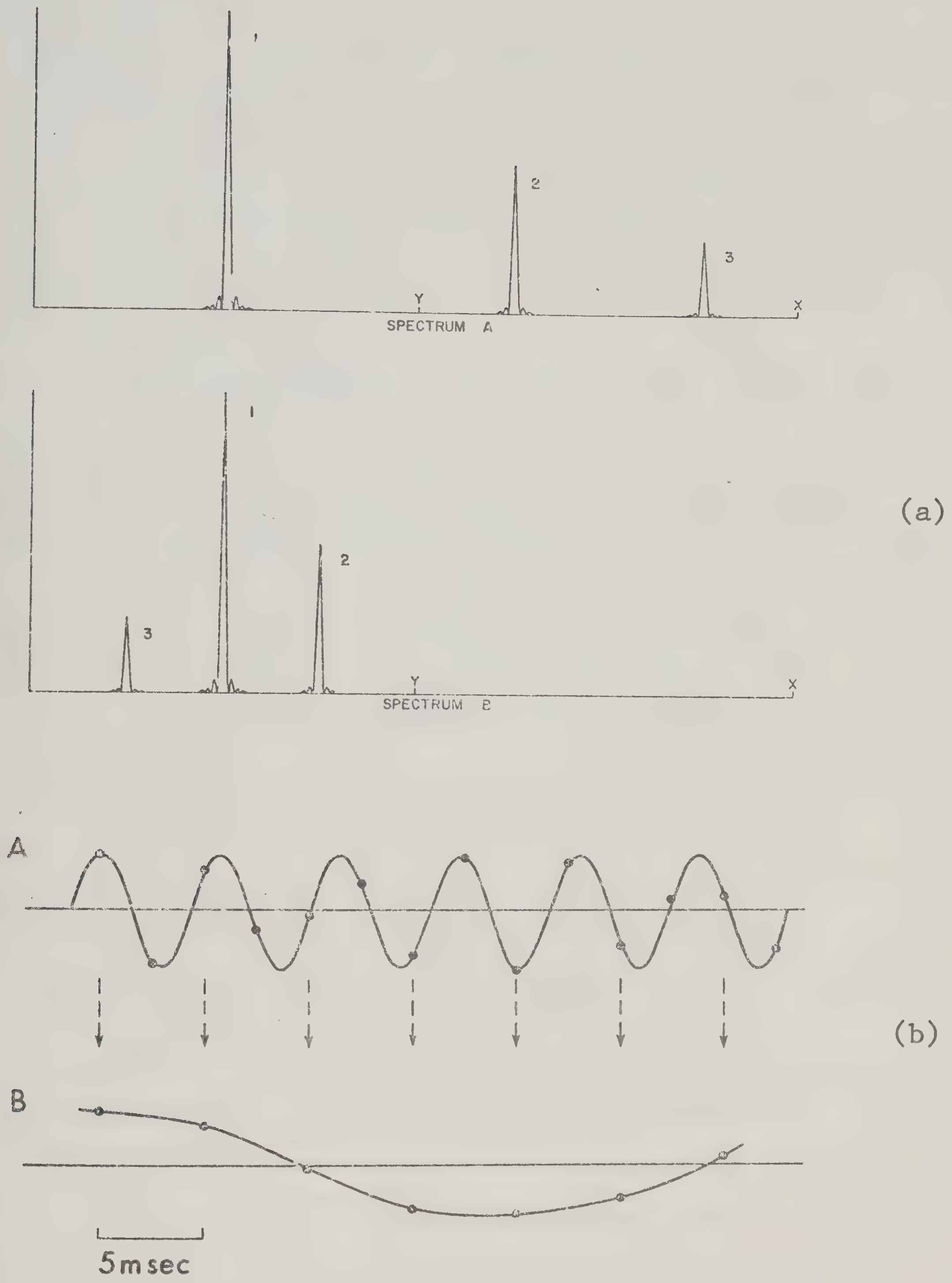

Figure 7. Illustration of aliasing. (a) Aliasing of spectral peaks due to undersampling of the interferogram. (b) Aliasing of a 175 Hz sine wave to a 25 Hz sine wave by undersampling.

The 175 Hz sine wave sampled at a 400 Hz rate is shown labelled as A. Every other sampled point is omitted, simulating the undersampling in spectrum B, and the remaining points are connected (shown labelled as B). A 25 Hz sine wave is the result. A similar exercise with a 125 Hz sine wave would result in an alias of a 75 Hz sine wave.

It is important to note that if peak 1 were not present, the fold over of peaks 2 and 3 would not be serious as it occurs in an exactly predictable manner. Of course, the approximate frequency range of the signals must be known to predict whether the spectrum is aliased. Therefore, in practice, it is the bandwidth of the signal and not just the highest frequency which determines whether a certain sampling rate is acceptable.

In the previous example (Figure 7), if peak 1 did not exist and the bandwidth was known to be only 100 Hz (from Y=100 Hz to X=200 Hz), a sampling rate of 200 Hz would still aliase the spectrum (as in spectrum B). However, the spectrum can be interpreted because an a priori knowledge of the bandwidth eliminates the possibility that peaks 2 and 3 are in the 0 to 100 Hz region. There is no overlap of regions so that a sampling rate twice the signal bandwidth is acceptable. But, care must be exercised in the proper labeling of the frequency axis.

Normally, in Fourier transform spectroscopy, aliasing is avoided as the undersampled modulation frequencies show up as spurious spectral information (fold over). This can be very confusing when there is much broadband energy present. However, with line spectra, as commonly measured in atomic spectroscopy, it is possible to use aliasing to advantage. To be useful one must have an a priori knowledge of the sampling rate and the spectral region of the signal. The bandwidth of the signal must be known, but it can be determined from the instrumental components. Factors limiting the bandwidth are: optical transmission of the beamsplitter, beamsplitter support and compensator materials; reflectivity of the mirrors and/or lenses used in the system; source output; detector response, both spectral sensitivity and frequency response; detector amplifier and electronic filter bandwidth; and any optical filters placed in the light path to intentionally block out some spectral regions.

A practical illustration of the use of aliasing is the measurement of the flame emission spectra of lithium, potassium, rubidium and cesium with the Fourier transform spectrometer. Table I lists the emission lines of these elements in the near-IR region along with the region from Table II in which they fall. Table II will be explained shortly. Figure 8 gives a schematic diagram

TABLE I

Major Emission Lines of Na, Li, K, Rb, Cs in the Near-IR

Element	nm	cm^{-1}	Region(in Table II)
Na	589.00	16,978	9
	589.59	16,961	9
Li	670.78	14,908	8
K	766.49	13,046	7
	769.90	12,989	7
Rb	780.02	12,820	7
	794.76	12,582	7
Cs	852.11	11,736	6
	894.35	11,181	6

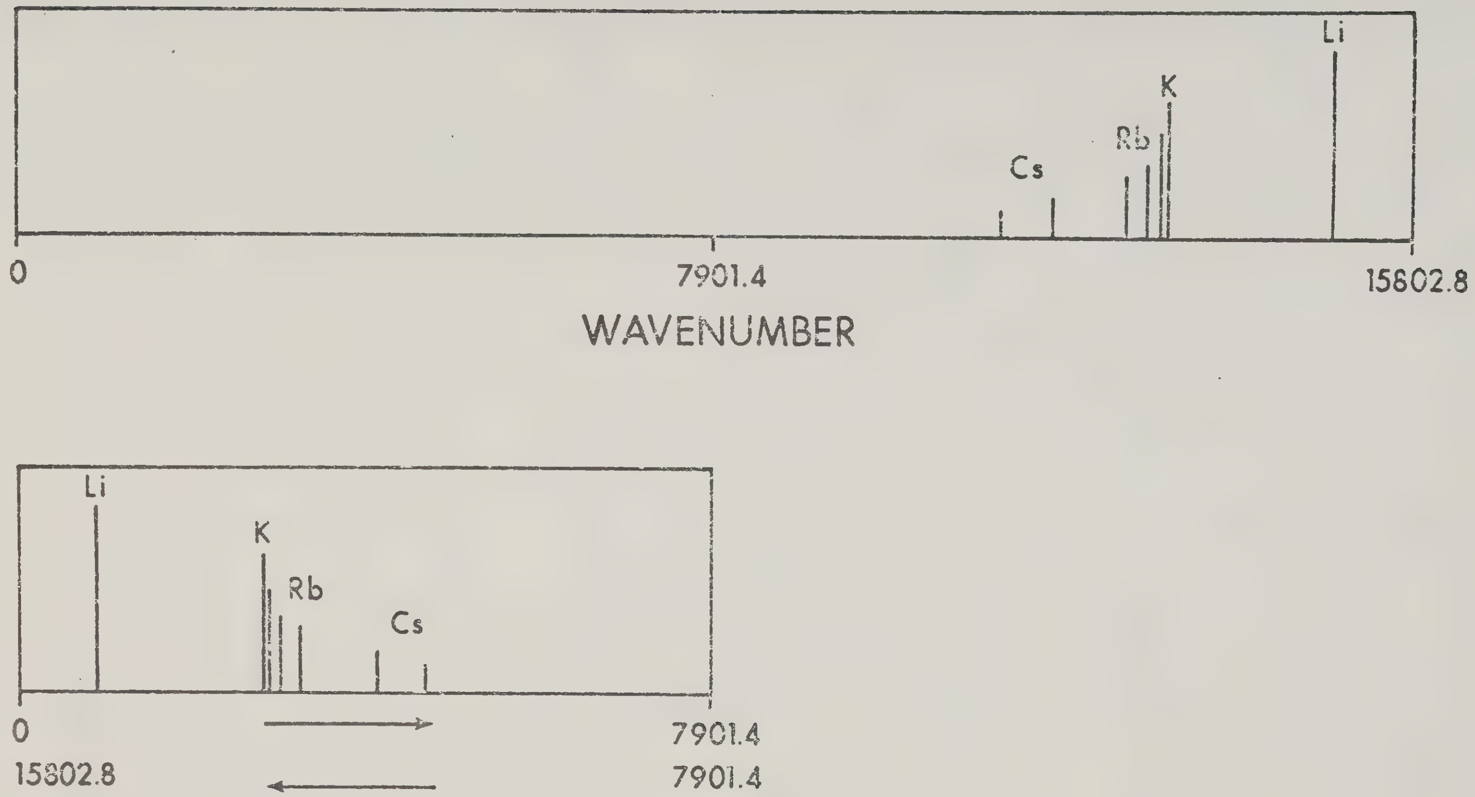

Figure 8. Schematic spectrum of Li, K, Rb, and Cs and the aliased schematic spectrum for a 0.6328 um sampling interval.

of a spectrum of these elements with the frequency axis in wavenumbers. The amplitude of the lines are arbitrary.

In order to measure these lines of Li, K, Rb, and Cs without aliasing, a bandwidth of 15,802.8 cm^{-1} is necessary. However, the standard He-Ne laser used as a reference has a wavelength of 0.6328 um (15,802.8 cm^{-1}). The clock signal for sampling is derived from the laser fringes generated by the interferometer. A clock pulse is generated for every 0.6328 um of optical retardation; that is, the signal interferogram is sampled at 0.6328 um intervals. This means that the shortest wavelength of light that can be properly sampled without aliasing is 1.2656 um (7901.4 cm^{-1}). To achieve the bandwidth of 15,802.8 cm^{-1}, the sampling interval must be 0.3164 um. With the 0.6328 um sampling interval, the bandwidth covered is 7901.4 cm^{-1}. The 7901.4 to 15,802.8 cm^{-1} region then becomes aliased and overlaps the 0 to 7901.4 cm^{-1} region. This is shown in the bottom diagram of Figure 8. In this case the overlap is not serious since there is no signal in the 0-7901.4 cm^{-1} region (due to the Si photodiode detector's insensitivity and the quartz beamsplitter not being efficient in the mid-IR region). Therefore, as long as one is aware of the aliasing, the frequency axis can be labelled properly and the spectrum can be interpreted.

Now, what if there is spectral signal above

15,802.8 cm^{-1}? An example is where sodium is present along with the previous four elements, shown schematically in Figure 9. Even if the sampling interval were 0.3164 um (31,605.6 cm^{-1}), the Na doublet at 589 nm would still be aliased. The overlap is shown in the middle diagram of Figure 9 where the Na doublet is aliased to a position between the K and Li lines. With the 0.6328 um sampling interval, the result is shown in the bottom diagram. The Na doublet has been aliased twice. There is spectral information from more than one aliased region and interpretation is less trivial. But, as long as the aliased lines do not overlap exactly, interpretation is possible. One possible method to determine which region a line belongs is to use an optical filter to block out the other region or regions and measure the spectrum again. The disappearance or continued presence of a line will locate the region in which that line belongs. Also some regions may be ruled out due to lack of detector response.

Another example is diagrammed in Figure 10. The chromium triplets at 427 nm and 360 nm are shown unaliased in the top diagram. If the sampling interval were 0.3164 um, the triplets would be folded over into the 0-15,802.8 cm^{-1} region pivoting about the 15,802.8 cm^{-1} point (middle diagram). With a 0.6328 um sampling interval, the bandwidth is 7901.4 cm^{-1} and the Cr 427 nm triplet is folded over again about the 23,704.2 cm^{-1} point.

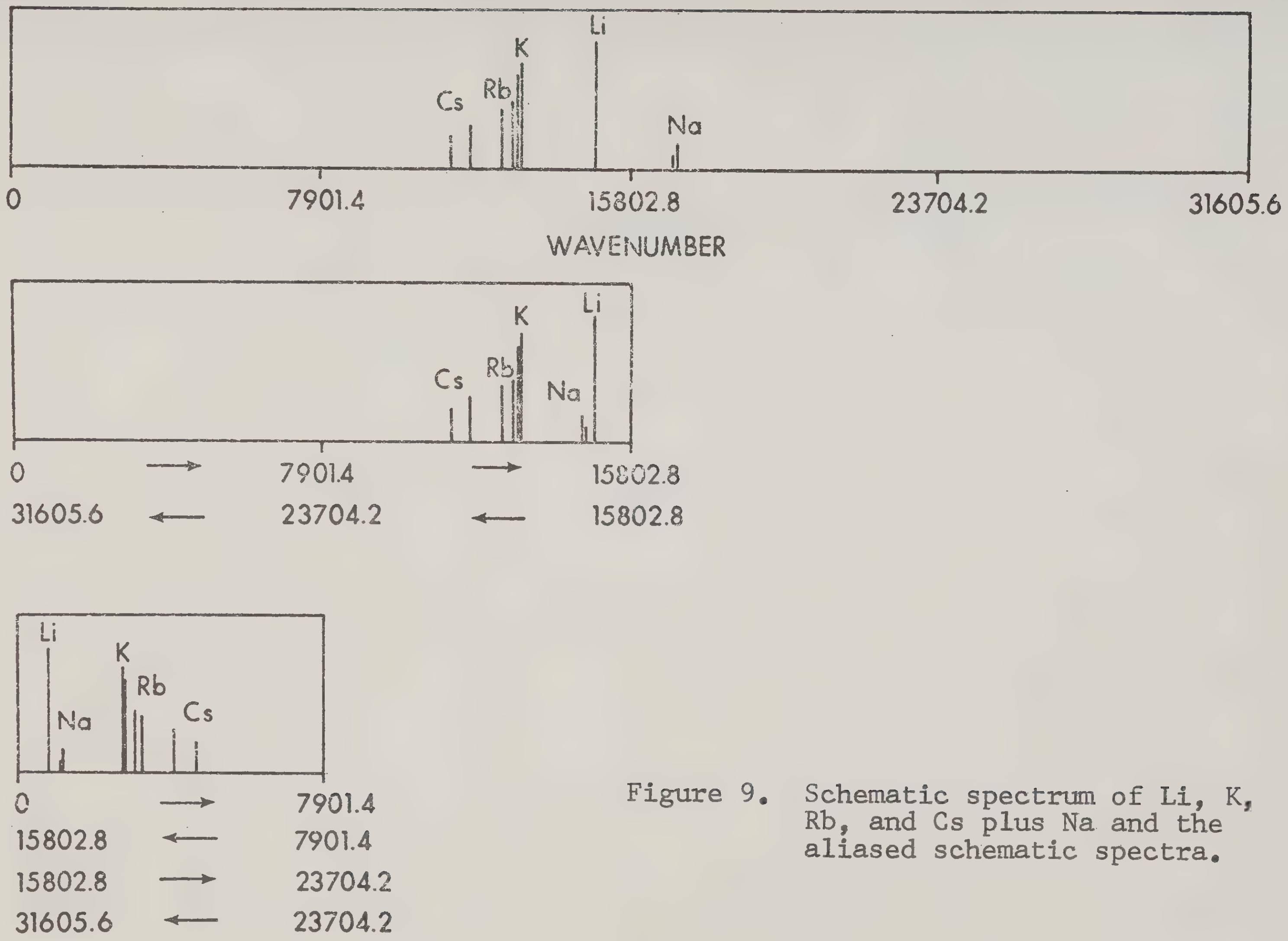

Figure 9. Schematic spectrum of Li, K, Rb, and Cs plus Na and the aliased schematic spectra.

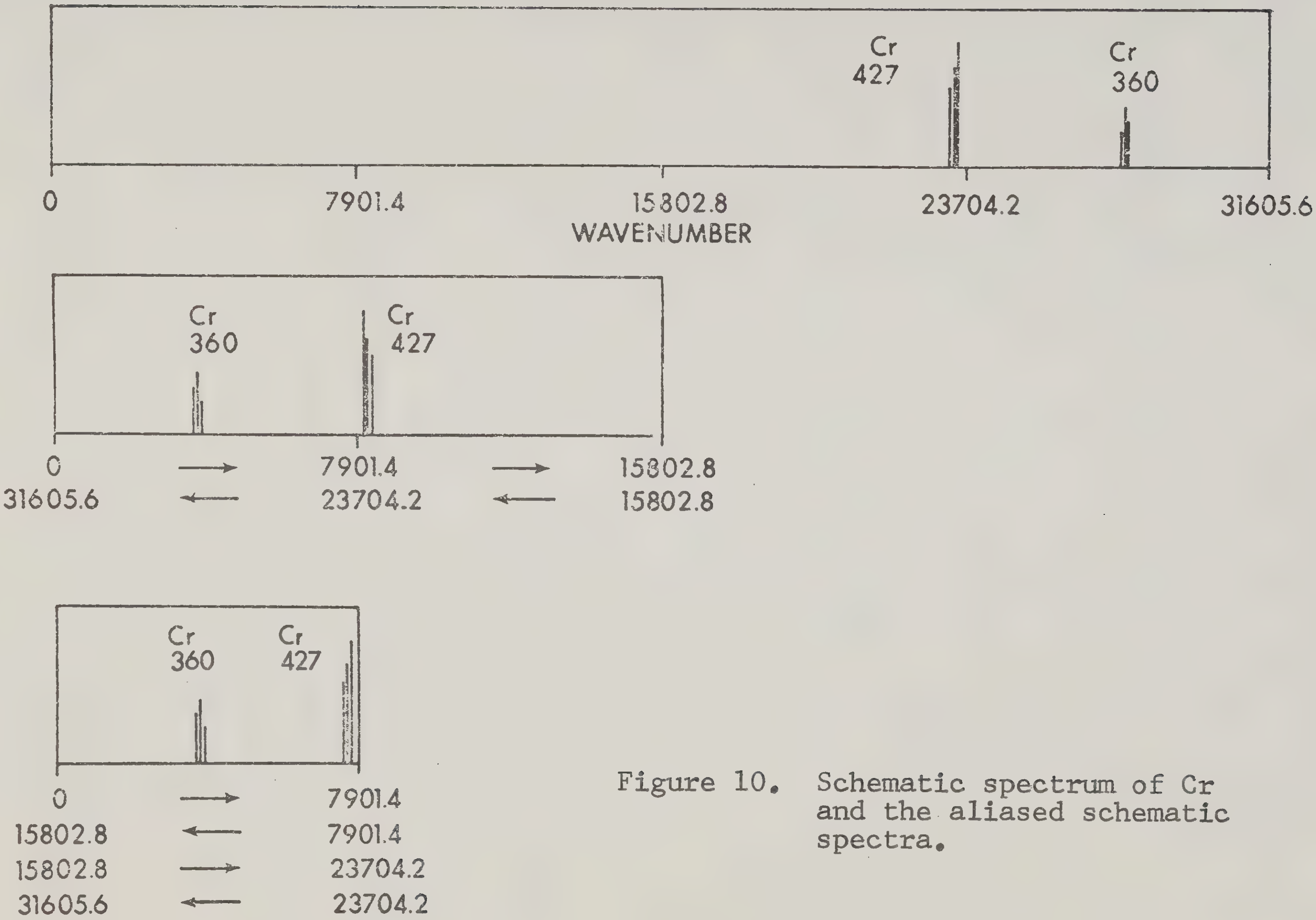

Figure 10. Schematic spectrum of Cr and the aliased schematic spectra.

This overlapping of spectral regions due to aliasing is tabulated in Table II based on the sampling rates derivable from the He-Ne laser 632.8 nm line. Column III is the overlapping regions for a 0.6328 um sampling interval which has a bandwidth of 7901.4 cm^{-1}. This is termed the direct sampling rate since a data point is taken for every laser fringe (0.6328 um optical retardation). In order to avoid confusion, the notation used will be explained. The regions are numbered at the left of Table II. When reference is made, for example, to the 15,802.8-7901.4 cm^{-1} region under the direct sampling rate, that region will be called region (5-8). Not all the regions listed under one sampling rate will be present in an aliased spectrum. As mentioned before, some regions can be optically eliminated. Another method is by using low and high filters to electronically block out regions. For example, if the mirror drive velocity is set to give a laser fringe of 4 kHz, this means that an optical signal of 632.8 nm is modulated to a fringe frequency of 4 kHz and lower wavelengths (higher optical frequencies) are modulated to a higher fringe frequency. If the frequency response of the detector amplifier is limited by a low pass filter set at about 4 kHz, all optical signals which are modulated to a frequency greater than 4 kHz (all wavelengths less than 632.8 nm) will be eliminated. A high pass filter can also be set to

TABLE II

Aliasing Table for ÷4, ÷2, Direct, X2, and X4 Sampling Rates

Region No.	I		II		III		IV		V	
	÷4 SAMPLING RATE (2.5312 μm)[a]		÷2 SAMPLING RATE (1.2656 μm)		DIRECT SAMPLING RATE (0.6328 μm)		x2 SAMPLING RATE (0.3164 μm)		x4 SAMPLING RATE (0.1582 μm)	
	Region(cm^{-1})	Region(μ)	Region(cm^{-1})	Region(μ)	Region(cm^{-1})	Region(μ)	Region(cm^{-1})	Region(μ)	Region(cm^{-1})	Region(μ)
1	0 - 1975.35	∞ - 5.0624	0 - 3950.7	∞ - 2.5312	0 - 7901.4	∞ - 1.2656	0 - 15,802.8	∞ - 0.6328	0 - 31,605.6	∞ - 0.3164
2	3950.70 - 1975.35	2.5312 - 5.0624								
3	3950.70 - 5926.05	2.5312 - 1.6875	7901.4 - 3950.7	1.2656 - 2.5312						
4	7901.40 - 5926.05	1.2656 - 1.6875								
5	7901.40 - 9876.75	1.2656 - 1.0125	7901.4 - 11,852.1	1.2656 - 0.8437	15,802.8 - 7901.4	0.6328 - 1.2656				
6	11,852.10 - 9876.75	0.8437 - 1.0125								
7	11,852.10 - 13,827.45	0.8437 - 0.7232	15,802.8 - 11,852.1	0.6328 - 0.8437						
8	15,802.80 - 13,827.45	0.6328 - 0.7232								
9	15,802.80 - 17,778.15	0.6328 - 0.5625	15,802.8 - 19,753.5	0.6328 - 0.5062	15,802.8 - 23,704.2	0.6328 - 0.4219	31,605.6 - 15,802.8	0.3164 - 0.6328		
10	19,753.50 - 17,778.15	0.5062 - 0.5625								
11	19,753.50 - 21,728.85	0.5062 - 0.4602	23,704.2 - 19,753.5	0.4219 - 0.5062						
12	23,704.20 - 21,728.85	0.4219 - 0.4602								
13	23,704.20 - 25,679.55	0.4219 - 0.3894	23,704.2 - 27,654.9	0.4219 - 0.3616	31,605.5 - 23,704.2	0.3164 - 0.4219				
14	27,654.90 - 25,679.55	0.3616 - 0.3894								
15	27,654.90 - 29,630.25	0.3616 - 0.3375	31,605.6 - 27,654.9	0.3164 - 0.3616						
16	31,605.60 - 29,630.25	0.3164 - 0.3375								
17	31,605.60 - 33,580.95	0.3164 - 0.2978	31,605.6 - 35,556.3	0.3164 - 0.2812	31,605.6 - 39,507.0	0.3164 - 0.2531	31,605.6 - 47,408.4	0.3164 - 0.2109	63,211.2 - 31,605.6	0.1582 - 0.3164
18	35,556.30 - 33,580.95	0.2812 - 0.2978								
19	35,556.30 - 37,531.65	0.2812 - 0.2664	39,507.0 - 35,556.3	0.2531 - 0.2812						
20	39,507.00 - 37,531.65	0.2531 - 0.2664								
21	39,507.00 - 41,482.35	0.2531 - 0.2411	39,507.0 - 43,457.7	0.2531 - 0.2301	47,408.4 - 39,507.0	0.2109 - 0.2531				
22	43,457.70 - 41,482.35	0.2301 - 0.2411								
23	43,457.70 - 45,433.05	0.2301 - 0.2201	47,408.4 - 43,457.7	0.2109 - 0.2301						
24	47,408.40 - 45,433.05	0.2109 - 0.2201								
25	47,408.40 - 49,383.75	0.2109 - 0.2025	47,408.4 - 51,359.1	0.2109 - 0.1947	47,408.4 - 55,309.8	0.2109 - 0.1808	63,211.2 - 47,408.4	0.1582 - 0.2109		
26	51,359.10 - 49,383.75	0.1947 - 0.2025								
27	51,359.10 - 53,334.45	0.1947 - 0.1875	55,309.8 - 51,359.1	0.1808 - 0.1947						
28	55,309.80 - 53.334.45	0.1808 - 0.1875								

---

[a] Sampling Interval

eliminate low optical frequencies.

Clearly then, to work in the UV-visible region, either the sampling rate must be increased or aliasing must be tolerated. The frequency of the reference laser modulation can be increased by use of optical techniques such as double passage of the laser through the interferometer or by electronic frequency multiplication using phase locked loops (54). However, the high sampling rate necessary to sample the UV-visible modulation frequencies without aliasing quickly results in a prohibitively large number of data points that must be digitized in the interferogram to achieve reasonable resolution. Thus, the alternative of aliasing the spectral information in the interferogram must be used.

To show that electronic multiplication of the laser modulation frequency was possible, the reference clock was frequency quadrupled using phase locked loop techniques. The analog laser fringes were also used as the spectral signal. Figure 11 shows the spectrum from the Fourier transform of the sampled laser interferogram. The sampling interval was 0.1582 um (x4 sampling rate) because a data point was taken at every 1/4 wavelength of the laser. The bandwidth was 31,605.6 cm^{-1} (Column V in Table II) and the laser line should be exactly at the midpoint of the spectrum at 15,802.8 cm^{-1}. The peak does occur at this position. Spectrum (a) is the output with no

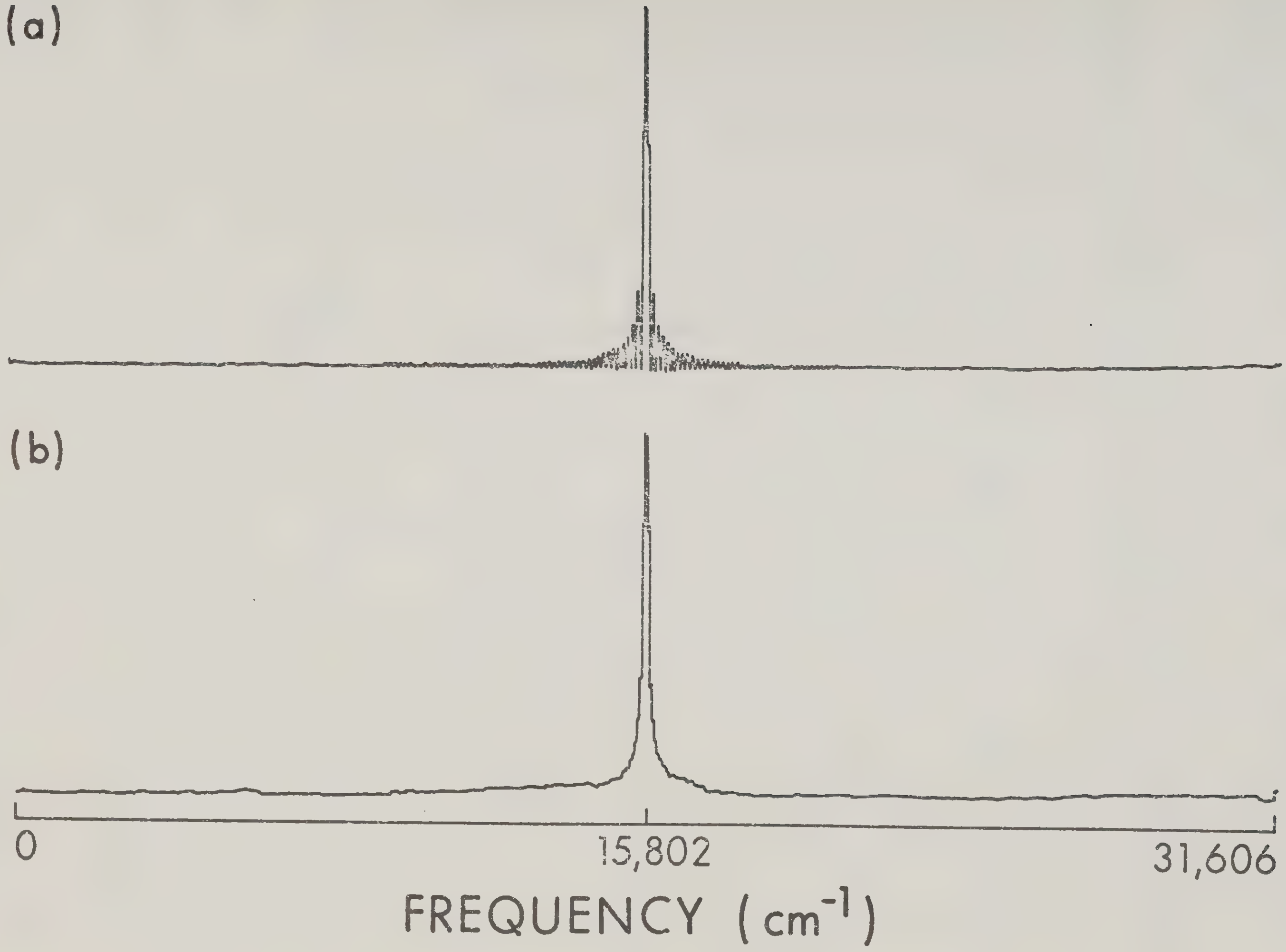

Figure 11. He-Ne laser 0.6328 um line, interferogram sampled at X4 sampling rate. (a) No apodization. (b) Triangular apodization.

apodization of the interferogram. Spectrum (b) is the result of triangular apodization before performing the Fourier transform. Apodization will be discussed in Chapter IV.

Electronic frequency doubling by the same technique gives a sampling interval of 0.3164 um. The interferogram of the flame emission of a Li, K, Rb, Cs solution was sampled at this rate (x2 sampling rate) and the resulting spectrum is shown in Figure 12(a). At this sampling interval, the bandwidth is 15,802.8 cm^{-1} and all the spectral lines are properly sampled. There is no aliasing. The direct sampling rate with a bandwidth of 7901.4 cm^{-1} results in spectrum (b) where all the lines have been aliased. These are the real spectra that were diagrammed in Figure 8. It should be noted that all the spectra measured with a Fourier transform spectrometer has an axis which is linear in frequency (wavenumber) and not linear in wavelength. This set of data was taken with the PDP-8/e system which had a limit of a 512 point transform.

With the limited number of data points and the wide spectral coverage (over 220 nm), the resolution is quite poor. The potassium doublet is not resolved at all and the rubidium doublet is only partially resolved in spectrum (a). In spectrum (b), the resolution is doubled. This is due to the fact that the sampling interval is twice as long; therefore, with the same number of data

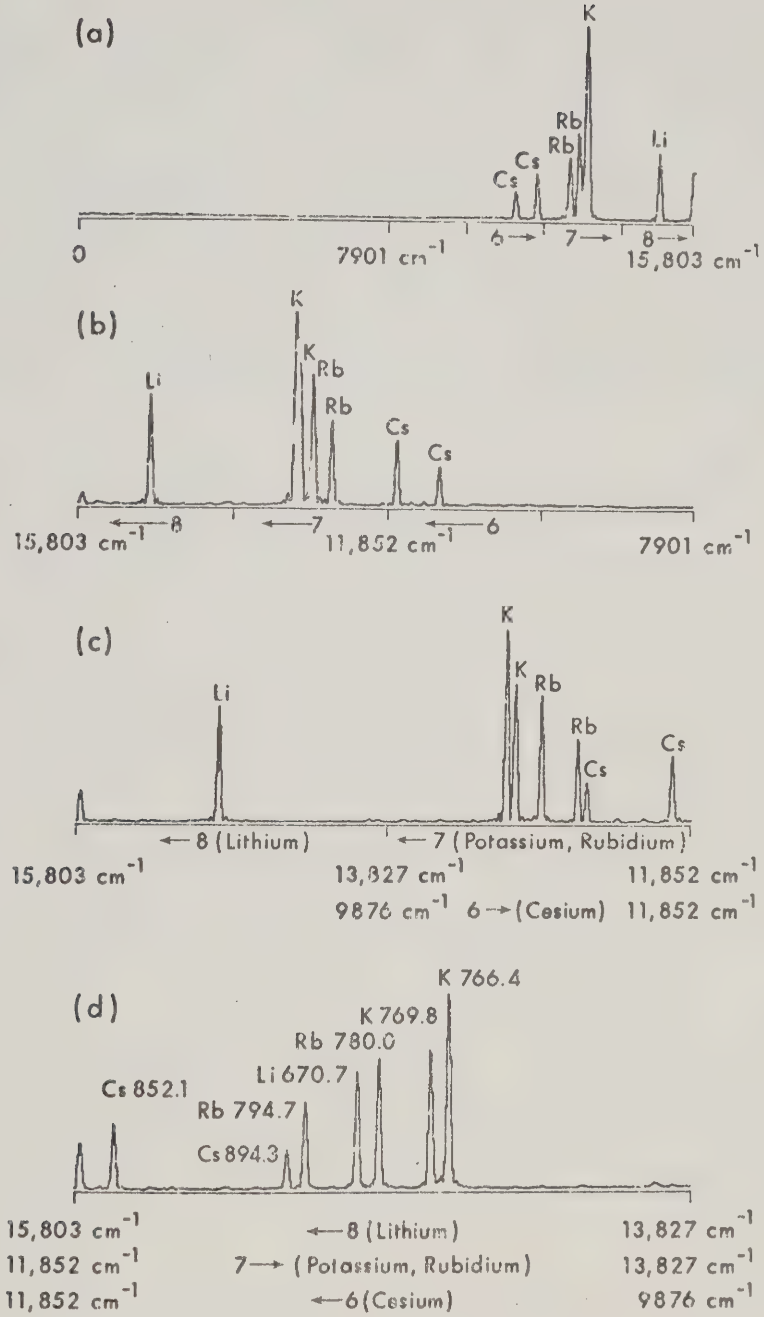

Figure 12. Spectra of Li, K, Rb, and Cs using (a) X2 sampling rate, (b) direct, (c) ÷2, and (d) ÷4 sampling rate.

points (512 in this case), the interferogram has been sampled to twice the optical retardation which determines the ultimate resolution. Table III tabulates the resolution that can be achieved with a triangularly apodized interferogram using different sampling intervals. The resolution is also given in wavelength units at 770 and 280 nm. It should be noted that the resolution is constant in wavenumber for one situation; therefore, the resolution increases with decreasing wavelength. For example, 16 cm^{-1} resolution at 770nm results in 0.95 nm resolution; but, at 280 nm, the resolution is 0.125 nm.

If the sampling interval is 1.2656 um (a data point every other laser fringe), the bandwidth is 3950.7 cm^{-1}. The overlapping of the regions due to aliasing is tabulated in Column II of Table II. This is the ÷2 sampling rate. The spectrum is shown in Figure 12(c). The resolution is again doubled and now the potassium doublet is resolved. The cesium lines (in region 6) have aliased into the potassium-rubidium region (number 7). The region numbers are those given in Table II.

If the sampling interval is made even coarser to 2.5312 um, the bandwidth is 1975.35 cm^{-1}. The regions overlap further (Column I of Table II) with all three regions overlapping via aliasing. The spectrum is shown in Figure 12(d). The theoretical resolution at the

TABLE III

Resolution with a Triangularly Apodized Double-sided Interferogram of (a) 512 points, (b) 4096 points

Sampling Rate	Resolution		
	cm^{-1}	nm at 770nm	nm at 280nm
X4	(a) 256	15.5	2.00
X2	(a) 128	7.7	1.00
Direct	(a) 64	3.8	0.50
÷2	(a) 32	1.9	0.25
÷4	(a) 16	0.95	0.125
Direct	(b) 8	0.47	0.063

different sampling rates is given in Table III for a triangularly apodized double-sided interferogram of 512 points. Since the potassium doublet has a 3.4 nm separation, it is expected not to be resolved until the sampling interval was 1.2656 um. The spectra point this out.

The flame emission was measured again when the new data system with the PDP-11/10 minicomputer was available. With 4096 point interferograms, the resolution is better with the direct sampling rate than with a ÷4 sampling rate and a 512 point interferogram. Figure 44 in Chapter VII shows a spectrum of the above four metals plus sodium from a 4096 point interferogram. The Na doublet has only a 0.59 nm separation, but it is resolved. Table III predicts this, pointing out that the resolution capability is fairly close to the calculated resolution.

From the series of spectra in Figure 12, it is clear that aliasing can be used to advantage in optimizing spectral coverage and resolution when making Fourier transform atomic spectrochemical measurements.

CHAPTER IV

APODIZATION AND ITS EFFECTS

As mentioned earlier, the interferogram of a monochromatic source is a cosine wave. If the source were infinitely narrow, the cosine wave would continue for infinitely large optical retardation. However, in practice, this is not observed. First, certain spectral or instrumental conditions result in the interferogram being damped as optical retardation increases. Factors contributing to this are natural line broadening and solid angle effects (15). Second, the interferogram is sampled to an optical retardation of x_{max} and not to infinity. This truncation of the interferogram is a type of self-apodization. The term apodization refers to the multiplication of the interferogram by a relatively simple function. The effect of multiplying the interferogram by a function is equivalent to the convolution of the spectrum resulting from the Fourier transform of the interferogram with the Fourier transform of that function. This is shown in Figure 13 where the asterisk "*" refers to convolution. The bottom diagrams describe apodization and the top diagrams describe convolution where the spectral peak is convolved with the instrumental line shape to give the output spectrum.

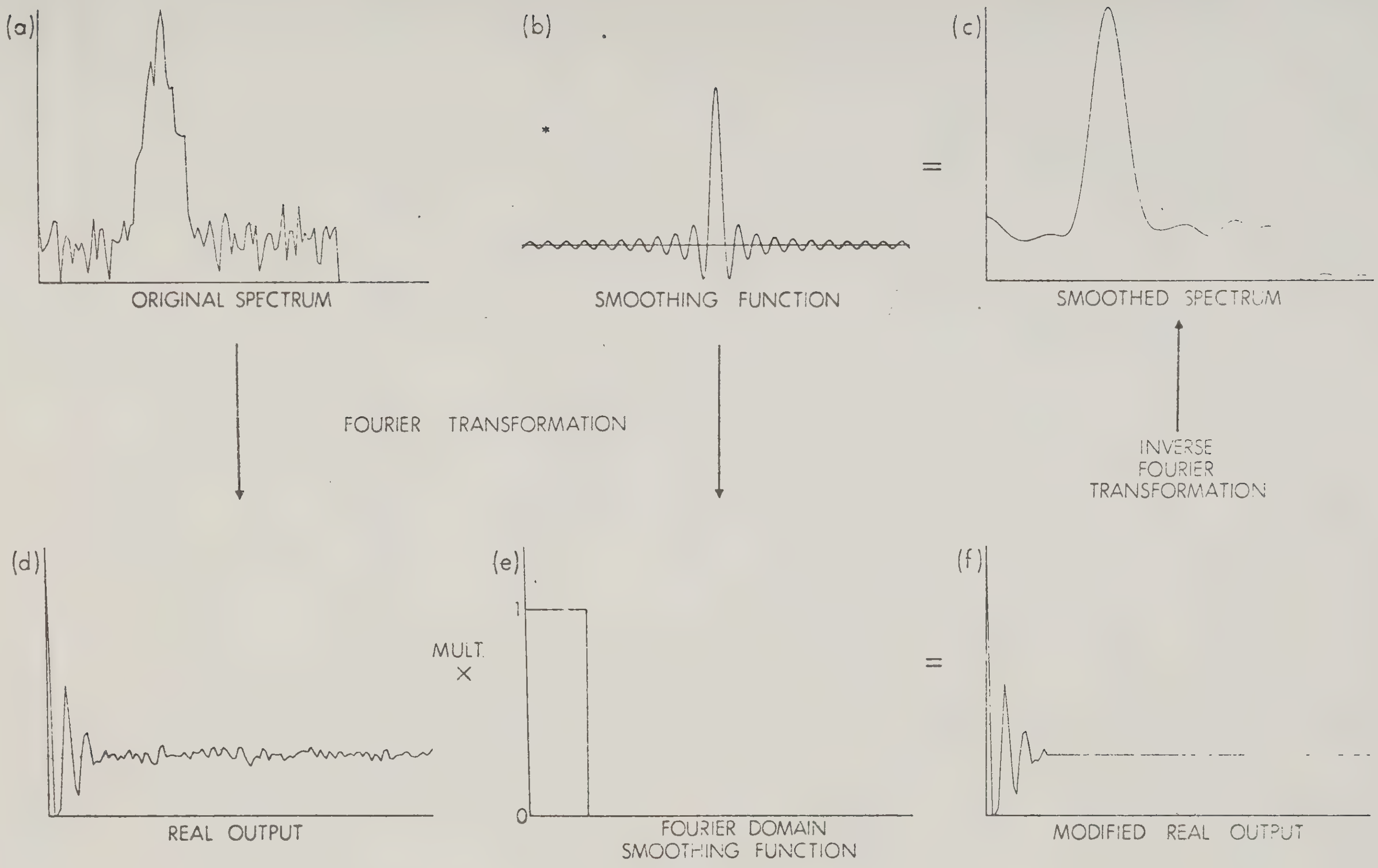

Figure 13. The relationship between convolution and apodization: (a), (b), (c) convolution, (d), (e), (f) apodization.

The truncation of the interferogram at the end of the sampling at x_{max} can be thought of as multiplying the interferogram by a boxcar function where the interferogram is multiplied by one if x is less than x_{max} and multiplied by zero if x is greater or equal to x_{max}. The shape of the truncation function is shown in Figure 14(a). This truncation imposes the instrumental line shape to the spectral lines (50) of the form $\sin(2\pi v x_{max})/(2\pi v x_{max})$. The peak shape is shown in Figure 15(a). Because of the method of computation, the negative side lobes of the sine x/x function appear positive. The peaks in Figures 15 and 17 were generated by Fourier transforming a 4096 point interferogram consisting of a cosine wave sampled at 4 points per cycle with the appropriate apodization. This is the resultant instrumental line shape when there is no intentional apodization, that is, when the interferogram is not multiplied by a function after the interferogram is acquired. When the term no apodization is used, it means that no intentional apodization has been performed on the interferogram. The resolution that can be obtained in this case is given by $1/2x_{max}$. For most of the spectra presented here, the interferograms are 4096 points long with the direct sampling rate and equal number of data points on either side of the ZPD position; therefore x_{max}=0.1296 cm (2048 X 6.328 X 10^{-5} cm). The nominal

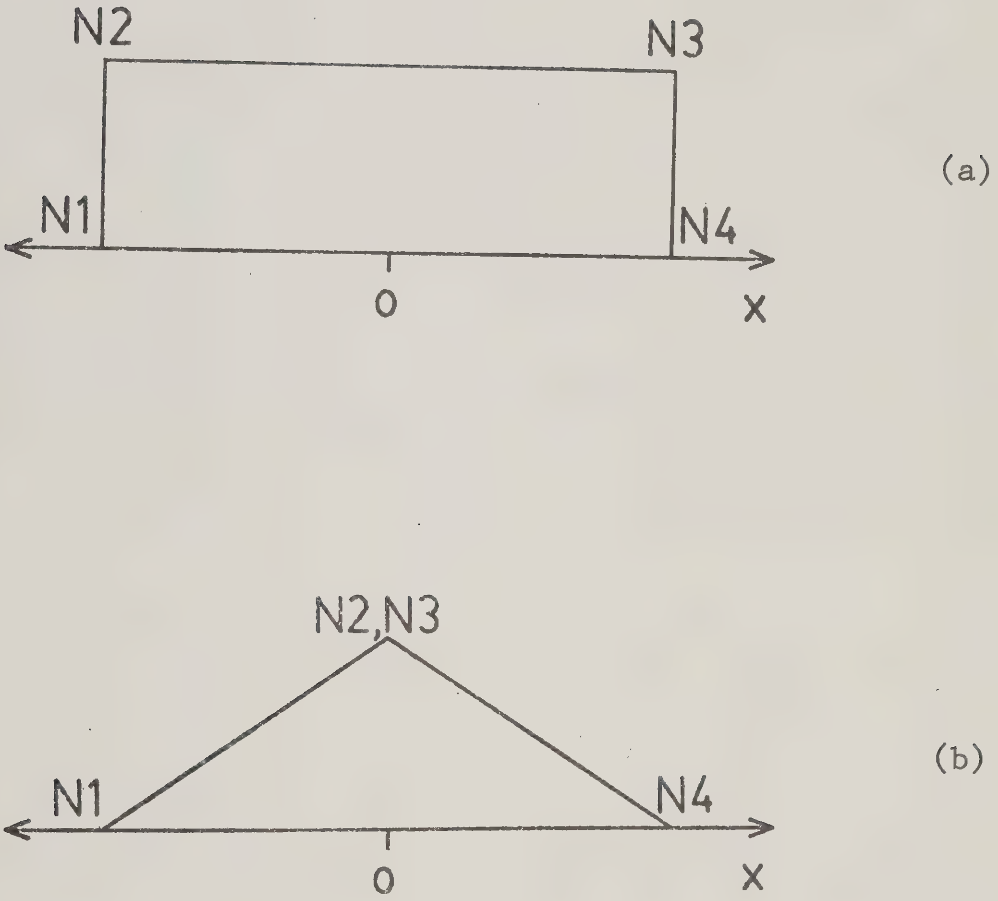

Figure 14. Apodization functions:
(a) boxcar, (b) triangular.

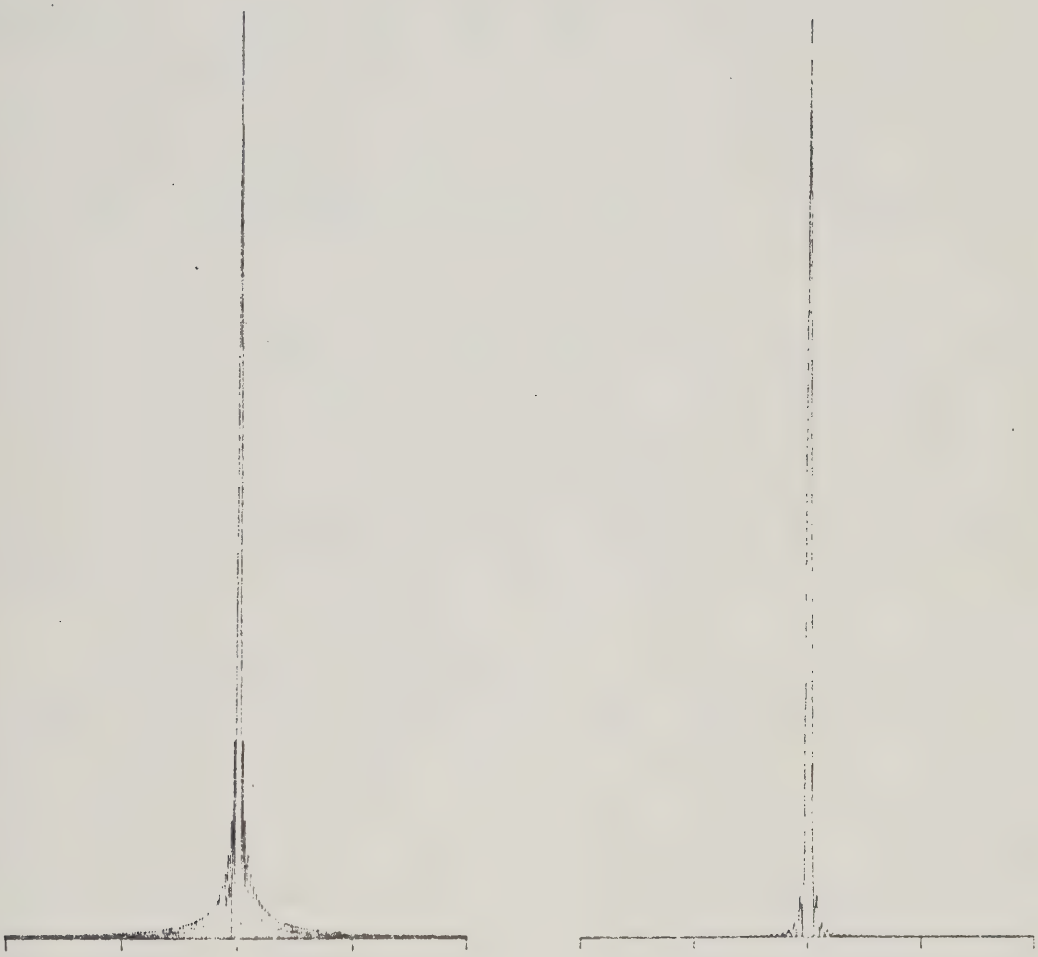

(a) (b)

Figure 15. Peak shapes resulting from (a) boxcar, (b) triangular apodization.

resolution is about 4 cm^{-1}. However, the peak shape with the truncated interferogram gives large side lobes, the first side lobe being about 20% of the peak maximum. In many cases, the side lobes can cause confusion, especially if small peaks are close to large peaks.

To improve the instrumental line shape, the interferogram can be multiplied by a mathematical function before the Fourier transform is performed (23,25,55-57). This function is usually normalized so that the value is between zero and one. In general, apodization functions do not necessarily have to reach zero. The apodization is performed easily since the interferogram is already stored in the computer. Typical functional dependencies include linear, exponential and Gaussian function.

A consequence of apodizations that give more weight to small $\underline{x}$ and less to large $\underline{x}$ is the improvement in signal-to-noise ratio in the final spectrum. This comes about because the rapid changes (high spatial frequencies) in the spectrum are represented in the interferogram at larger optical retardations than the slower changing information. Noise tends to be of higher spatial frequency than spectral peaks, therefore the noise is reduced. But there is the standard trade-off of resolution and S/N ratio. The spectral peaks also contain some high spatial frequencies which determine the sharpness of the peak. Therefore, when the noise is

reduced by apodization, the resolution decreases.

The boxcar apodization function shown in Figure 14(a) can be implemented by a routine that multiplies the interferogram data points less than N1 and greater than N4 by zero and leaving points between N2 and N3 unchanged.

A linearly decreasing function, called triangular apodization (Figure 14(b)), can be implemented with the routine by setting N2 and N3 to the data point corresponding to the ZPD position. All points between N1 and N2, and between N3 and N4 are multiplied by the $\underline{y}$ value of the slope which varies linearly between 0 and 1. Points less than N1 and greater than N4 are set equal to zero. The instrumental line shape resulting from triangular apodization is $\sin^2 (2\pi v x_{max})/(2\pi v x_{max})^2$. The peak shape is shown in Figure 15(b). Note that the side lobes are less prominent than for the boxcar apodization. The resolution possible with triangular apodization is $1/x_{max}$ or half the resolution of a boxcar apodization. For the example given earlier (4096 point, double-sided interferogram), this means a nominal resolution of about 8 cm^{-1}.

The type of apodization found to be more useful with narrow emission type signals is the Gaussian function. The form of the function used is

$$\mathrm{FCN(I)} = \exp\left(-\mathrm{FAC} \left(\frac{|\mathrm{I-Z}|}{\mathrm{NP-Z}} \right)^2 \right) \qquad (11)$$

where I=point number, Z=point number of the ZPD position, NP=total number of points, and FAC=a factor that determines the width of the Gaussian function. The Gaussian apodization is shown in Figure 16. The ZPD position is shown at point 2048 (for 4096 point double-sided interferograms). Plot A results when the variable FAC=10.0, plot B when FAC=5.0, and plot C when FAC=2.5. The peak shapes resulting from Gaussian apodization are shown in Figure 17(a) for FAC=2.5 and in Figure 17(b) for FAC=5.0. The resolution, when Gaussian apodization is applied, should be similar to triangular apodization if FAC is approximately 2.5. For larger values of FAC, the function is more heavily damped and therefore resolution will be lower. The side lobe suppression with the FAC=2.5 Gaussian apodization is more effective than with the triangular function while retaining similar resolution. The FAC=5.0 Gaussian function almost reaches zero at maximum optical retardation with the result that side lobes are not evident (actually they are less than 0.5% of the peak amplitude); however, the resolution is lower.

A practical example of apodization is shown in Figures 18 and 19. The flame emission of a sodium solution was measured (details in Chapter VII). Figure 18 shows 3000 points of the 4096 point double-sided interferogram that resulted from time averaging 50 successive scans. That two emission lines are present can be deduced

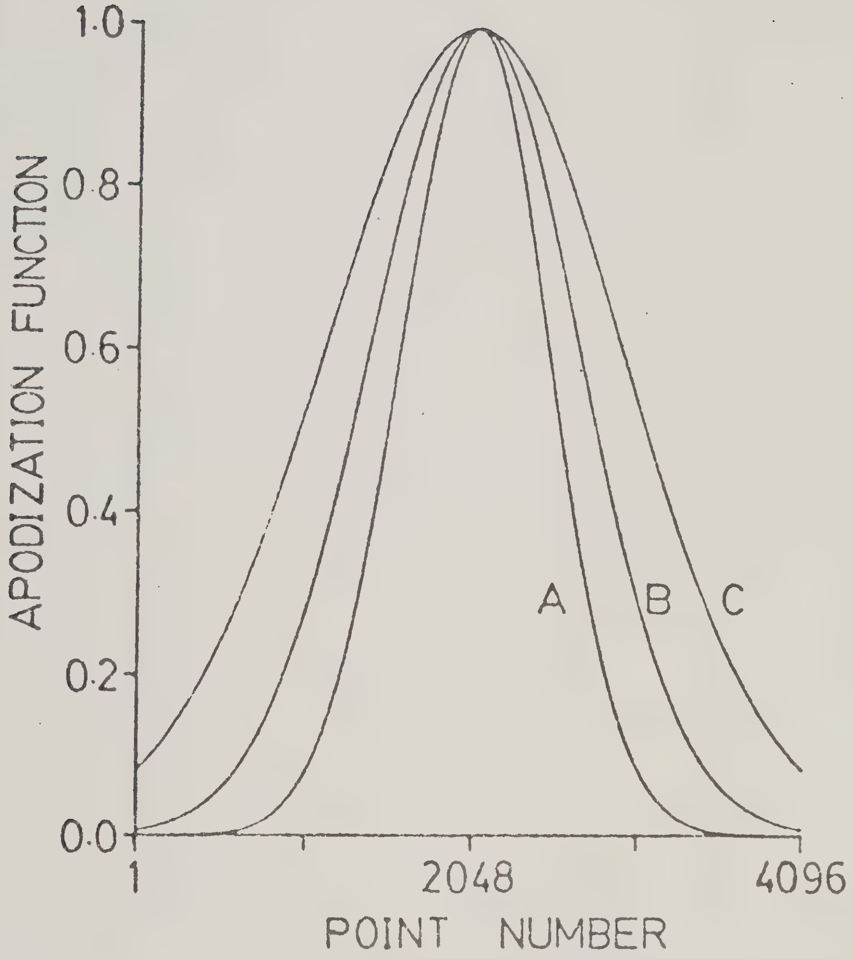

Figure 16. Gaussian apodization functions: A--FAC=10.0, B--FAC=5.0, C--FAC=2.5. See text for details.

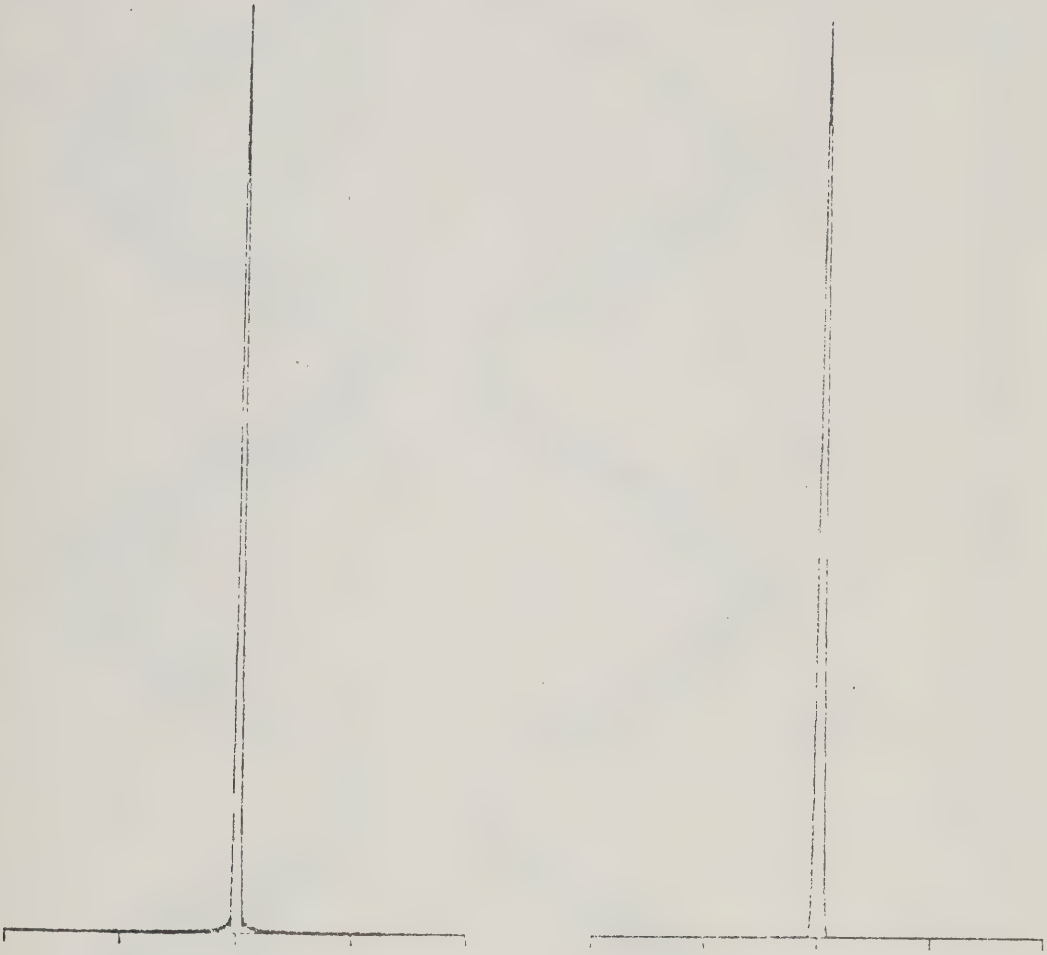

(a) (b)

Figure 17. Peak shapes resulting from Gaussian apodization: (a) FAC=2.5, (b) FAC=5.0.

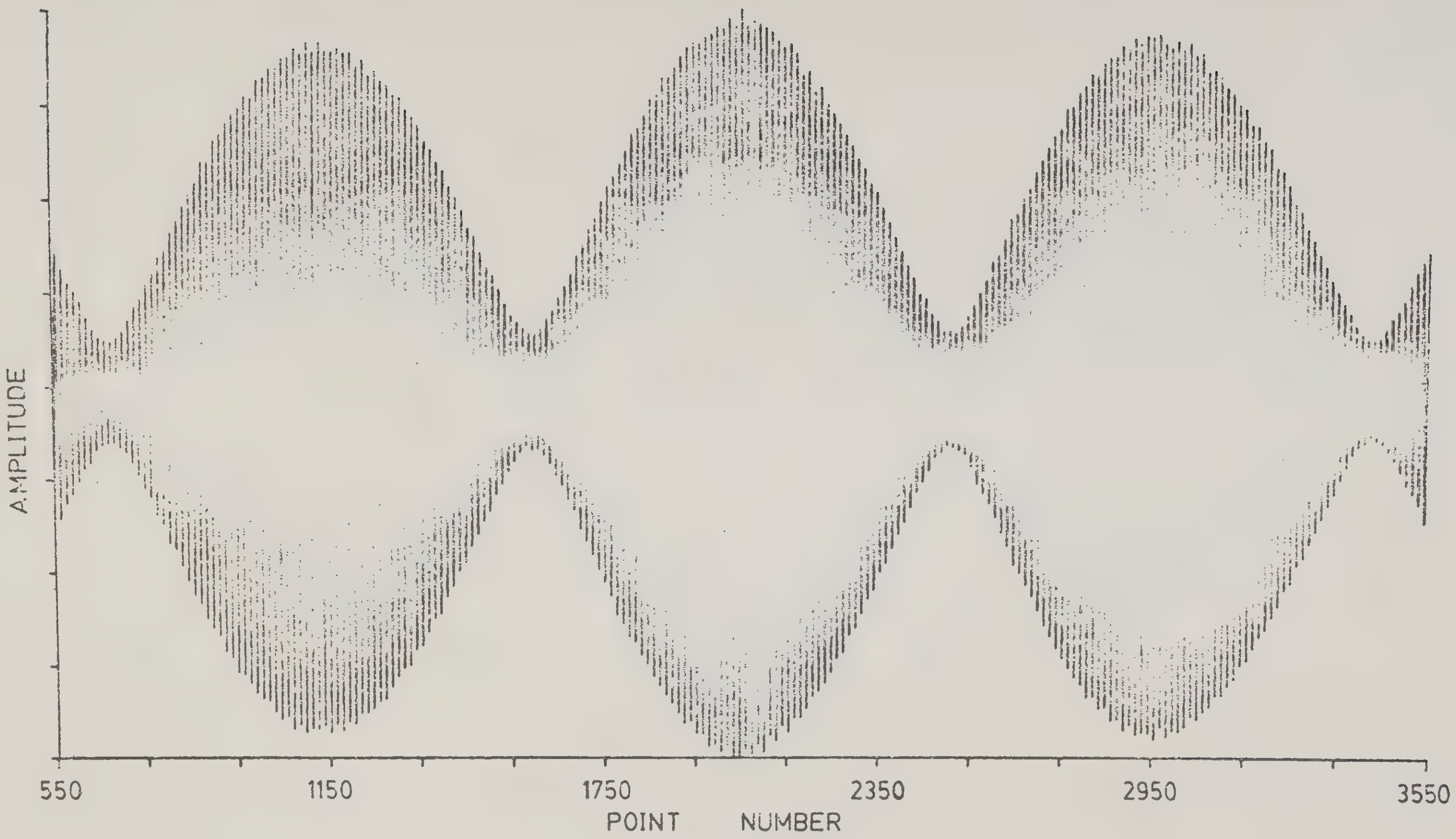

Figure 18. Interferogram of Na 589 nm doublet (3000 of the 4096 points shown).

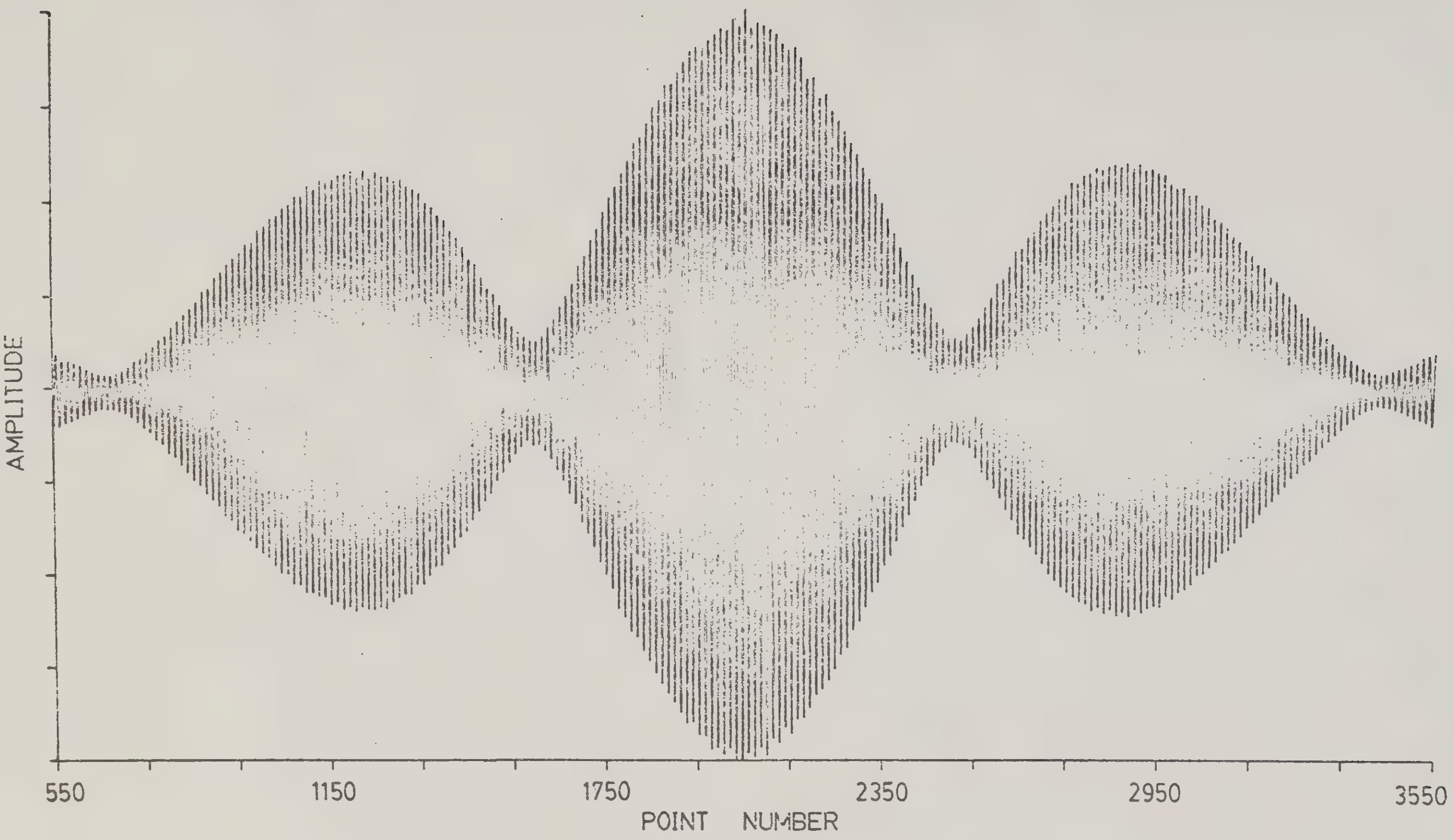

Figure 19. Interferogram of Na589 nm doublet after Gaussian apodization (FAC=2.5).

from the interferogram. The beat pattern is the result of the summation of two cosine waves of slightly differing frequencies. Figure 19 shows the result of multiplying the interferogram shown in Figure 18 with a Gaussian function (FAC=2.5). Again only the middle 3000 points of the 4096 point interferogram are plotted. The Fourier transform is performed on both interferograms and the amplitude spectra are shown in Figures 20(a) and 20(b). Only the part of the spectrum around the Na doublet is plotted to show the instrumental line shape that has been imposed by the apodization. It can be seen that the spectrum from the apodized interferogram is more amenable to interpretation.

The apodization process does not give any more information than is present in the unapodized spectrum; in fact, information can be lost by apodization. This can occur if the apodization results in a lower resolution and causes two lines to become unresolved. Therefore the implementation of apodization must be done with care to give the desired instrumental line shape without removing essential information in the spectrum.

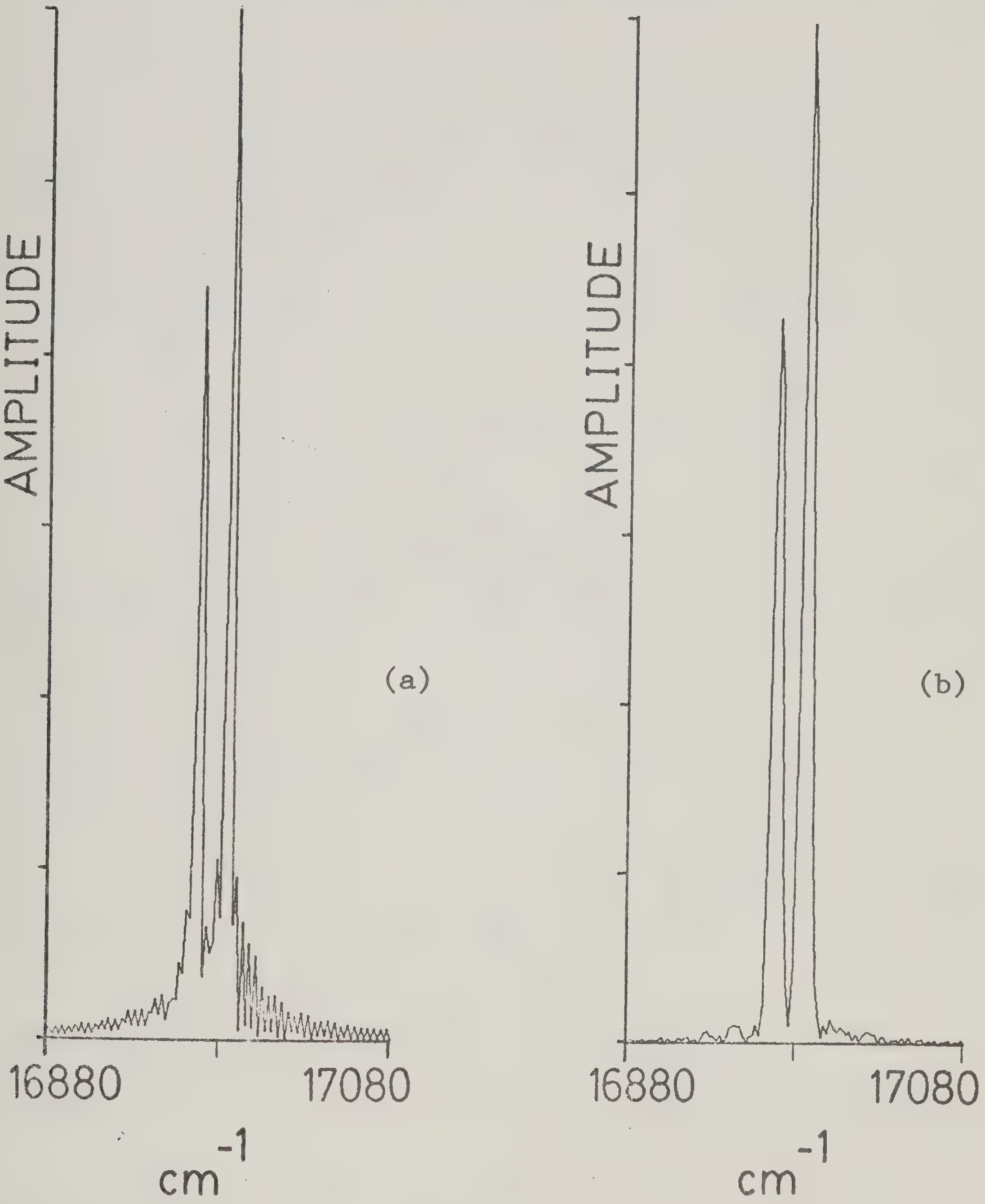

Figure 20. Na 589 nm doublet spectral peak shape: (a) with no apodization, (b) with Gaussian apodization (FAC=2.5).

CHAPTER V

PHASE PROBLEMS IN FOURIER TRANSFORM SPECTROSCOPY

The technique of Fourier transform spectroscopy involves the recording of the interferogram that results from the two beam interference of light via a Michelson interferometer. Ideally, the interferogram is a symmetric function of the optical path difference. That is, the function is the same from 0 to $+x_{max}$ as from 0 to $-x_{max}$. Therefore, only one side need be recorded in this ideal case.

However, several factors contribute to give an asymmetric interferogram. If all the optical and electronic components were perfect, at zero path difference (ZPD) every spectral frequency would be at zero phase. But this is not the case and phase errors are always present. The fact that the light passes through real and not perfect optics may cause different spectral frequencies to have slightly differing phases at the ZPD position. Also the sampled interferogram may not contain a data point exactly at the ZPD position. This results in a constant phase error due to sampling. Detector electronics may have phase response that is dependent on the frequency of the input. This is especially true if electronic filters are used to limit the frequency bandwidth of the signal. Hence, imperfect optics and measurement

electronics produce phase errors that are varying functions of the spectral frequencies.

The detailed mathematical description of phase errors and correction methods have been well documented since it is a problem that is always present with single-sided interferograms and must be corrected to give an accurate output spectrum (15,23,58-61). The discussion given here will be of a qualitative nature and will emphasize the phase problem with respect to line emission type signals in the UV-visible-near IR regions.

A special problem arises when the interferogram is sampled at a rate that results in aliasing. Since the phase error is dependent on the spectral frequency of the signal, each aliased region requires a different phase correction. This makes it next to impossible to phase correct an aliased spectrum. It should be mentioned that problems with phase correction of line emission spectra in the IR (not aliased) have been reported (62,63).

Measurements taken with the first data system using the PDP-8/e minicomputer will illustrate the phase problem. Only single-sided interferograms could be acquired at that time. The flame emission of Li, K, Rb, and Cs was studied. Figure 21 shows the spectrum from a potassium solution (1000 ppm). Spectrum A results from the Fourier transform of the triangularly

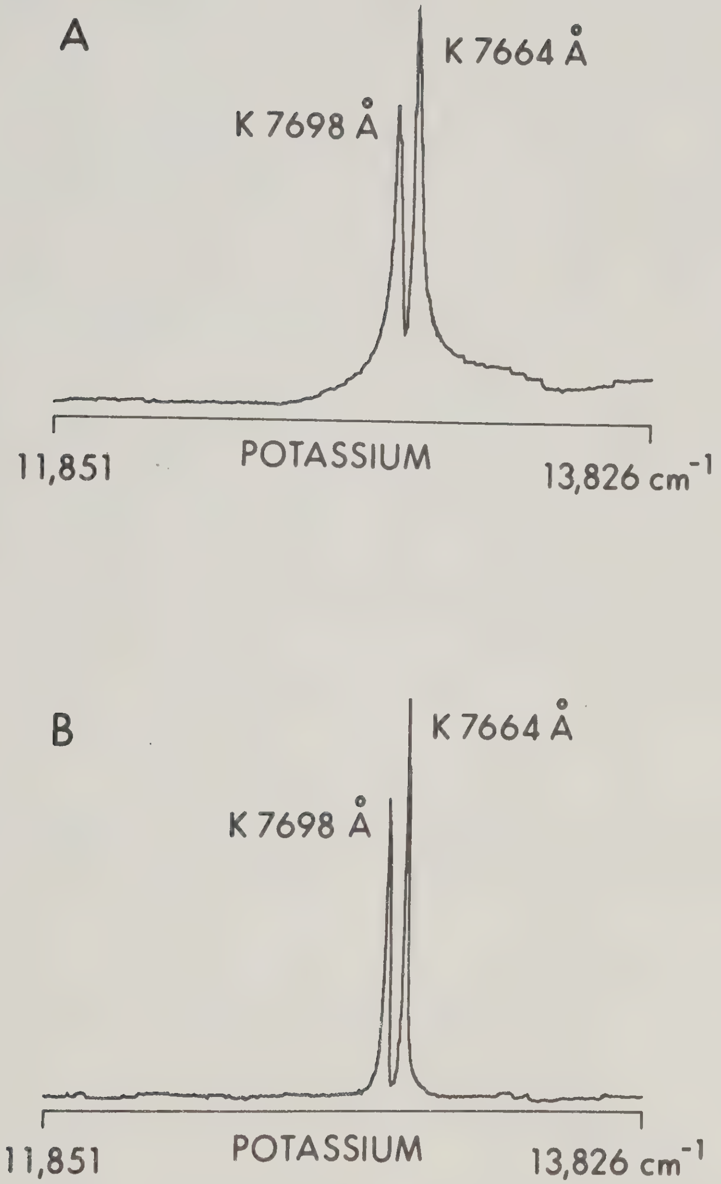

Figure 21. Potassium spectrum from a single-sided interferogram (512 points). A: no phase correction, B: phase corrected.

apodized interferogram. The K doublet is obviously very distorted.

Phase correction procedures utilized in Fourier transform NMR (64) were attempted on these flame emission spectra. The procedure for phase correction involves convolving all the points in the real and imaginary spectra with a cosine and sine wave. The phase angle required to correct a peak is obtained by inspection of the line shape in the real or imaginary spectra. If the spectral peak needs no phase correction, the real and imaginary outputs from the FFT would resemble Figure 22(a). If the real part were distorted, the phase angle is estimated from an inspection of a chart of peaks distorted from 0 through 360 degrees. Figure 22 shows peaks at 0,30,90,120, and 180 degrees of phase error.

The phase corrected K spectrum is shown in spectrum B of Figure 21. Considerable improvement has been made. Similar phase correction procedures were performed for the Li, Rb, and Cs spectra and the results are shown in Figure 23. The analog interferograms of the four elements are shown in Figure 24. The digitized interferograms sampled at 2.5312 um intervals are shown in Figure 25. The aliasing can be seen in the digitized interferograms. If sampling was done at a rate high enough to avoid aliasing, the digital interferogram would have the same appearance as the analog signals.

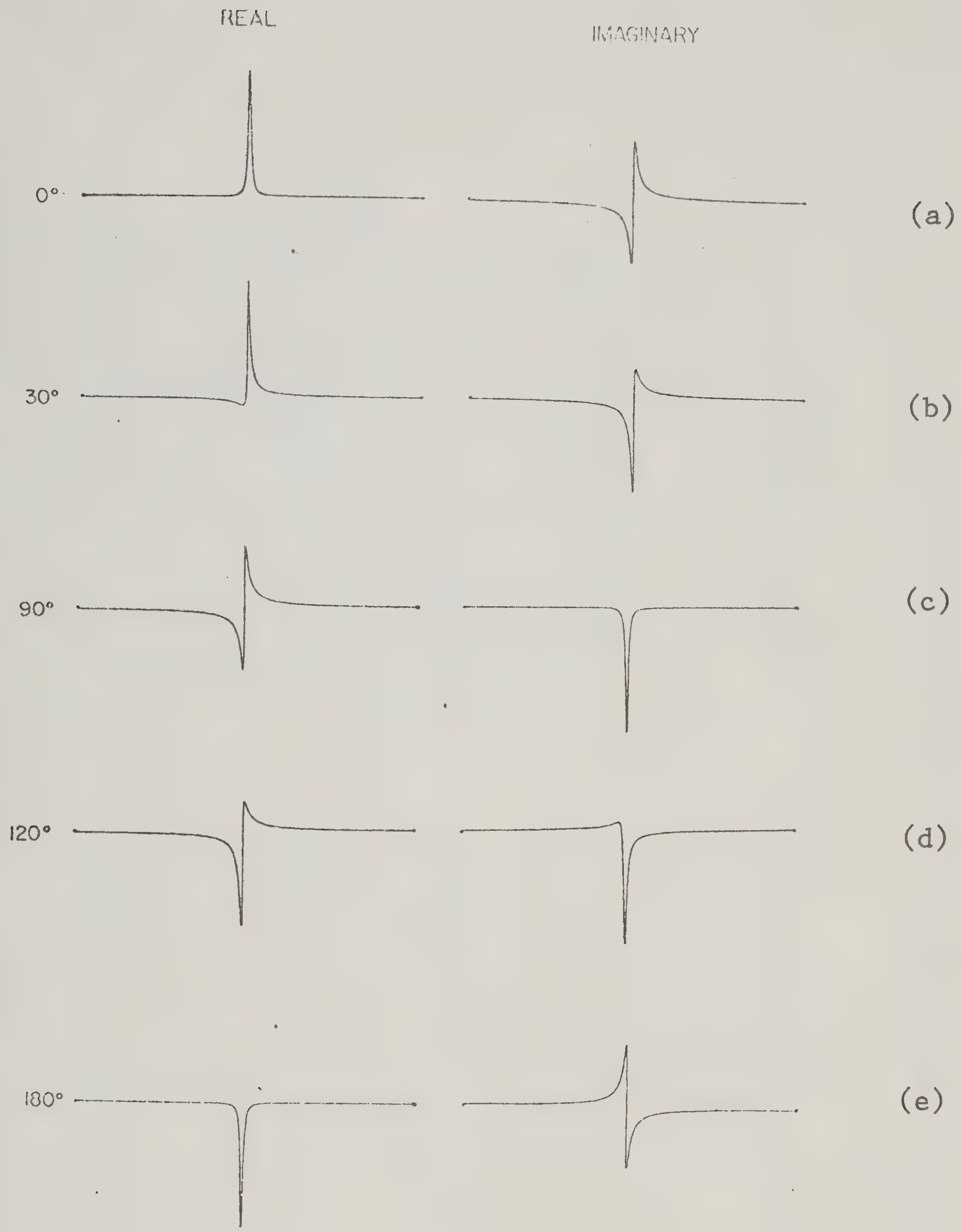

Figure 22. Real and imaginary output peak shapes for phase errors of 0, 30,90,120, and 180°.

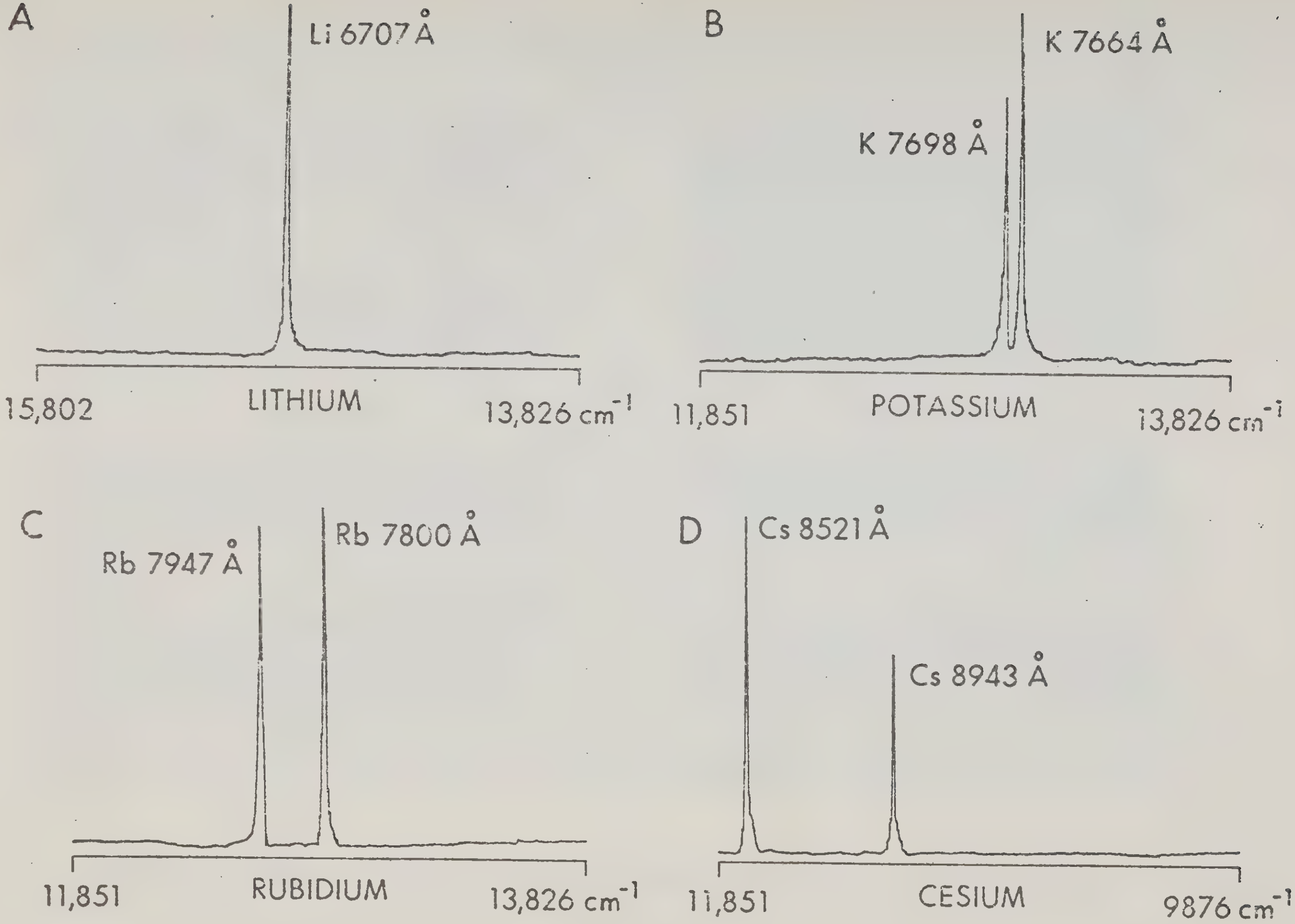

Figure 23. Phase corrected spectra of Li, K, Rb, and Cs.

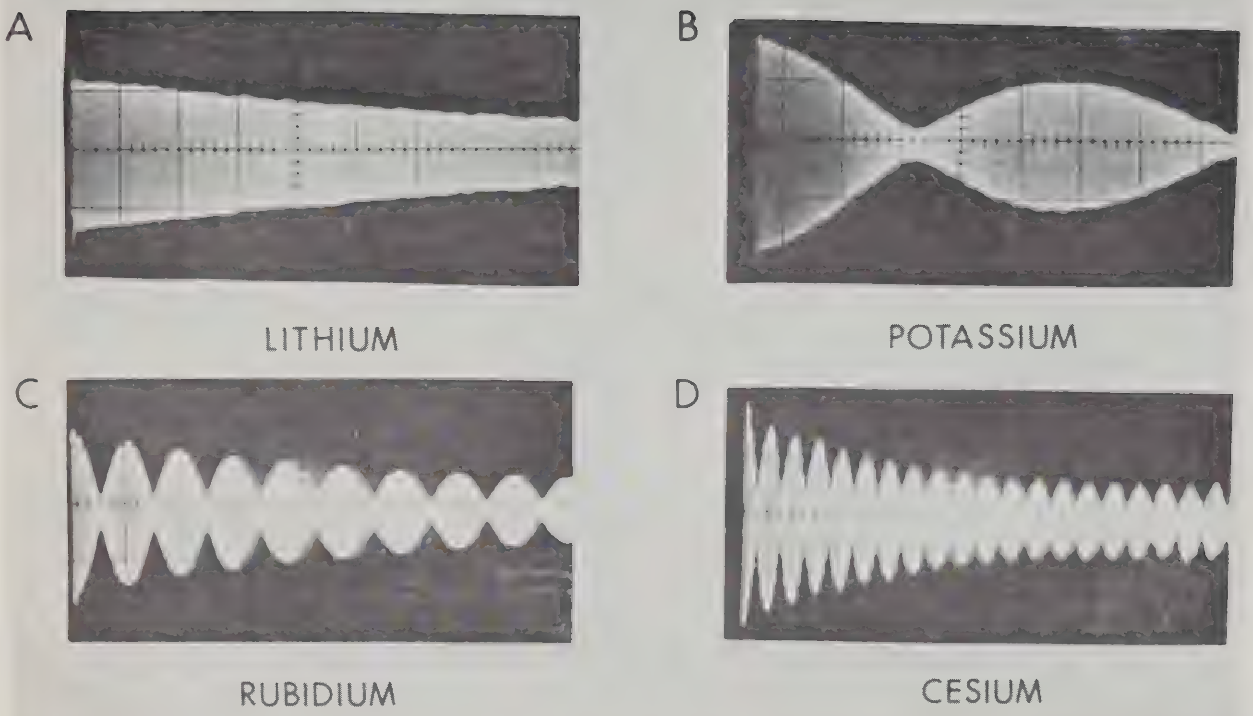

LITHIUM

POTASSIUM

RUBIDIUM

CESIUM

Figure 24. Analog interferograms of Li, K, Rb, and Cs.

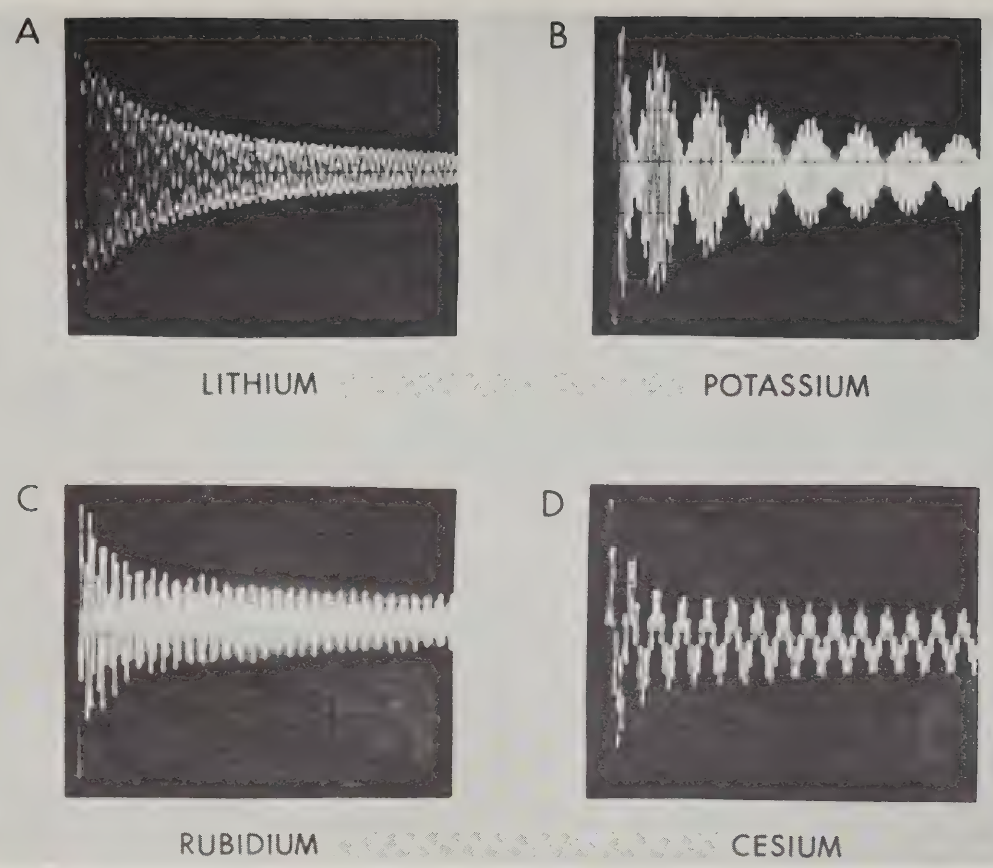

Figure 25. Digitized interferograms of the analog signals shown in Figure 24.

However, when a solution of all four elements was measured (Figure 26), the spectrum was very distorted and similar phase correction procedures could not improve the spectrum to any great extent. This is because the spectral lines are in different aliased regions and each region requires a different phase correction angle. The cumulative effects of the use of different correction angles for each spectral region produces distortions of its own,thus making overall correction of the spectrum impossible.

A method of phase correction that has been fairly successful in Fourier transform infrared measurements does not seem to work as well for line emission spectra. The reason it works for most IR measurements is due to the fact that these spectra are of the absorption type; that is, there is broadband information present. This allows the calculation of a reference phase spectrum which can be used to correct the sample spectrum. A low resolution reference phase spectrum is satisfactory and this can be calculated from a small portion of the interferogram on both sides of the ZPD position. The phase correction procedure is described in reference (23). For line emission type signals, there is little or no broadband information; hence, an accurate reference phase spectrum is difficult to obtain. This makes phase

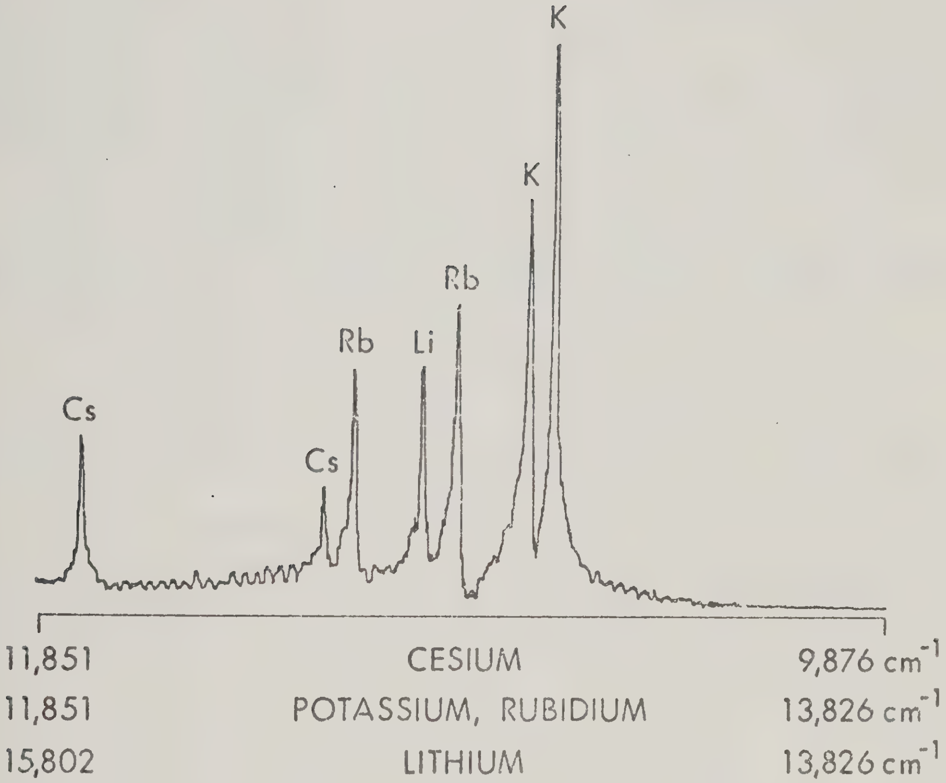

Figure 26. Multielement spectrum of Li, K, Rb, and Cs (not phase corrected).

correction of line emission type signals not very successful.

The problem of phase correction can be totally eliminated if the interferogram is sampled from $-x_{max}$ to $+x_{max}$; that is, a double-sided interferogram is acquired. If the amplitude spectrum is calculated (the amplitude spectrum is the square root of the sum of the real and imaginary parts squared), the results are independent of the phase (Chapter 12 of reference 32).

This is shown in Figure 27. A double-sided interferogram was acquired using a hollow cathode lamp as a source (most of the lines shown are due to the neon gas filler of the lamp). Triangular apodization was applied and the result is spectrum (b). The peaks show no distortion. To produce the single-sided interferogram, the points to the left of the ZPD position were set equal to zero. The apodizing functions are shown above the spectra. Triangular apodization was applied and the result is shown in spectrum (a). Distortions similar to the flame emission data (Figure 26) can be seen.

The flame emission measurements of Li, K, Rb, and Cs were taken using double-sided interferograms and the results are shown in Figure 12(d) in Chapter III. This spectrum and the one in Figure 26 can be compared directly. It should be noted that the improvement in

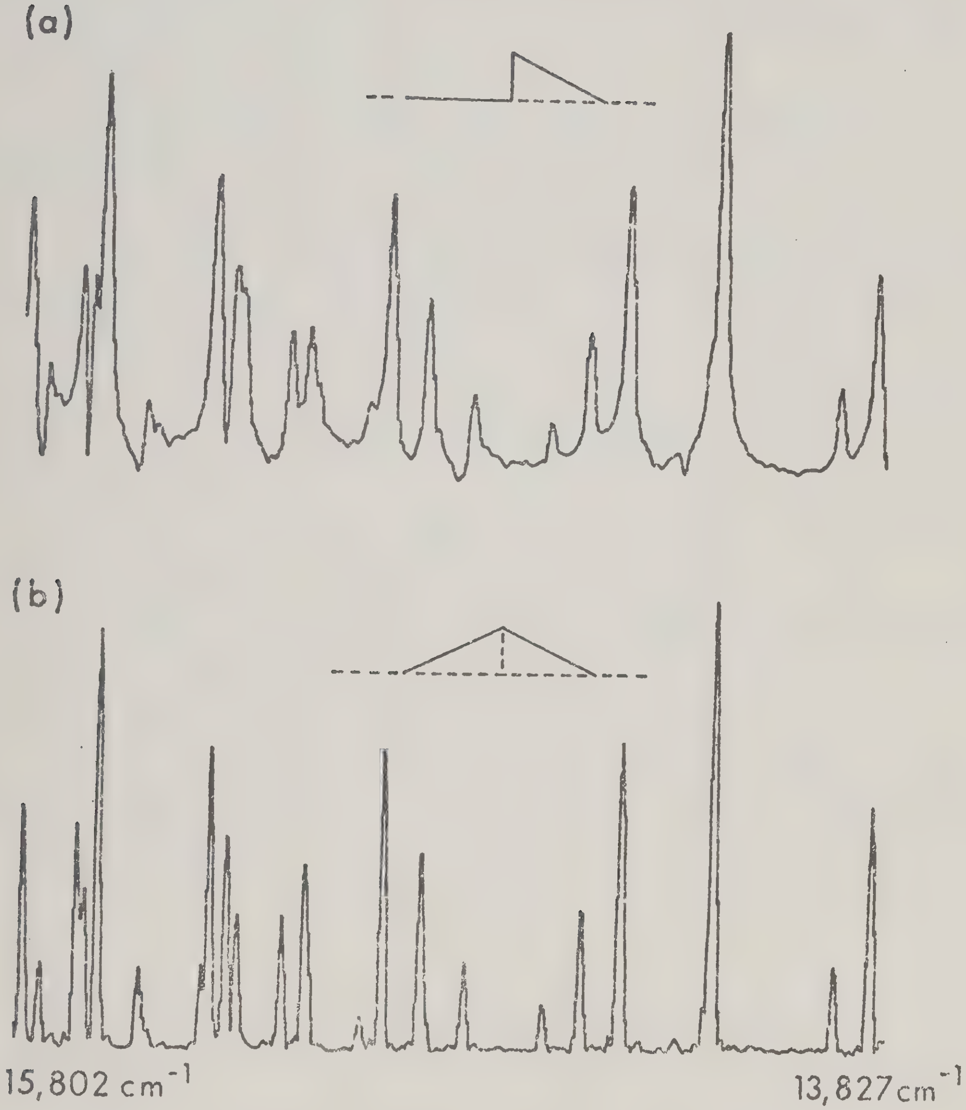

Figure 27. Hollow cathode lamp spectrum resulting from (a) single-sided, (b) double-sided interferogram.

quality of the spectrum in Figure 12(d) occurs in spite of the fact that resolution is lower by a factor of two (same number of data points but a single-sided interferogram samples to twice the optical retardation of a double-sided interferogram).

The question arises as to why double-sided interferograms are not used exclusively. There are several reasons. A major reason is that double-sided interferograms need twice as many data points for the same resolution compared to single-sided interferograms. The resolution depends on the maximum optical retardation, x_{max}. Sampling from $-x_{max}$ to $+x_{max}$ gives the same resolution as from 0 to $+x_{max}$. With twice as many points the computing time for the Fourier transformation is greatly increased. Also the computer memory needed must be doubled if an "in-core" FFT is used. Other factors are that the time required to acquire the double-sided data is doubled, and the moving mirror must be driven twice as far.

The above considerations make the acquisition of double-sided interferograms impractical for extremely high resolution measurements where in the order of hundreds of thousands of points need to be acquired.

However, for line emission type signals and medium resolution, the double-sided interferogram is not impractical. In fact, it is essential if proper spectra

are to be obtained, because of the lack of adequate phase correction procedures for line emission signals.

CHAPTER VI

THE MICHELSON INTERFEROMETER SYSTEM

A. Description of the Michelson Interferometer

The current Michelson interferometer has evolved over several years. The initial interferometer design was developed at the Department of Aerospace Engineering, High Altitude Engineering Laboratory at the University of Michigan by L. W. Chaney in cooperation with Goddard Space Flight Center for balloon borne and space experiments (65,66). A non-repetitive slow scanning mirror drive system was built at the University of Illinois (52). It has been substantially modified and developed into the current interferometer design. This chapter will describe the interferometer in detail.

A block diagram of the interferometer system is shown in Figure 28. There are three optical inputs to the interferometer: a He-Ne laser, a white light source (tungsten bulb), and the spectral signal of interest. Laser fringe referencing is used to sequence digitization. The laser fringes are also used to control and stabilize the velocity of the moving mirror using phase locked loop techniques. The mirror drive system consists of an electromechanically driven piston supported by an air bearing and a mirror mounted on the piston. The mirror

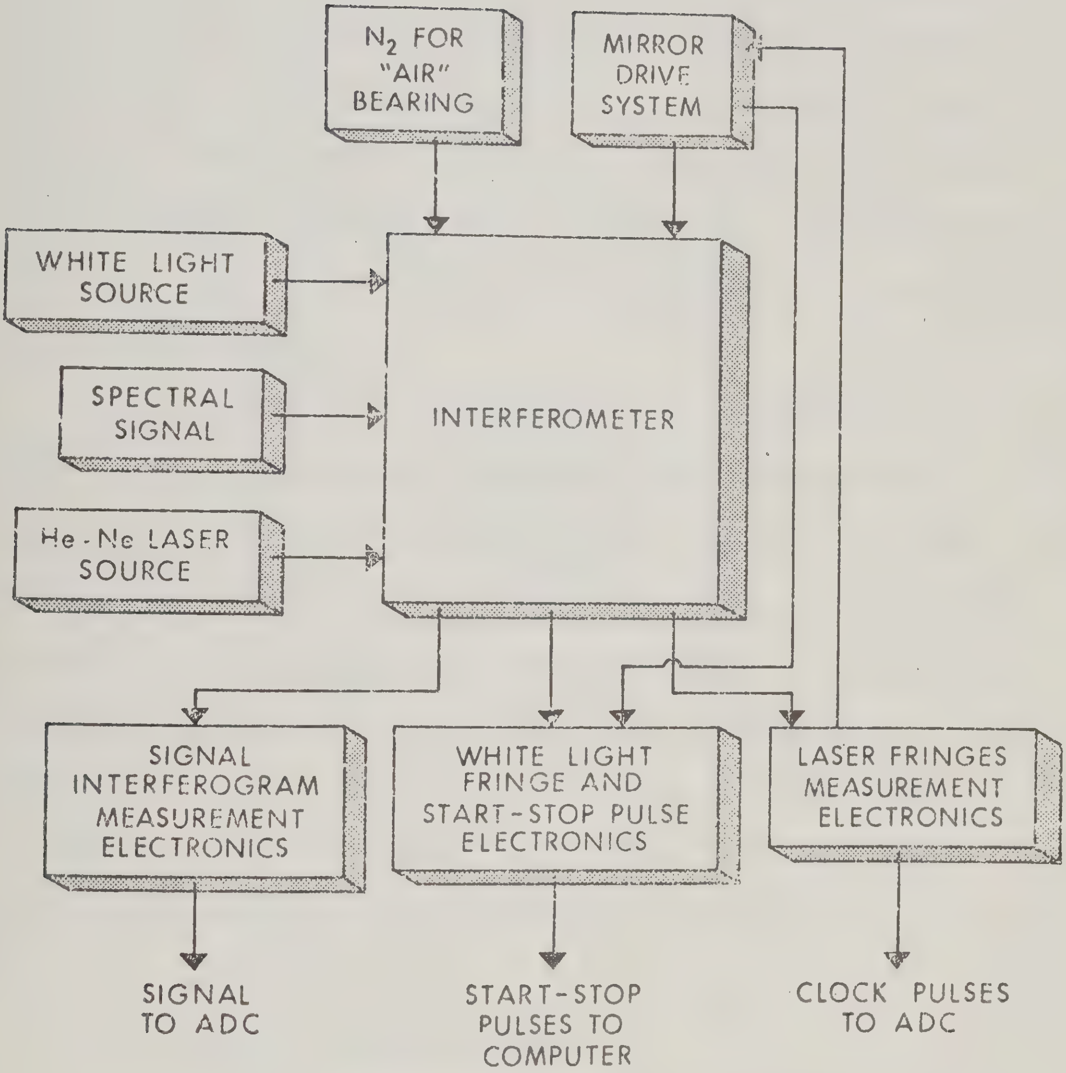
N$_2$ FOR "AIR" BEARING
MIRROR DRIVE SYSTEM
WHITE LIGHT SOURCE
SPECTRAL SIGNAL
He-Ne LASER SOURCE
INTERFEROMETER
SIGNAL INTERFEROGRAM MEASUREMENT ELECTRONICS
WHITE LIGHT FRINGE AND START-STOP PULSE ELECTRONICS
LASER FRINGES MEASUREMENT ELECTRONICS
SIGNAL TO ADC
START-STOP PULSES TO COMPUTER
CLOCK PULSES TO ADC

Figure 28. Block diagram of the Michelson interferometer system.

movement is repetitive and both the scan rate and length can be easily set or altered. With the control signals derived from the white light interferogram and the laser fringes, spectral signal interferograms can be precisely time averaged. A unique "pretrigger" approach allows acquisition of any desired number of data points before and after the zero path difference position. All three optical inputs share the same beamsplitter and Michelson mirrors. This feature greatly facilitates alignment of the interferometer.

The concept of the design is to be flexible in order to ease alignment, assembly, and modifications. Therefore the interferometer consists of modules, each of which can be changed easily. For example, the source, beamsplitter, and detector can be changed and the interferometer realigned in a few minutes. A schematic diagram of the interferometer is shown in Figure 29. It will be useful to refer to Figures 28-30 and the photographs shown in Figures 31 and 32 during the following discussion.

1) Central Mounting Cube

The mounting cube is the central unit of the interferometer. All the other modules mount onto the cube. The cube is approximately 10.8 cm (4.25 inches) and was machined out of a solid piece of aluminum. The entrance port visible in Figure 31(a) is 6.05 cm (2.38 in.)

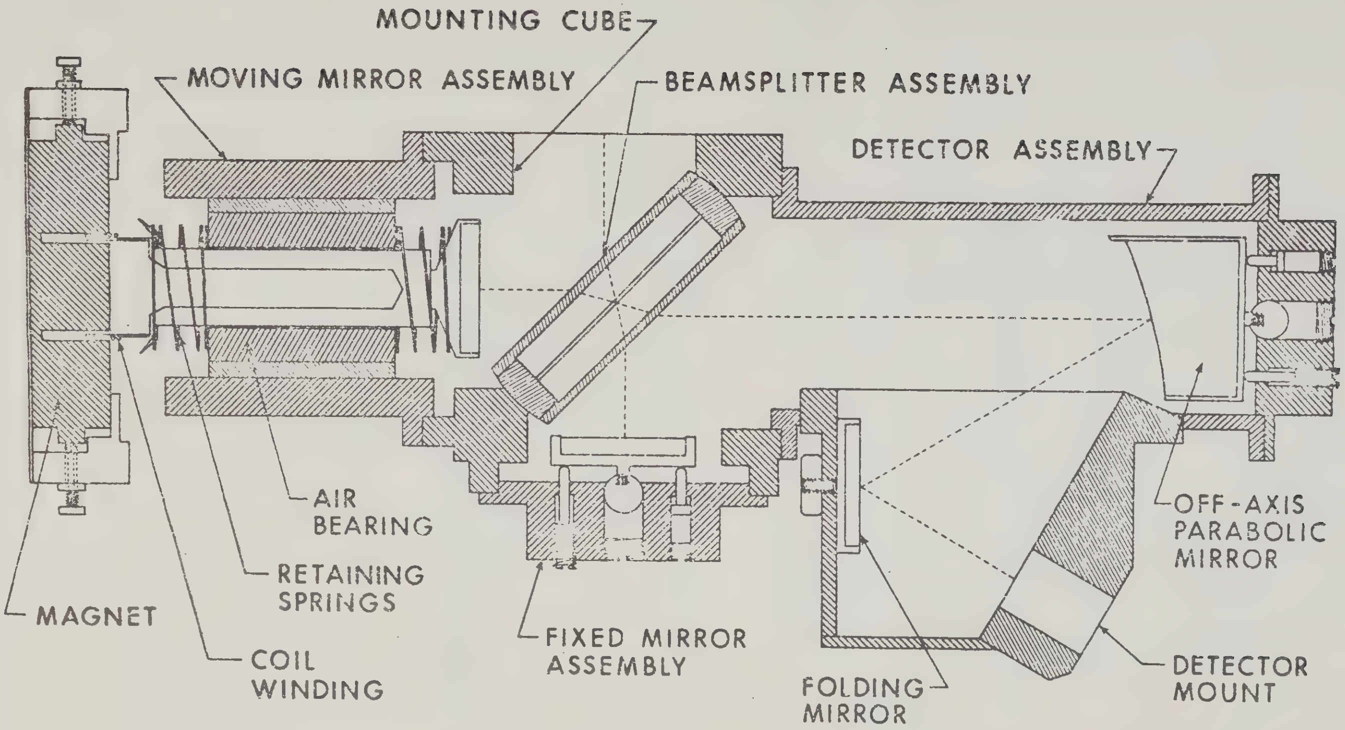

Figure 29. Schematic diagram of the Michelson interferometer.

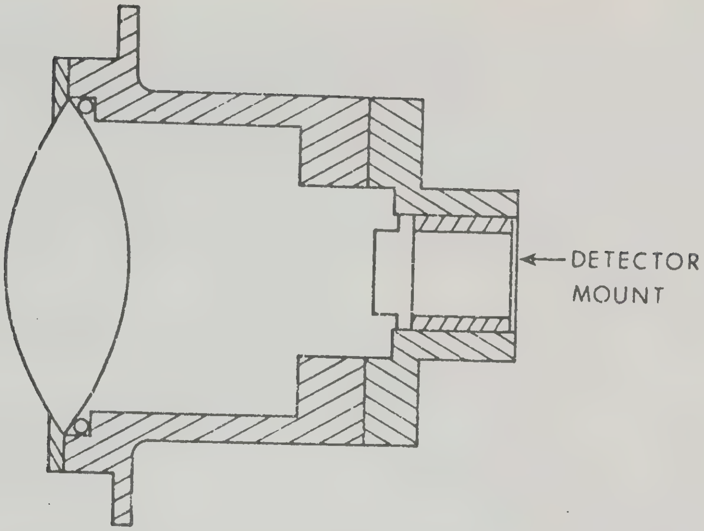

(a) DETECTOR ASSEMBLY

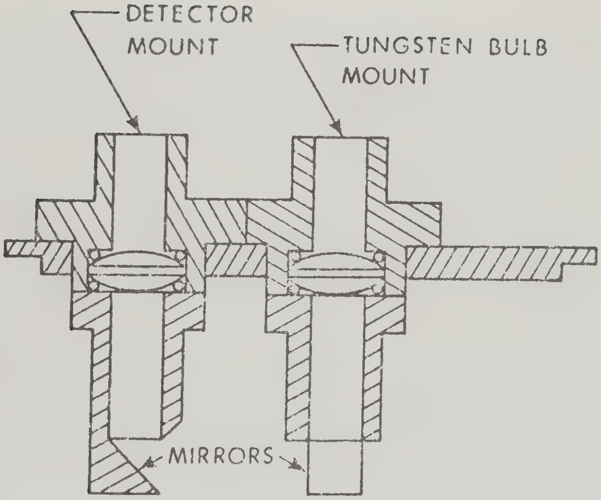

(b) WHITE LIGHT
REFERENCE ASSEMBLY

Figure 30. (a) Lens detector assembly.
(b) White light reference assembly schematic.

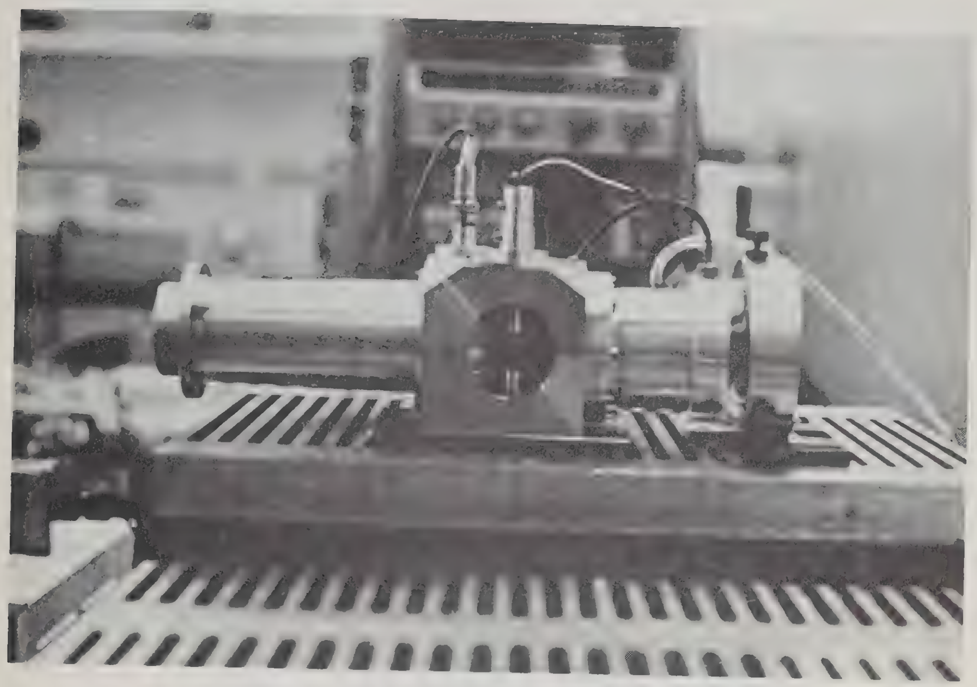

(a)

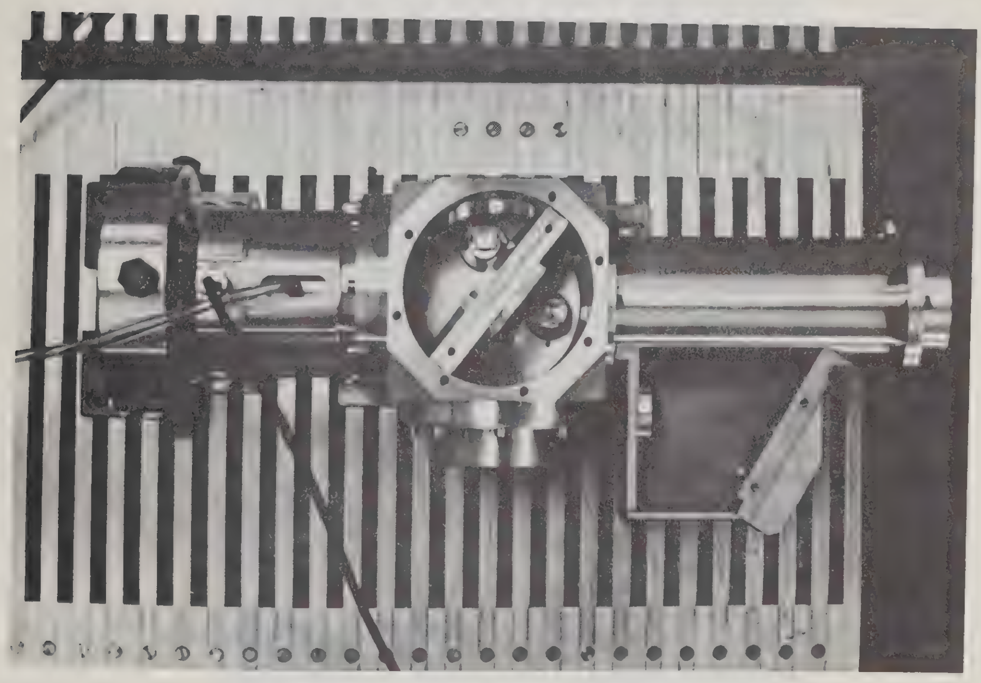

(b)

Figure 31. Photographs of the interferometer: (a) front view, (b) top view.

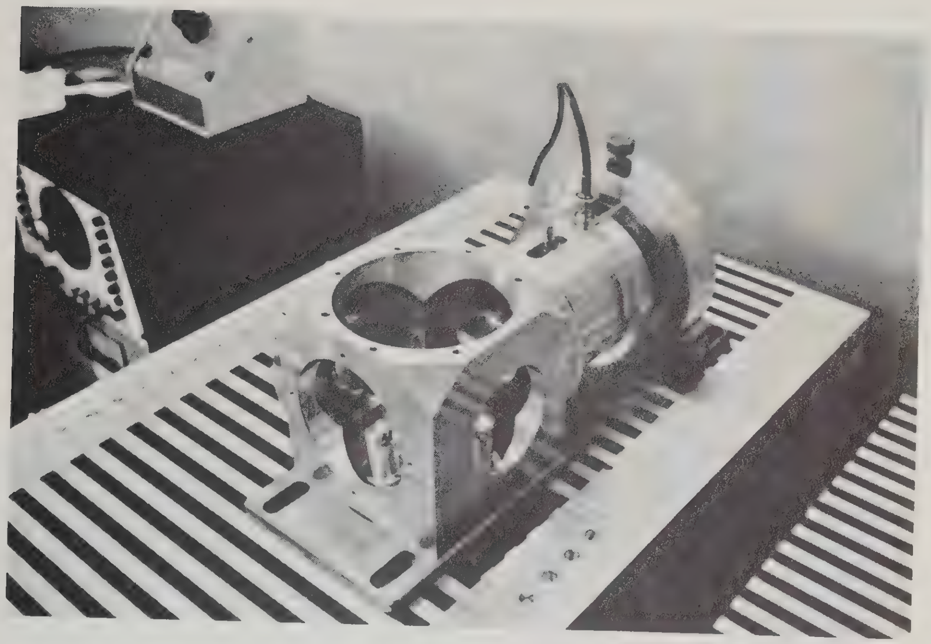

(a)

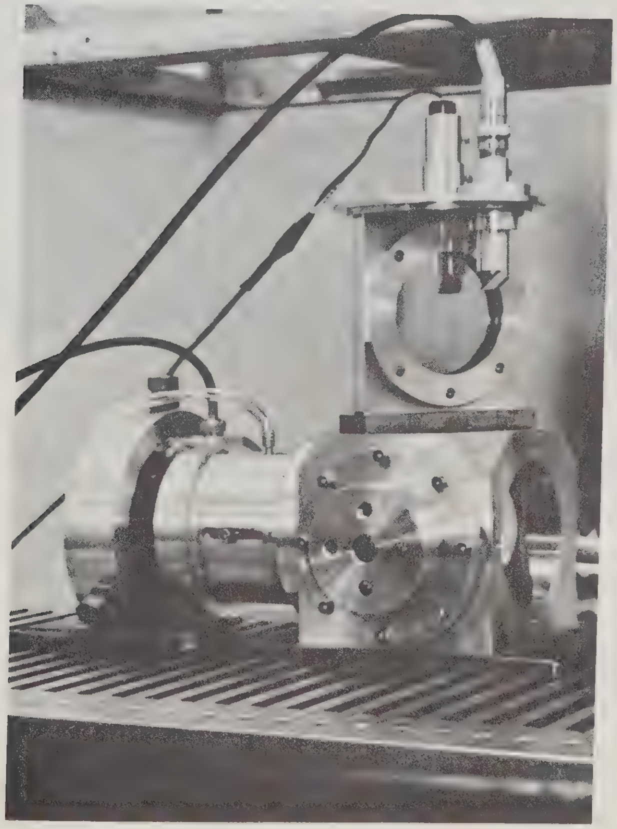

(b)

Figure 32. Photographs of the interferometer:
(a) mounting cube partially disassembled,
(b) beamsplitter and white light assembly.

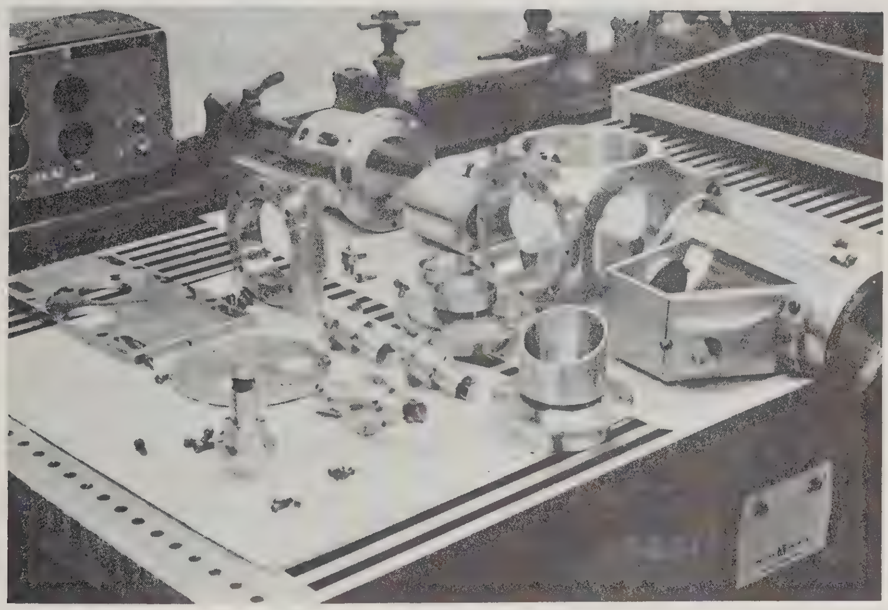

(c)

Figure 32 (c). The interferometer totally disassembled.

in diameter. In order to allow the He-Ne laser input module to be mounted from the bottom, the cube is mounted on a brass plate over a hole in the optical table.

2) Beamsplitter Assembly

The beamsplitter assembly is best seen in Figure 32(b) where it is raised out of the central cube. It is mounted under the top face plate of the interferometer. The assembly consists of two optical flats (a beamsplitter substrate upon which the beamsplitter coating is deposited and a compensator) mounted on two aluminum holders separated by an aluminum spacer. The beamsplitter substrate and compensator are each 7.62 cm (3.00 in.) in diameter and 0.953 cm (0.375 in.) thick and their dimensions should be matched as closely as possible. For work in the UV, visible and near-IR, fused silica flats were used (from L. H. Sampson Co., 22730 Orchard Lake Road, Farmington, Michigan 48024) with flatness to $\lambda/10$ in the visible. For work in the mid-IR, NaCl flats were used. The salt flats are flat to better than 1λ in the visible (obtained from Frank Cooke Inc., 59 Summer Street, North Brookfield, Mass. 01535).

Germanium was used as the beamsplitter material and was coated on the substrates by a local optical shop at the University of Alberta. The germanium was coated on until the transmittance was approximately 50% in the spectral region of interest. Figure 33 shows the

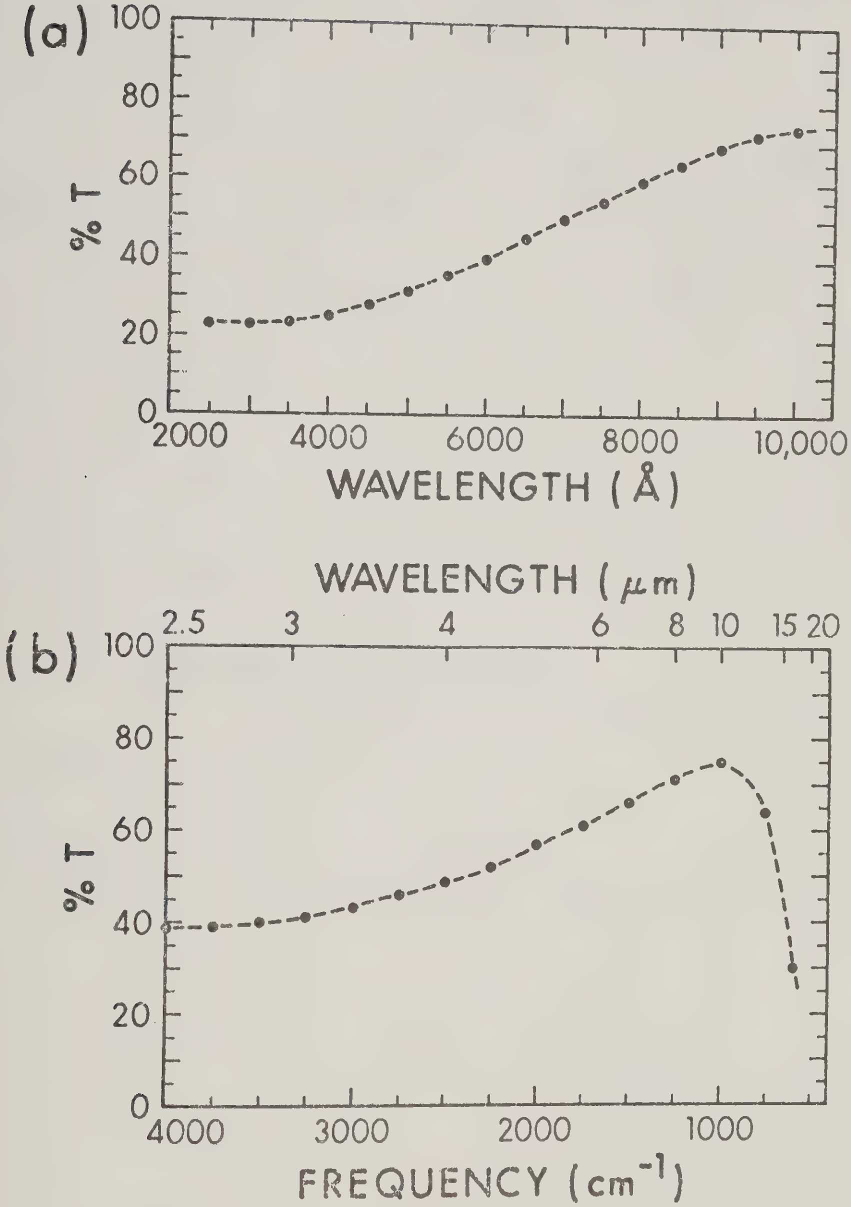

Figure 33. Transmission spectra of the beamsplitters:
(a) quartz substrate for UV, visible,
(b) NaCl substrate for mid-IR.

transmission spectra (light incident at 90°, air reference) of the fused silica substrate and the NaCl substrate beamsplitter assemblies.

3) Fixed Mirror Assembly

The fixed mirror assembly consists of a spring loaded ball-in-socket mount with two sets of opposing spring loaded plungers and screw-driven adjustments. This design has proven to be very stable. The fixed and moving mirrors are both 4.2 cm (1.64 in.) in diameter, 0.64 cm (0.25 in.) thick, flat to $\lambda/10$ in the visible and coated with aluminum. (The mirrors were obtained from L. H. Sampson Co.).

4) Moving Mirror Assembly

The moving mirror assembly is based on an air bearing suspension system driven by a standard loudspeaker magnet and coil assembly. (The air bearing, Model L.B.-10, was obtained from Bearing Specialty Co., 90 Windom Street, Boston, Mass. 02134). The moving mirror is mounted on a piston inserted inside the air bearing. The loudspeaker coil is mounted at the other end of the piston and rides into the magnet assembly. Weak retaining springs keep the piston assembly roughly centered in the air bearing. Tank nitrogen (20-25 psi) is used to float the moving mirror piston. The complete air bearing assembly can be shifted back and forth in the moving mirror assembly for coarse positioning of the

moving mirror static position. The magnet holder is the only unit of the modules not physically attached to the interferometer cube. It is mounted on the optical table. A plexiglass dust cover encloses the gap between the magnet holder and the moving mirror assembly. With the present design the maximum mirror movement is about 1 cm.

5) White Light Reference System

The white light reference system consists of two assemblies mounted on the top face plate of the interferometer. One assembly contains a tiny tungsten bulb and collimating lens (see Figure 30(b)). The collimated white light source is reflected into the interferometer by a small diagonal mirror, such that only a small part of the top of the Michelson mirror is used for this signal. At the output end, the white light signal is reflected back up to a silicon photodiode detector by another small diagonal mirror and focusing lens. The arrangement of this important periscope system is more clearly shown in Figure 32(b) where the top face plate, with attached beamsplitter has been pulled out of the central mounting cube. This photograph also emphasizes the modular nature of the interferometer and the fact that the beamsplitter can be exchanged easily.

6) He-Ne Laser Reference System

The He-Ne laser reference system is very similar to the white light reference system and is mounted

on the bottom face plate of the interferometer. The two periscopes project through the hole in the optical table over which the central cube is mounted. The beam from the He-Ne laser (Spectra Physics Model 133), mounted under the top surface of the optical table, is reflected up into the periscope and through the interferometer by two small right angle prisms. The laser path through the interferometer uses only a small part of the bottom of the Michelson mirrors. Since the laser beam is inherently collimated, no lenses are needed in either periscope of the laser system. At the output periscope the laser signal is reflected down a custom made interference filter to a Si photodiode detector. (The filter bandpass is centered at 632.8 nm and was supplied by Infrared Industries, Inc., Thin Film Products, 84 Fourth Ave., Waltham, Mass, 02154). The filter is mounted in the same manner as the lenses for the white light assembly. The laser periscopes can be seen in Figures 31(b)and 32(a).

7) Detector Assembly

Two detector assemblies have been used with the interferometer. One is based on a lens to focus the light to the detector (Figure 30(a). Both glass and salt lenses have been used. The salt lens was ground in our own laboratory from a NaCl cylinder. Both lenses have a diameter and focal length of 5.97 cm (2.35 in.).

However, at the short wavelengths of the UV-visible

region, a short focal length single lens is prone to aberrations that could affect the quality of the output signal. Therefore, the second detector assembly consists of an off-axis parabolic mirror (Figure 29, 31(b)), folding mirror and detector mount. The off-axis parabolic mirror is mounted on a sub-assembly identical to the fixed mirror assembly. The focal length of the off-axis parabolic mirror is 16.8 cm (6.6 in.) with the focal point 6.1 cm (2.4 in.) from the inner edge. (The parabolic mirror was obtained from Optronics International Sales Corp., 7 Stuart Rd., Chelmsford, Mass. 01824).

Several detectors have been used: TGS (triglycine sulphate) pyroelectric for mid-IR measurements (series T-300 unit from Barnes Engineering Co., 30 Commerce Rd., Stamford, Conn. 06902), Si photocell for near-IR and visible, 1P28 (RCA) photomultiplier tube (PMT) for visible, and R166 solar blind (Hamamatsu) PMT for ultraviolet measurements.

It should be pointed out that the focal length of the off-axis parabolic mirror represents a compromise. The radius of the first fringe $\underline{y}$ in the focal plane of the output of a Michelson interferometer is equal to $f(\lambda/d)^{1/2}$ where $\underline{f}$ is the focal length of the output mirror, $\underline{\lambda}$ the wavelength and $\underline{d}$ the optical retardation. To get maximum sensitivity, it is desirable for the detector to see the entire central (zero) fringe. A smaller detector

aperture will give a lower signal level. But an aperture larger than the central fringe will degrade the signal because the detector will be observing more than one fringe simultaneously.

Thus, for optimal IR performance in the 2-15um region, the focal length of 16.8 cm is too long as it results in a fringe size (y=1.47 cm for 10um wavelength and d=0.13 cm) that overfills our TGS detector (element 1 mm x 1 mm) by a considerable amount, particularly at the longer wavelengths. This results in lower sensitivity. However, for visible and especially UV performance, the longer focal length is desirable. Typical IR detectors have small sensor areas and thus act as their own apertures. With a PMT, a circular aperture must be mounted in the exit focal plane in front of the PMT. A short focal length, combined with working at wavelengths over an order of magnitude shorter, would result in a very small fringe radius making fabrication of an appropriately small aperture difficult and also making focusing much more critical. For example, with f=5.08 cm (2.0 in.), 250 nm wavelength and d=0.13 cm, y=0.07 cm. Also, the problem becomes increasingly severe as one goes to higher resolution measurements; that is, as _d_ increases, _y_ decreases further. Since our initial experimental goals were to investigate the applicability of our Fourier transform spectrometer to UV and visible

measurements, we chose a longer focal length (16.8 cm) than would be optimal for a purely IR instrument in order to use larger exit apertures with the PMT detectors. Because of the modular nature of the interferometer, it would be easy to design a separate detector assembly optimized for IR performance.

8) Input Optics

The spectral input to the interferometer is collimated by an off-axis parabolic mirror (identical to the one in the detector assembly). The source is placed at the focal point of the mirror. Sources that have been used are hollow cathode lamps and a modified Varian burner (see Chapter VIIA for details) for UV-visible-near IR measurements and a globar for mid-IR measurements. A filter holder for 2 in. x 2 in. filters can be placed at the interferometer entrance port if it is necessary to block unwanted portions of the spectral region.

B. Consequence of Using Only One Interferometer

The design of our interferometer uses the same Michelson mirrors and beamsplitter for all three optical signals. The white light channel uses the top section of the Michelson mirrors, the He-Ne laser channel the bottom section and the spectral signal the center of the mirrors. This is a major difference compared to most commercially available systems which use two or even three independent interferometers for these signals. We have found the single interferometer design to be both simple and effective. In particular, alignment and the maintenance of alignment are greatly facilitated since only one mirror needs to be adjusted.

If the interferometer is grossly misaligned, as it would be if the beamsplitter were changed, the procedure for alignment is as follows. The detector assembly is easily removed and, using the laser signal, coarse adjustment is made visually by lining up the laser beams from the two arms of the interferometer. Then, with the moving mirror scanning, the fixed mirror is fine tuned to locate and maximize the laser fringes signal. The alignment at this point is nearly optimal. The white light interferogram signal is then maximized. With these two signals aligned, the spectral signal channel is automatically aligned as only one mirror is involved.

In contrast, systems with multiple interferometers can be very time consuming to adjust; particularly the spectral signal and white light channels.

Since the thickness of Ge required for an effective mid-IR beamsplitter is such as to be essentially opaque in the visible, this design does require that small windows of higher transparency be left on the top and bottom of the salt beamsplitter to allow the white light and laser signals to pass. This is easily achieved via a two step coating procedure using a mask on the second coating. In addition, even though salt flats can only be obtained with a one wavelength flatness specification, the white light and laser fringes are of excellent quality with our mid-IR salt beamsplitter assembly. For the near-IR and visible beamsplitter, one coating is sufficient; windows of different %T being unnecessary for the white light and laser.

Another major consequence of the single interferometer design is the coincidence in time (and mirror position) of the white light and spectral signal interferograms. The occurence of the white light interferogram peak is normally used as a precise start flag when time averaging repetitive interferograms. This means that only single-sided interferograms can be acquired with no points acquired before the central fringe of the spectral signal interferogram. Single-sided interferograms

make it difficult, if not impossible, to phase correct the spectra properly as shown in the chapter dealing with phase. In fact, this is the major reason why, in most designs, a separate interferometer is used for the white light channel. Thus, one of the Michelson mirrors of the white light channel can be offset so that the white light central fringe occurs several hundred laser fringes before the spectral signal central fringe. That is, the zero path difference(ZPD) point for the white light channel occurs before the ZPD point for the spectral signal.

To overcome the single-sided interferogram problem, a versatile hardware and software system was developed to precisely acquire and time average any desired number of data points both before and after the signal central fringe. The procedure involves generating a start flag (some imprecise point before the ZPD position) to initiate taking data. Then a stop flag (precise because it is generated by a preset number of laser fringes after the white light central fringe) is used to halt the data acquisition. The time averaging is then performed from the last data point backwards. This "pretrigger" approach and how it is accomplished is explained in detail in the next section.

C. Interferometer Electronics

The interferometer control electronics is shown in Figure 34 and the timing sequence of the various electronic signals is illustrated schematically in Figure 35. The two key control signals generated by the interferometer are shown in Figure 36(a). The white light fringes signal measured at the output of OA1 is shown in Figure 36(a) (upper trace). The laser fringes signal, simultaneously measured at the output of OA2, is shown in Figure 36(a) (lower trace). These signals will be referred to as the white light analog and laser analog signals. The white light signal, in combination with the laser signal, is used to generate a precise stop flag in order to sequence averaging of many scans. The laser signal is used to stabilize the velocity of the moving mirror and to initiate digitization accurately.

1) Moving Mirror Drive

The basic mirror drive signal is a triangular waveform obtained from a function generator (Heath Model EU-81A). This signal is amplified by a power amplifier (Hewlett-Packard Harrison 6824A Power Supply Amplifier) to provide the current to drive the loudspeaker coil. The drive rate and length are set with these two units. Most of our measurements have been carried out with a drive frequency of about 0.2 Hz

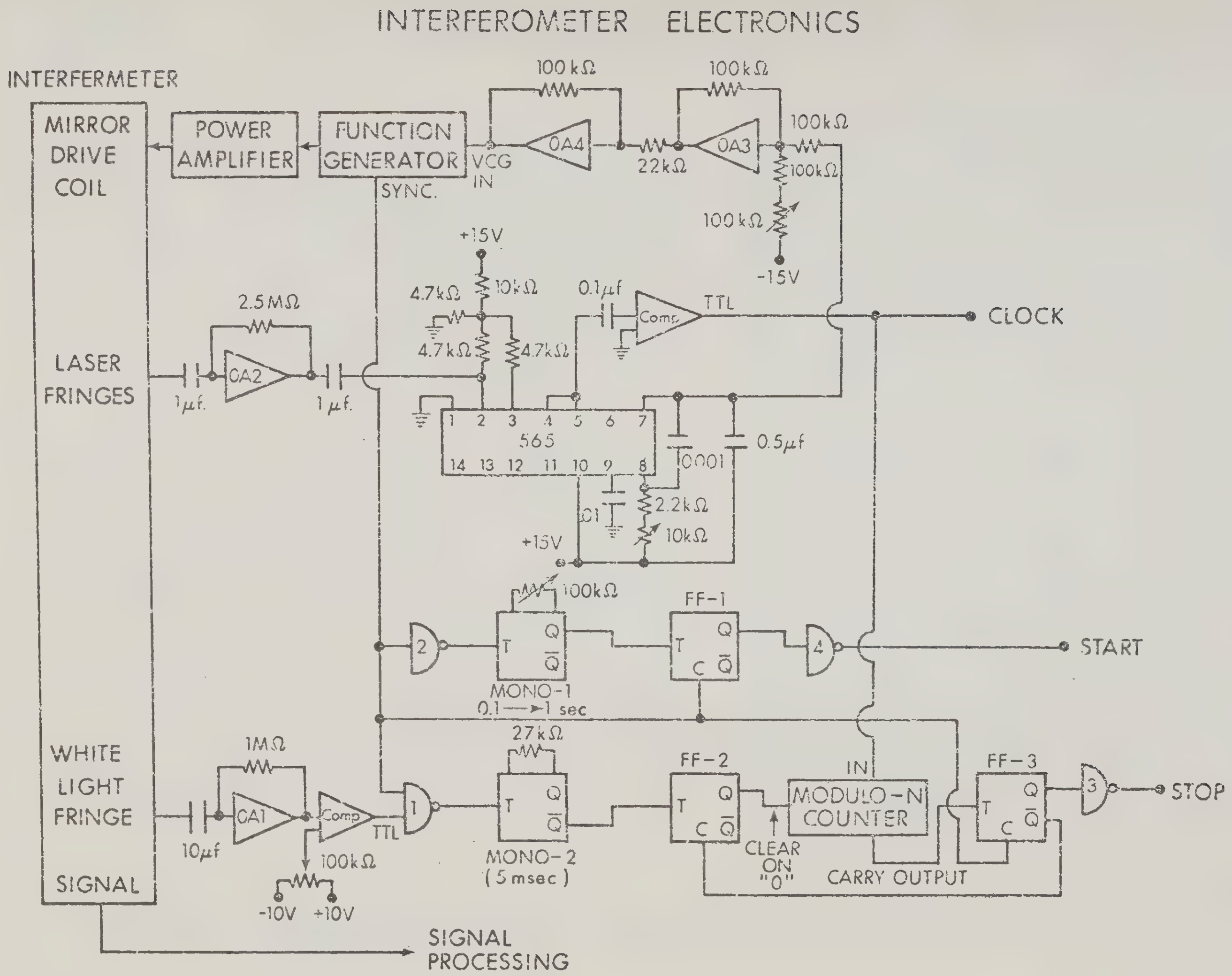

Figure 34. Interferometer electronics with the PDP-11/10 computer.

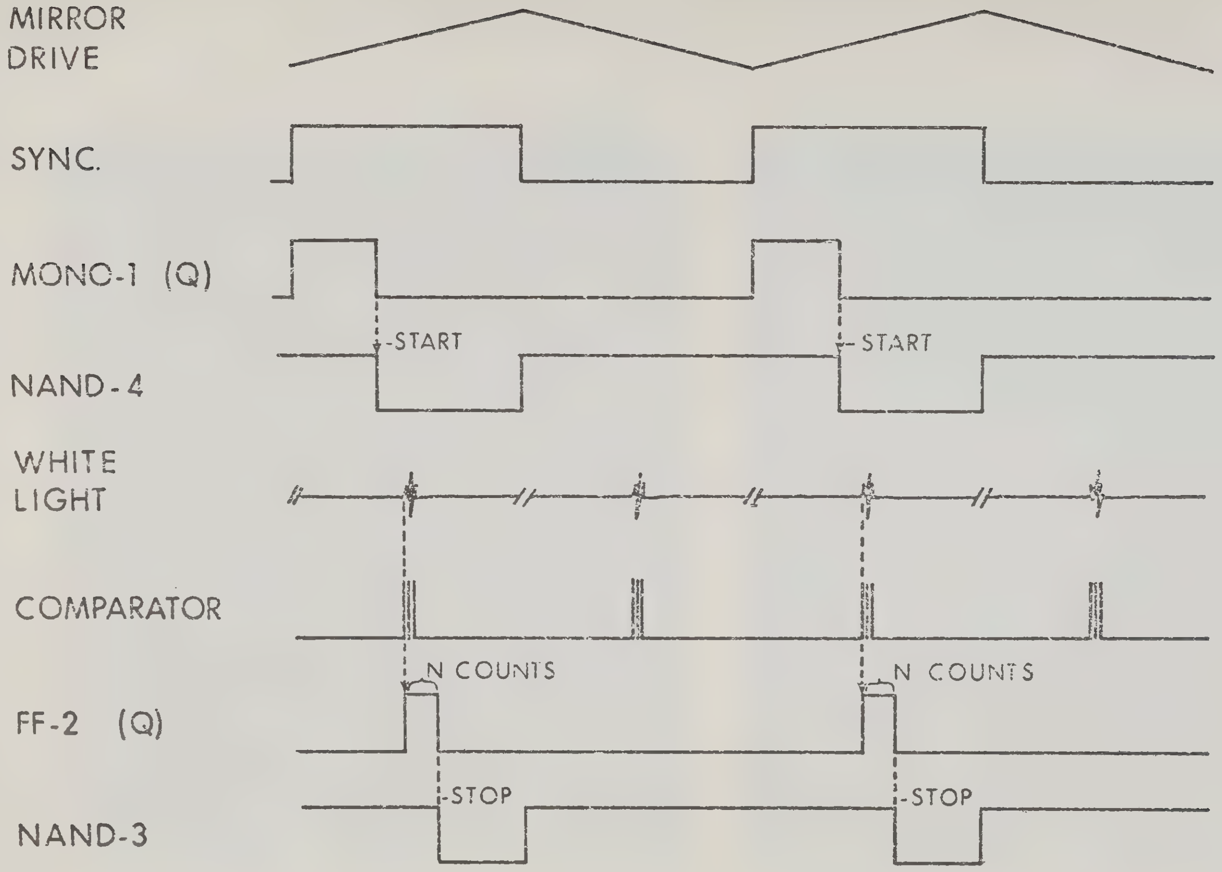

Figure 35. Schematic diagram of the control signals' timing sequence.

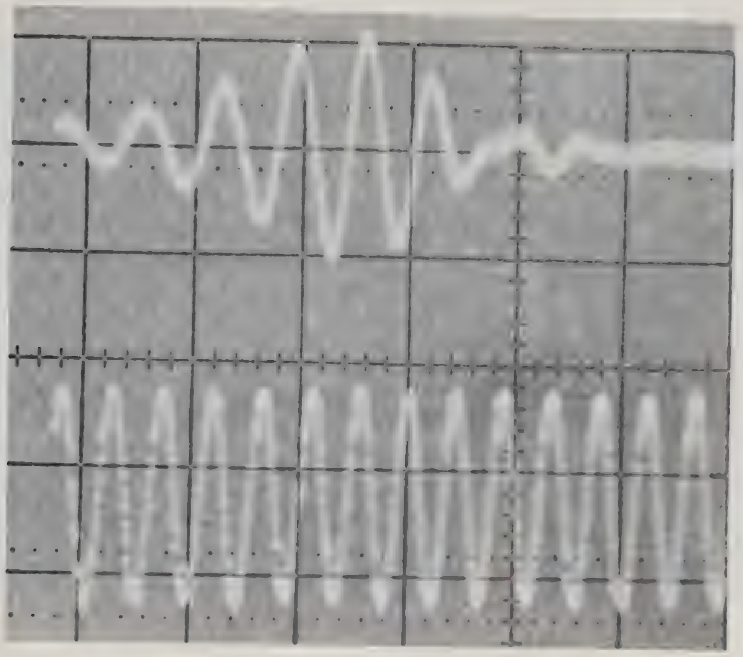

(a)

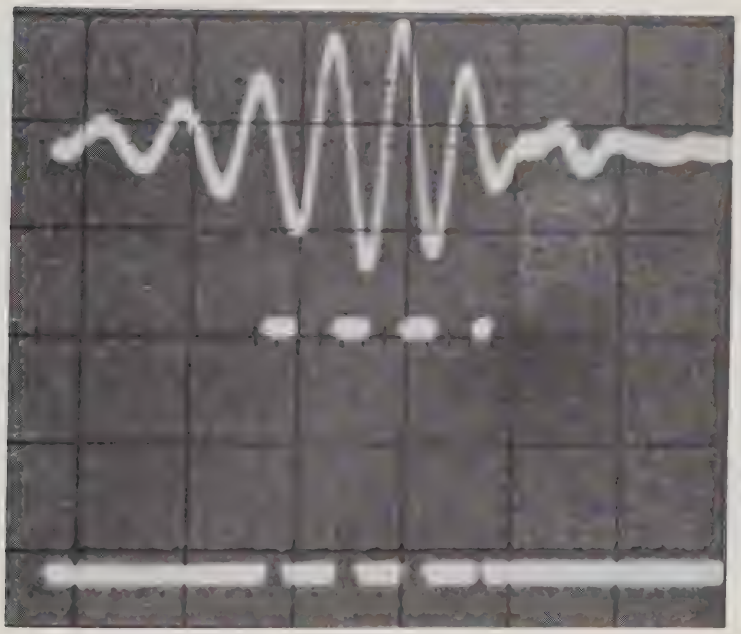

(b)

Figure 36. (a) White light analog (upper trace) and laser analog (lower trace) signals.
(b) White light analog (upper) and white light digital (lower) signals.
(Scope time base: 0.2msec/division)

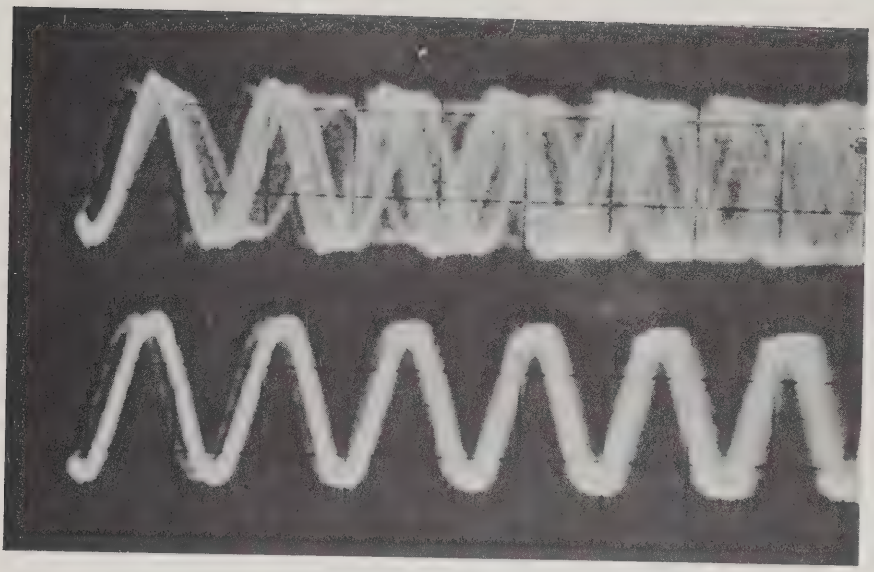

(a)

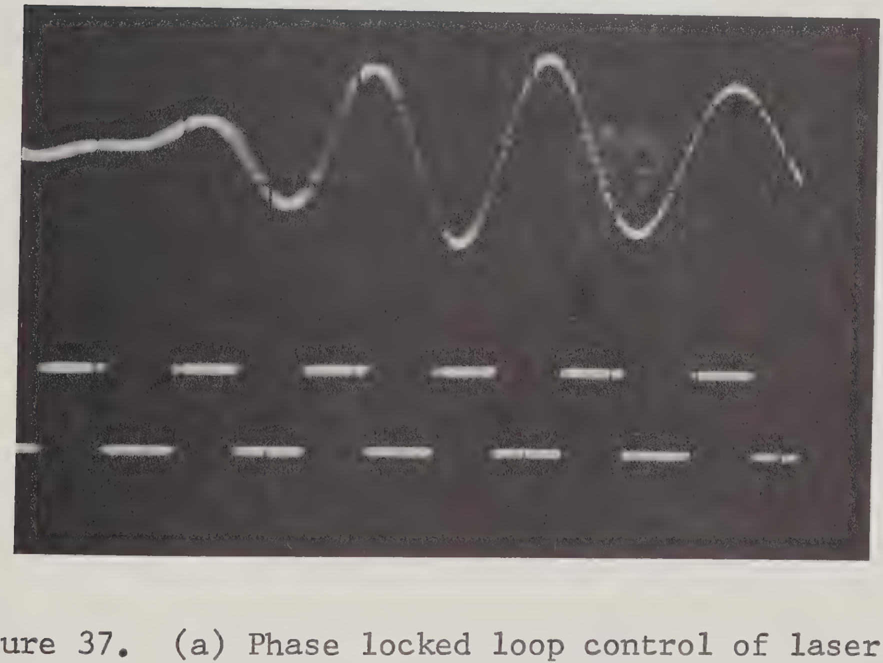

(b)

Figure 37. (a) Phase locked loop control of laser analog signal: upper, no PLL control; lower, with PLL control.
(b) White light analog (upper) and laser digital (lower) signals.
(Scope time base: 0.05 msec/division)

and an amplitude sufficient to drive the mirror 0.3-0.5 cm. This produces laser fringes at a frequency around 4kHz.

2) Laser Channel

The signal interferogram must be sampled at accurate distance intervals. For each cycle of the laser fringe signal shown in Figure 36(a) (lower trace) the mirror moves 0.3164 um and the optical path length changes 0.6328 um. Thus this signal can be used to provide an accurate clock for digitization. The frequency of this clock is determined by the velocity of the moving mirror. Even though this clock will accurately mimic any velocity changes in the mirror, it is still desirable to stabilize the mirror velocity because of the variable effects that low and high pass electronic filters will have on an interferogram signal whose frequency composition is changing due to mirror velocity changes. In our system, the mirror velocity is stabilized using a phase locked loop feedback control system.

A phase locked loop (PLL) consists of a phase comparator, a low pass filter and a voltage controlled oscillator (VCO) (54,67) and it can be obtained as a single integrated circuit (IC) package. In our circuit we have used a Signetics 565 PLL. Functionally the PLL compares the phase and frequency of an input frequency to the internal VCO frequency and generates an error

voltage proportional in sign and magnitude to the phase and frequency difference of the input and VCO frequencies. This error signal is applied through the low pass filter to the VCO control input (internal connection on the IC) and drives the VCO until it is at exactly the same frequency as the input frequency, that is, the VCO output becomes locked to the input frequency. Clearly, no stabilization of the mirror velocity is achieved merely by just locking the VCO of the PLL to the laser frequency. But the error signal discussed above is available as an output from the integrated circuit (pin 7). This error signal is applied, with appropriate polarity, to the external voltage control input of the mirror drive function generator.

This input of the function generator allows an offset to the basic drive frequency (about 0.2 Hz) so that the actual drive frequency depends on the polarity and amplitude of the error signal. For example, if the error signal is momentarily positive, the drive frequency is greater than 0.2 Hz for that time. This feedback loop (OA3 and OA4) stabilizes the mirror velocity and hence the laser fringe frequency. The capability of this system in stabilizing the mirror velocity is shown in Figure 37(a). The upper trace is the laser analog signal without feedback control and the lower trace with feedback control. Each trace is a 0.5 second time

exposure taken during one scan of the mirror drive.

Complete details on the operation of the 565 PLL can be obtained from Signetics (68). Only those connections pertinent to this application will be discussed. The VCO free running frequency is set by the value of the capacitor to ground from pin 9 and the resistance to +15V from pin 8. The frequency is set by the 10k ohm potentiometer to about 4 kHz. The 0.5 uf capacitor from pin 7 to +15V sets the internal loop low pass filtering and the 0.001 uf capacitor between pins 7 and 8 is for decoupling. Pin 7 is the error voltage output and hence provides the feedback signal for the mirror drive stabilization loop. Pins 2 and 3 are the external inputs to the phase comparator. The laser analog signal is connected to pin 2. The voltage divider network on pins 2 and 3 is necessary for proper operation of the PLL integrated circuit from a single power supply. Pin 4 is the VCO output which, when the complete system is interconnected, is phase locked to the stabilized laser frequency. Pin 4 must also be connected to pin 5, which is the internal input to the phase comparator in order to close the loop on the integrated circuit. To complete the laser channel circuit, the VCO output is converted to a TTL level signal by the OA comparator. The output of the comparator will be referred to as the laser digital signal (Figure 37(b), lower trace) and is used to clock

the analog-to-digital converter (ADC).

3) White Light Channel

In order to time average interferograms, some type of precise control signal is required to insure coherent addition of repetitive scans. This is the primary function of the white light interferogram. As discussed in Chapter VIB, in the single interferometer design, the white light and signal interferogram central fringe occurs coincidentally. Since the white light fringe is the only accurately known point (zero path difference position) during the mirror scan, using it to initiate data acquisition results in single-sided interferograms (no data points acquired before the ZPD position of the signal interferogram). Chapter V discussed the problems with calculating acceptable spectra from single-sided interferograms.

Our approach to taking data on both sides of the ZPD position is to use the white light fringe to generate a precise stop flag. A flag is generated at some imprecise point before the ZPD position to start acquiring data points. When the white light fringe occurs, it is used to precisely start a modulo-N counter that counts the laser digital clock. The counter overflow pulse generates a stop flag which is used to terminate data acquisition. Repetitive interferograms can be coherently time averaged by sequencing addition from the last point

acquired rather than the first, in a sense, time averaging backwards. This is achieved easily with software. This system will now be described in detail. It will be helpful to refer to Figures 34 and 35 in this discussion.

The imprecise start flag is generated from a "sync" signal available from the function generator. It is a square wave of the same frequency as that of the mirror drive triangular wave. The positive edge of the sync. signal, which is inverted by NAND-2, triggers MONO-1 (monostable) which in turn triggers flip-flop-1 (FF-1) generating the imprecise start flag (the negative going edge of NAND-4). This initiates data acquisition. The approximate position of the start flag, with respect to the white light fringes, can be set easily using MONO-1. It is normally set to occur about 2200-2400 laser clock pulses before the ZPD position. The laser clock pulses are counted with a Heath Model EU-805 Universal Digital Instrument in the gated counter mode. The clock signal is applied to the counter input and the counter gate is a pulse derived from the exclusive-or (XOR) of NAND-3 and NAND4 signals. Hence the counter registers the number of clock pulses between the start and stop flags. The modulo-N is 2048 so the total count is adjusted to read approximately between 4200 and 4500, that is, 100 to 400 more points than necessary to allow for drift and jitter. The start flag is imprecise with

respect to the ZPD position because it is essentially impossible to oscillate an electromechanical assembly such as the moving mirror assembly and have it turn around at interferometrically accurate amplitude. The jitter in the start flag has a standard deviation of about 9 laser clock fringes.

The sync. signal is used for one other key function. Data is acquired on only one half cycle of the moving mirror oscillation. White light fringes are generated on both half cycles. The sync. signal is connected to NAND-1 to inhibit the generation of a spurious stop flag on the other half cycle of the moving mirror oscillation.

When the white light interferogram occurs, it is amplified by OA-1 then converted to a TTL level digital signal by a comparator. To provide noise immunity, the trigger level is set so that only the central three or four fringes fire the comparator. The white light analog and digital signals are shown in Figure 36(b) upper and lower trace respectively. The first pulse of the white light digital signal triggers MONO-2 which immediately triggers FF-2, the modulo-N counter gate. This allows the counter (N=2048 for our present interferogram length of 4096 points) to count the laser digital clock pulses. MONO-2 pulse width is set wide enough to block out subsequent pulses of the white light digital signal. The overflow (carry) pulse of the counter triggers FF-3

generating the stop flag which is precise in terms of mirror movement with respect to the white light fringe (ZPD position). This stop flag (negative going edge of NAND-4) terminates data acquisition by the computer. Time averaging of the acquired interferograms in the computer is sequenced backwards from the last data point, thereby providing coherent addition of interferograms.

Flip-flop 3, when it is triggered, also clears FF-2 thus closing the counter gate and preventing multiple stop flags. The second half cycle of sync. pulse clears FF-1 and FF-3 to be ready for the next scan sequence. The purpose of NAND-3 and NAND-4 is to buffer the flip-flops to meet the input characteristics of the data acquisition system.

The first pulse of the white light digital signal must be reproducible from scan to scan. These signals have been observed over several hundred scans. Also, over 500 repetitive interferograms have been time averaged and there has been no evidence of jitter in the first pulse of the white light digital signal.

4) Detector Electronics

The detector used for IR measurements was a TGS (triglycine sulphate) pyroelectric detector. A circuit was provided by the supplier to interface to the detector to provide a voltage of low output impedance. This voltage output was connected to a low noise preamplifier (Princeton

Applied Research Model 225). The input is ac coupled and the preamp provides variable low and high pass filtering and variable gain. The bandpass was set at 300 Hz to 10 kHz. The preamp output is the signal that is applied to the analog-to-digital converter (ADC).

A Si photodiode was used for visible and near-IR measurements. The output of the detector was applied to an operational amplifier (PAR Model 215) in the current amplifier mode and ac coupled input. The operational amplifier output was connected to the ac coupled PAR 225 low noise preamplifier before going to the ADC. The bandpass of the preamplifier was set for 300 Hz to 10 kHz.

Photomultiplier tubes (1P28 and R166 solar blind) were used for visible and UV measurements. The standard high voltage dynode chain circuit for photomultiplier tubes is for DC applications (Figure 38(a)). This was modified (69) for operation of the PMT for signals of high frequencies (Figure 38(b)). The PMT circuit was normally operated with a negative high voltage of 500V. D1 to D9 represent the nine dynodes of the PMT. The anode current drains through R_L to ground providing a voltage output. This was applied to the ac coupled low noise preamplifier, then to the PAR 215 operational amplifier in the voltage amplifier mode with gain of 10 and finally to the ADC. The response of the PMT circuit is down 3dB at $f=1/(2\pi R_L C_L)$. C_L is the coaxial

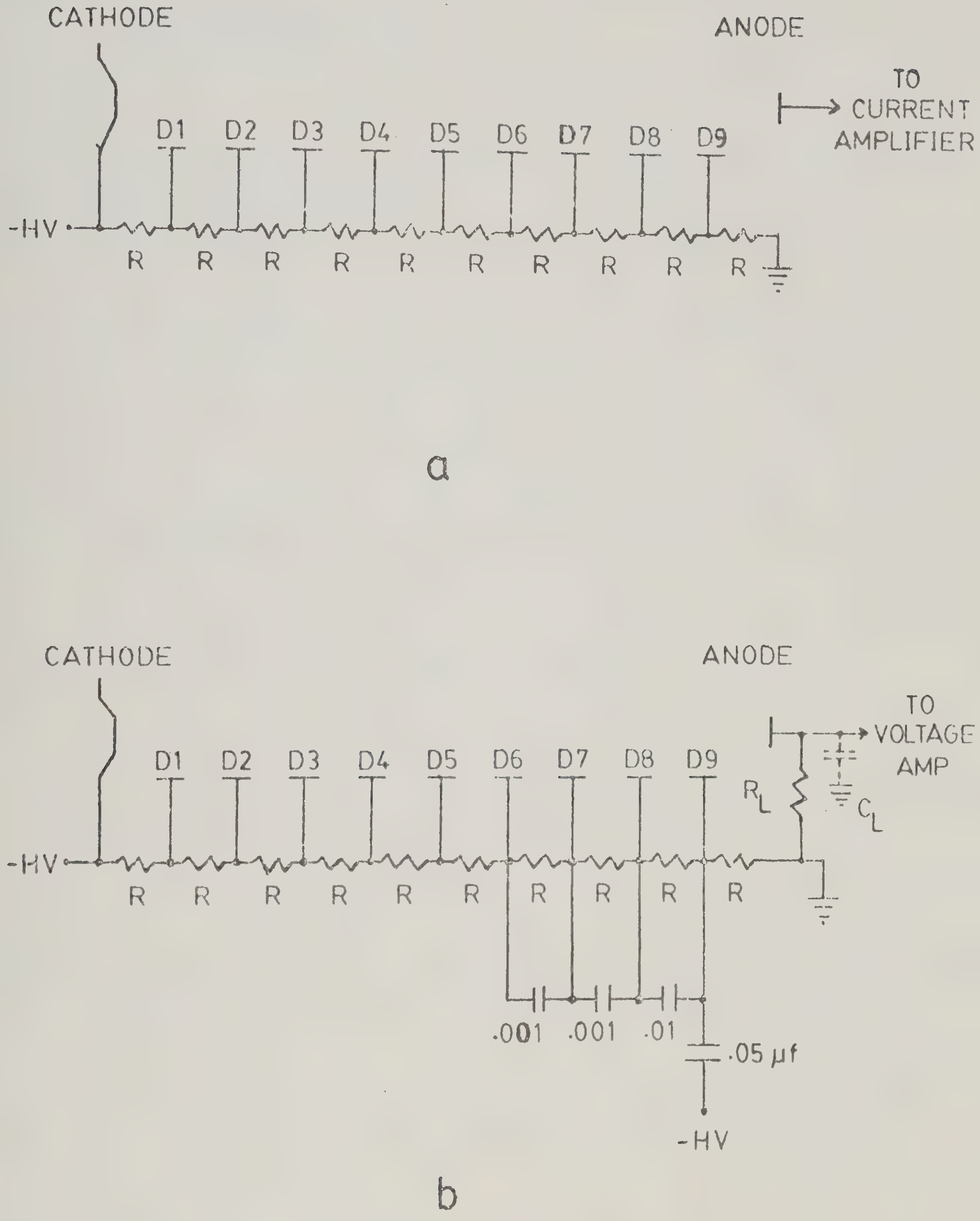

Figure 38. Photomultiplier tube schematic circuit for (a) DC operation, (b) AC operation.

cable capacitance and is about 100 pf. For response to around 30 kHz, R_L was chosen to be 50k ohms.

5) Sampling Rates

It is necessary with a versatile Fourier transform spectrometer system to be able to acquire data at various sampling rates. The importance of sampling rate and its relation to the frequency axis has been discussed in Chapter III. Most of the measurements are now taken using the direct sampling rate of the He-Ne laser fringes. Where the number of points for the Fourier transform is limited by the size of the computer memory (as in the PDP-8/e system used in the early development of this work and described in the following section) it is desirable to use a coarser sampling interval to optimize spectral coverage and resolution. These coarser sampling intervals (÷2 and ÷4 sampling rates) are achieved by software. Data is taken into the computer at the direct rate of the laser fringes. If the ÷2 rate is desired, the program is instructed to signal average every other point or for the ÷4 rate, every fourth point. This, however, does mean that 2000 data points must be acquired in order to time average a 500 point interferogram at the ÷4 rate.

The question arises as to why a hardware approach, simply a couple of flip-flops on the laser digital clock to divide by two or four, could not be used. Time

averaging could proceed directly and with simpler software. However, this is not possible in our system for a subtle reason. The ADC clock must be phase locked to the white light and signal interferograms. The laser digital clock satisfies this constraint. Figure 37(b) shows 20 superimposed repetitive scans of the laser digital and white light analog signals. The laser digital maintains the same phase with respect to the white light signal. But any clock signal generated from it by a modulo-2 or modulo-4 counter cannot be phase locked to the white light and signal interferogram because the state of the counter cannot be reproducibly set at the start of data acquisition (the start pulse is imprecise with respect to the white light interferogram).

It is also possible to take data at sampling intervals finer than that provided by the direct rate of the laser digital clock. This is useful for clarifying highly aliased spectra as shown in Chapter III. It turns out, in contrast to the above situation, that a phase locked clock of higher frequency can be generated by a hardware approach.

A phase locked loop can be used for precise frequency multiplication (54). It was mentioned in an earlier section that the internal loop of the 565 PLL between the VCO and the phase comparator was closed by connecting pin 4 and pin 5. If this connection is opened

and a modulo-K counter (K=2 or 4) is inserted, the loop will operate so as to drive the VCO at K times the frequency of the input laser analog signal. The VCO free running frequency must be adjusted to about twice the laser analog frequency before the PLL can lock onto it. Once lock is achieved, the VCO output at pin 4 will be precisely K times the laser analog signal frequency and phase locked to it. This approach has been used to generate X2 and X4 sampling rates.

6) Electronics with the PDP-8/e Computer

The computer system used for the early development of this work was a DEC (Digital Equipment Corporation) PDP-8/e. There are only two digital control lines into the computer (the other digital inputs are used for the data). One is used for the clock ADC flag to tell the computer that the conversion is done and the digital data is available to the computer. The other control line must then be used to start and also to stop taking data.

The interferometer electronics used with the PDP-8 is shown in Figure 39 and the timing sequence in Figure 40. The circuit for the laser channel and phase locked loop feedback control is basically the same as described earlier. The start flag, in this case, is a very short pulse (about 50 usec) from MONO-2 generated from MONO-1 and the sync. pulse. The white light fringe triggers MONO-3

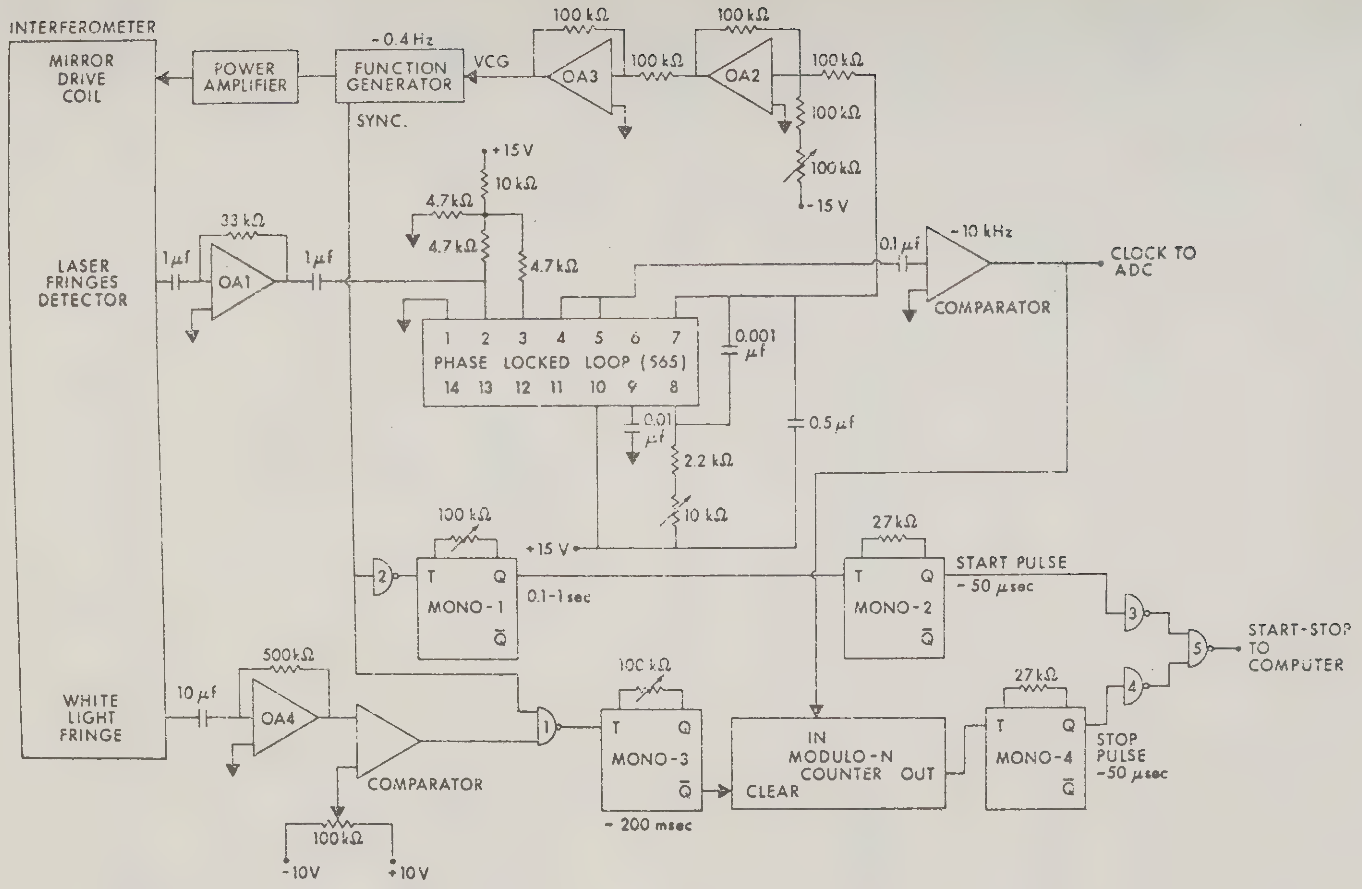

Figure 39. Interferometer electronics with the PDP-8/e computer.

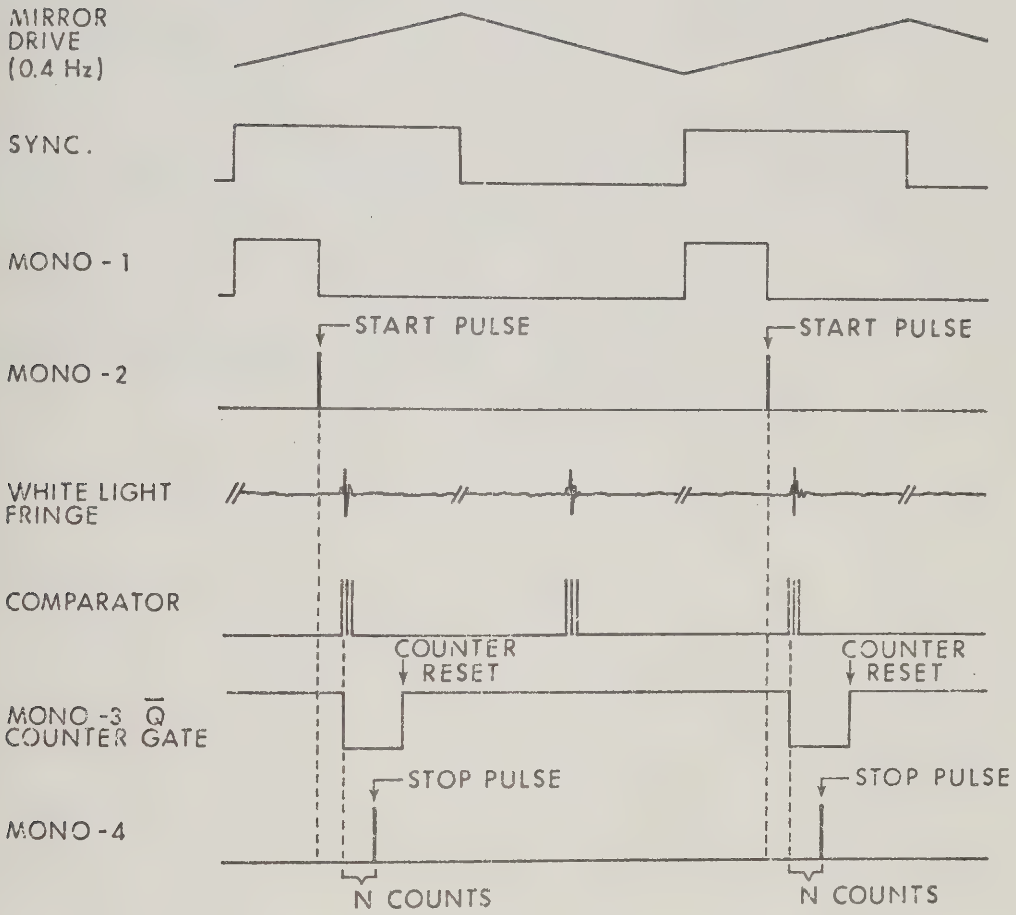

Figure 40. Schematic diagram of the control signals' timing sequence for the circuit in Figure 39.

which opens the modulo-N counter. The overflow pulse triggers MONO-4 which gives another very short pulse (about 50 usec) which is the stop flag. The counter reset used here is more crude than in the latest circuit (Figure 34). The counter gate, MONO-3, is adjusted to close in a time period longer than N counts but shorter than 2N counts to prevent multiple stop flags. Since only one control line is open for the start and stop flags, they are combined by a multiplex circuit (OR gate) to form one input into the computer. The computer program is instructed to sense the first pulse as a start flag and the next pulse as a stop flag.

D. Computer Processing

1) The Computer Systems

The first computer system available was a PDP-8/e from DEC, with 16k of core and a DEC-tape based OS/8 operating system (Figure 41). The associated digitizing system consists of a sample and hold module with a 50 nsec aperture time coupled to a 10-bit ADC with a 10 usec conversion time. Assembly language (SABR) commands were used to input data from the ADC and output data to the digital-to-analog converter via a DR8-EA 12 channel buffered digital I/O (input/output) board. All other programming was written in Fortran including the floating point FFT. The maximum number of points that can be transformed with this system is 512.

The present minicomputer data acquisition and processing system used with the interferometer is based on a DEC PDP-11/10 with 32k of memory and an LA-36 Decwriter terminal (Figure 42). The RT-11 (real time) operating system uses an RK-05 cartridge disk as the main storage medium. Accessory storage is provided by a TA-11 dual cassette unit. Versatile program editing and graphics capability is provided by a VT-11 graphic display processor with a VR-17 CRT. Hardcopy output is provided by a Zeta Research Series 100 incremental

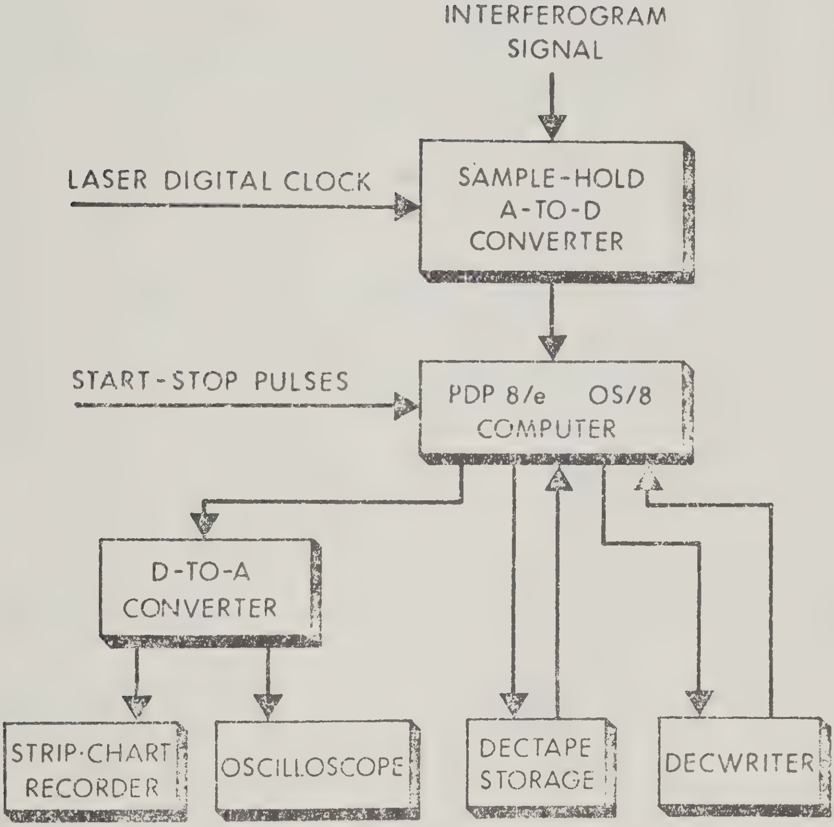

Figure 41. Minicomputer data acquisition and processing system based on the PDP-8/e.

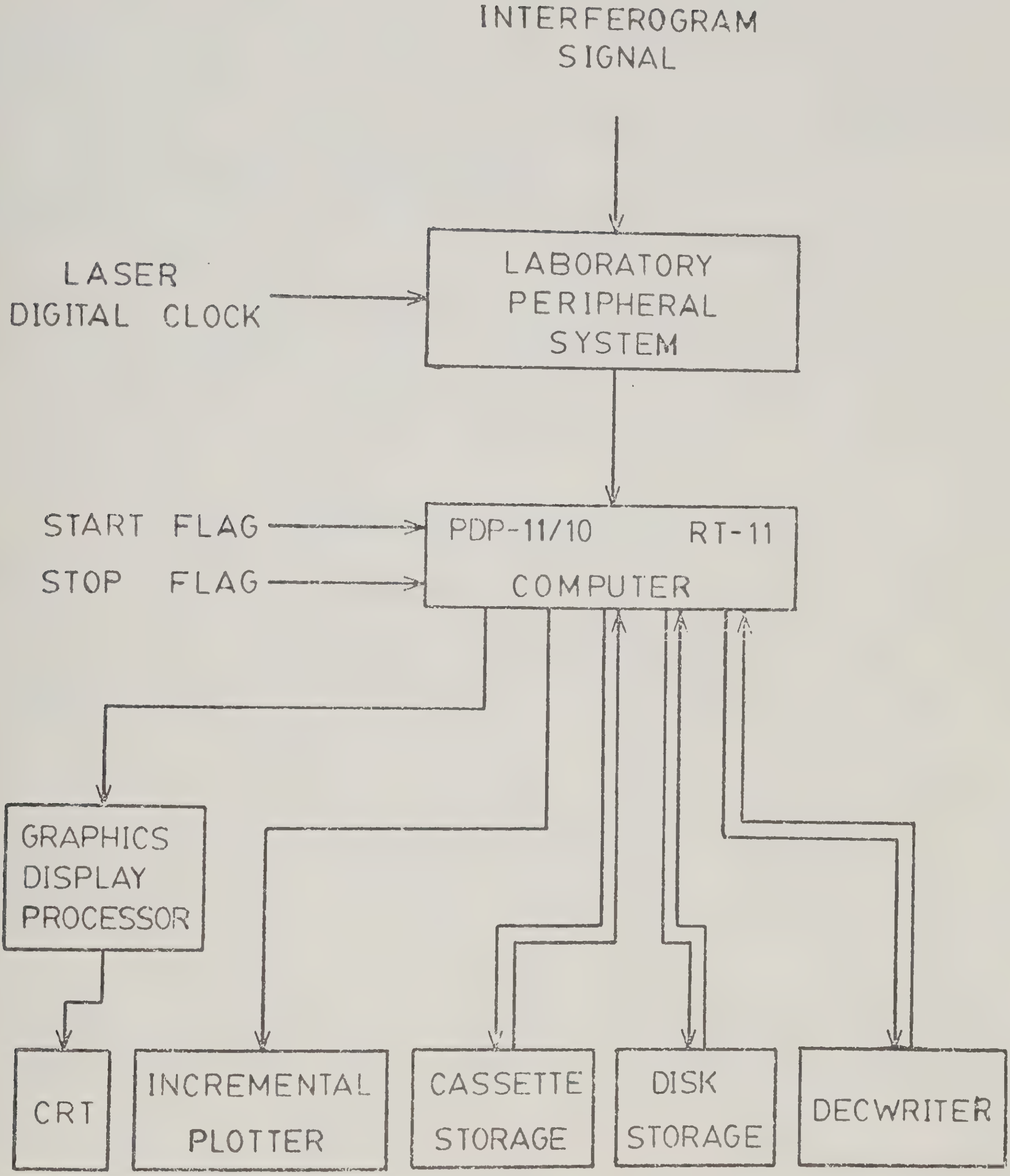

Figure 42. Minicomputer data acquisition and processing system based on the PDP-11/10.

plotter (Model 130-5).

The Michelson interferometer is interfaced to the computer by the DEC laboratory peripheral system (LPS) which contains the ADC and the sample and hold amplifier. The analog signal interferogram is connected to one of the eight channels of the LPS multiplexer and preamplifier before going to the sample and hold and 12-bit ADC (20 usec conversion time). The laser digital clock, the start and the stop flags are connected to the LPS 16-bit digital I/O.

The data acquisition program was written in assembly language (MACRO). All other programming was written in Fortran including the floating point FFT, graphics and plotting programs. The number of points that can be transformed is 4096. All the spectra shown in this work were calculated from 4096 point interferograms, unless otherwise stated. The interferograms were fully double-sided except those shown in Chapter V. Also the spectra were calculated as the amplitude spectra without using any phase correction techniques (except the spectra in Chapter V).

2) Computer Programming

The programs used to process the interferogram and manipulate the data are presented here in descriptive form. The actual programs and detailed commentary are presented in the Appendix. Figure 43

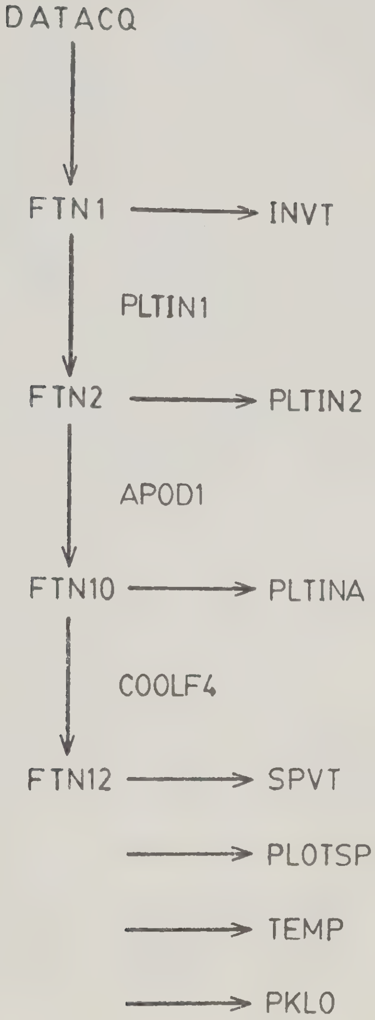

Figure 43. Program sequence for data acquisition and processing.

gives the program flow to process the data.

DATACQ is the data acquisition program. The actual acquisition subroutine is written in assembly language (MACRO). The program begins to acquire data upon arrival of the start flag with one point being stored for each laser digital clock pulse. The stop flag halts data acquisition. The raw interferogram is then summed (sequenced from the last data point) into an array which is double word to avoid addition overflow. The program then waits for the next start flag and the sequence repeats until the required number of scans have been taken. Then the summing array is divided by the number of scans and converted to single word to give the time averaged interferogram. The interferogram data points are written onto the disk as the file FTN1 in integer format.

PLTIN1 converts FTN1 to a floating point file which is stored as FTN2. FTN1 and FTN2 contain additional information about the parameters used, such as the number of points and scans, date and title, and the maximum and minimum values in the interferogram and their point locations.

APOD1 performs the apodization of the interferogram stored in FTN2. The interferogram is multiplied by a mathematical function which can vary from zero to one. There is a choice of functions: boxcar, triangular, and Gaussian. Others could easily be programmed. The degree of apodization is determined by the choice of the indices

in the case of boxcar and triangular functions. For the Gaussian function, the parameter FAC is entered to determine the width of the function and Z to determine the center point of the function (usually 2048 for a 4096 point double-sided interferogram). The apodized interferogram is stored in the file FTN10.

COOLF4 performs the fast Fourier transform on the data in FTN10 and outputs the unscaled amplitude spectrum onto the disk as the file FTN12.

Both the interferogram and amplitude spectrum can be viewed on the CRT with the programs INVT and SPVT respectively. Any portion of these data can be displayed and expanded. Listing of the data points on the terminal can also be obtained.

Hardcopy can be obtained on the incremental plotter of the interferogram, the apodized interferogram, and the spectrum with the programs PLTIN2, PLTINA, and TEMP respectively. Any portion of the data can be plotted with any desired expansion. The spectrum can also be scaled to give expanded amplitudes of small peaks with the program PLOTSP.

PKLO searches for peaks in the spectrum above a specified threshold value and outputs their point location, wavenumber and wavelength (for the specified aliasing region). The program also calculates the scaling factor so that absolute peak amplitudes can be

obtained for quantitative measurements.

One place where further program development is needed is in the number of points the Fourier transform program is capable of processing. At present, the computer memory of 32k on the PDP-11/10 limits the "in-core" transform size to 4096 points (floating point FORTRAN). To improve spectral resolution, longer interferograms (larger optical retardation) must be transformed. There are procedures for performing the Fourier transform in segments using the disk memory for temporary storage, therefore, allowing much longer interferograms to be processed by this computer. Another possibility to achieve this is to have a direct communications line from the PDP-11/10 to a large central computer. The mini-computer would perform the data acquisition, then, the interferogram would be transmitted to the large computer which performs the Fourier transform.

CHAPTER VII

SPECTRAL MEASUREMENTS WITH THE FOURIER TRANSFORM SPECTROMETER

The Michelson interferometer system was described in detail in Chapter VI. Earlier chapters discussed special factors that had to be considered in extending the use of Fourier transform spectroscopy to atomic spectrochemical measurements. A few spectra were shown to illustrate important points in the earlier chapters.

In order to explore the capabilities of the Fourier transform spectrometer that was built, various spectral sources in different spectral regions were measured. These include measurements from the near-IR, visible, ultraviolet, and mid-IR spectral regions. Representative spectra are shown to point out the versatility and capability of the spectrometer.

A. Near Infrared Measurements

The flame emission spectra of the alkali metals, Li, Na, K, Rb, and Cs, fall in the 600 to 900nm region. One detector which has response in this spectral region is the Si photodiode. Its maximum sensitivity is around 1 um. The detector is mounted in an aluminum housing which fits into the detector mount of the interferometer.

The instrumental setup for the flame source consists of a Varian Techtron manual gas control box, a Varian nebulizer and a premixed burner. The slot burner head was removed and a cylindrical flame head (70) was constructed. The burner head consists of an array of stainless steel capillary tubes of 1 mm inside diameter. The capillary tubes are stacked side by side and held together by epoxy inside the outer cylinder. The top surface of the array of about 60 capillaries is flat and the array is about 11 mm in total diameter.

The flame is then actually a composite of small flames, one from each capillary tube. The blue inner cones of the flame are 1 to 3 mm high, but the rest of the flame extends about 30 cm in height. The air/acetylene flame is very stable. For the alkali metals a cool flame is sufficient for excitation. The manual gas box was set for flows of air=7 units and acetylene=2.5 units. This corresponds to 12.3 and 1.8

liters/minute respectively. The burner was placed at the focal point of the input off-axis parabolic mirror to collimate the light to the interferometer. The observation height for the atomic emission was set by rotating the mirror so that the focal point was about 5 cm above the top of the burner.

Figure 44 shows a spectrum of the five alkali metals listed above. The spectrum was obtained by taking the Fourier transform of the interferogram resulting from a solution of the five elements at about 100 parts per million (ppm). The solutions were made from the chloride salts of the elements. Fifty consecutive scans were averaged and the interferogram was apodized with a Gaussian function (FAC=2.5). The sampling rate used was the direct rate derived from the He-Ne laser. The digitized interferogram is shown in Figure 45 where the middle 3000 points of the 4096 point double-sided interferogram is plotted. To illustrate again the point made in Chapter V about phase errors, note that the interferogram is quite asymmetric. Yet, the spectrum is not distorted because it is calculated from a double-sided interferogram. The Michelson moving mirror drive was set at about 0.2 Hz or 5 seconds per scan. The 4096 points of data on one scan were acquired in a 1 second period during the 5 second mirror drive cycle. Therefore, although about 4 minutes

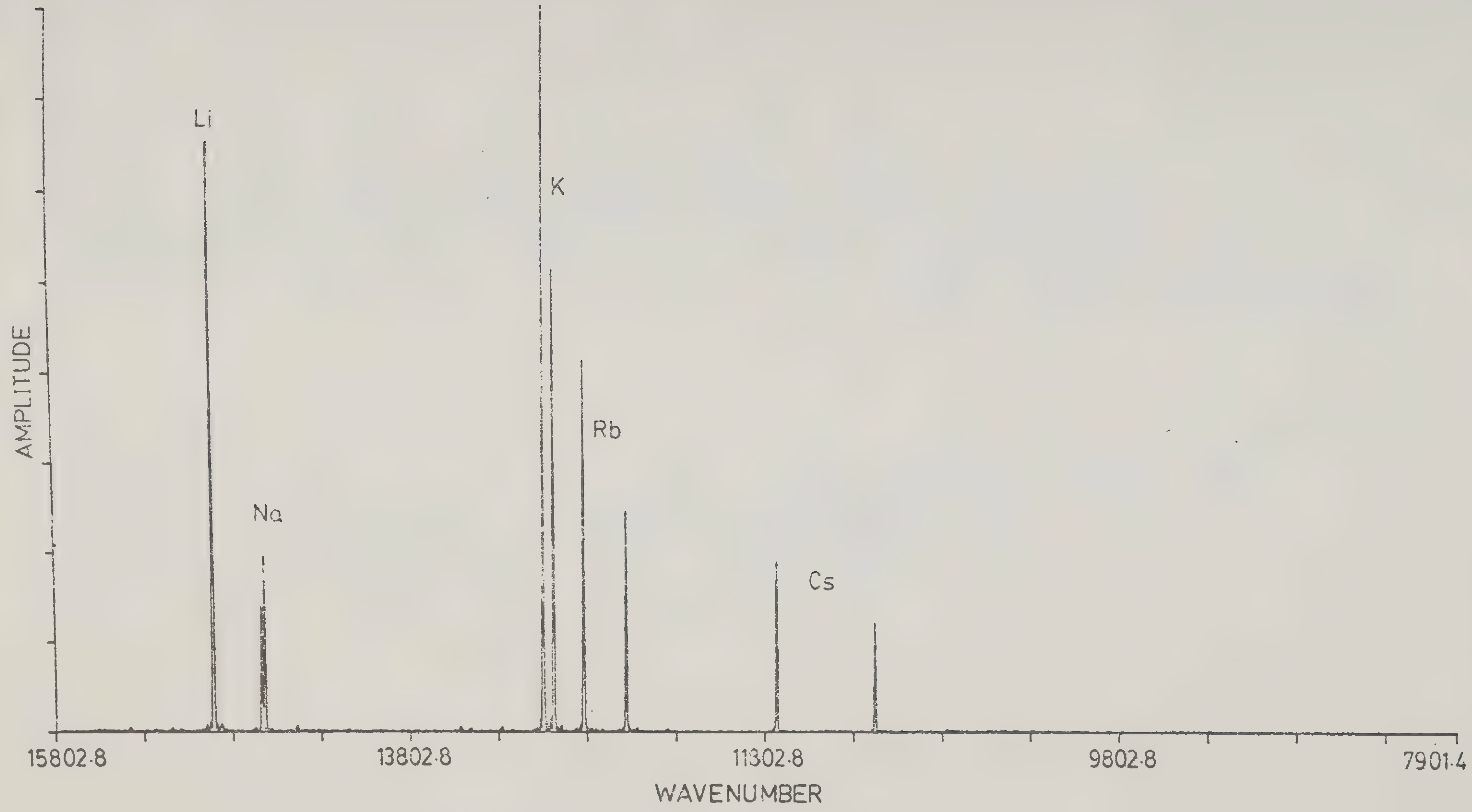

Figure 44. Flame emission spectrum of the alkali metals.

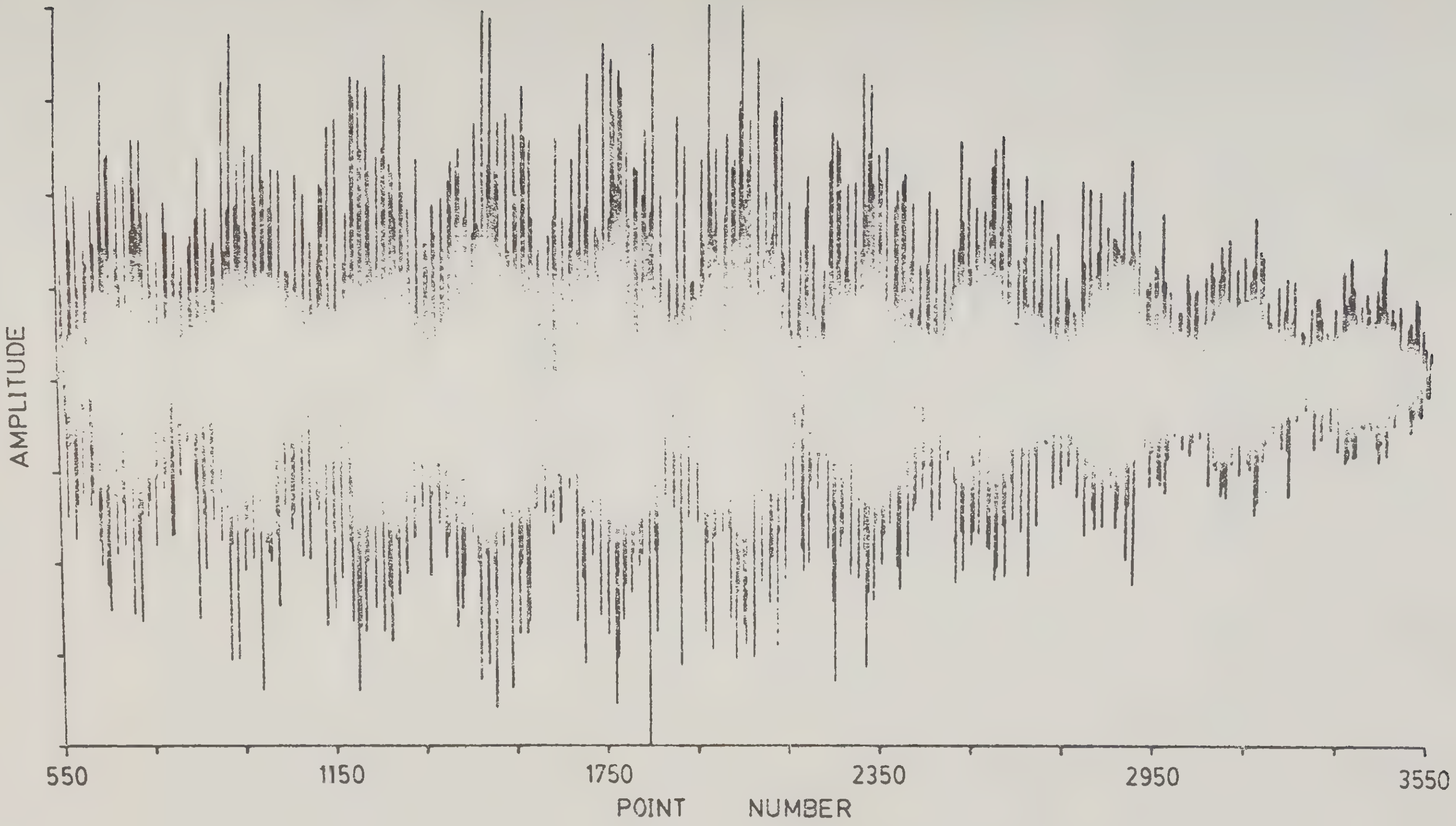

Figure 45. Digitized interferogram which produced the alkali metals spectrum in Figure 44.

are needed to acquire the data for 50 scans, the actual measurement time is only about 1 minute.

It should be noted that, since the sampling interval was 0.6328 um, all the lines in Figure 44 are aliased as explained in Chapter III. The wavenumber axis is labelled for region (5-8) (see Table II). The Li, K, Rb, and Cs peaks lie in this region, but the Na doublet is actually aliased in from region (9-12). The measured wavelengths are tabulated and compared with the literature values (71) in Table IV. The agreement is quite good. It should be emphasized that a spectral range of 300 nm is covered in this spectrum, illustrating the wide simultaneous spectral coverage possible with Fourier spectroscopy.

Quantitative aspects were studied with the lithium peak at 670.78 nm. An analytical curve for lithium flame emission is shown in Figure 46. The lower concentration limit is about 0.1 ppm at which point the S/N for the lithium peak decreases to about three. The slope of the straight portion of the log-log plot ranges from 0.95 to 1.05 for all the analytical curves that have been run. The slope in Figure 46 is 1.05. This shows that the Fourier transform spectrometer is capable of quantitative measurements.

The spectra for two of the points on the analytical curve are shown in Figures 47 and 48 for 5 ppm and 0.5 ppm

TABLE IV

Wavelengths Calculated From the Alkali Metals Spectrum Shown in Figure 44

Element	Literature (nm)	Experimental (nm)	Δ nm
Li	670.78	670.63	0.15
Na	589.59	589.47	0.12
	589.00	588.87	0.13
K	766.49	766.32	0.17
	769.90	769.74	0.16
Rb	780.02	779.93	0.09
	794.76	794.64	0.12
Cs	852.11	851.99	0.12
	894.35	894.17	0.18

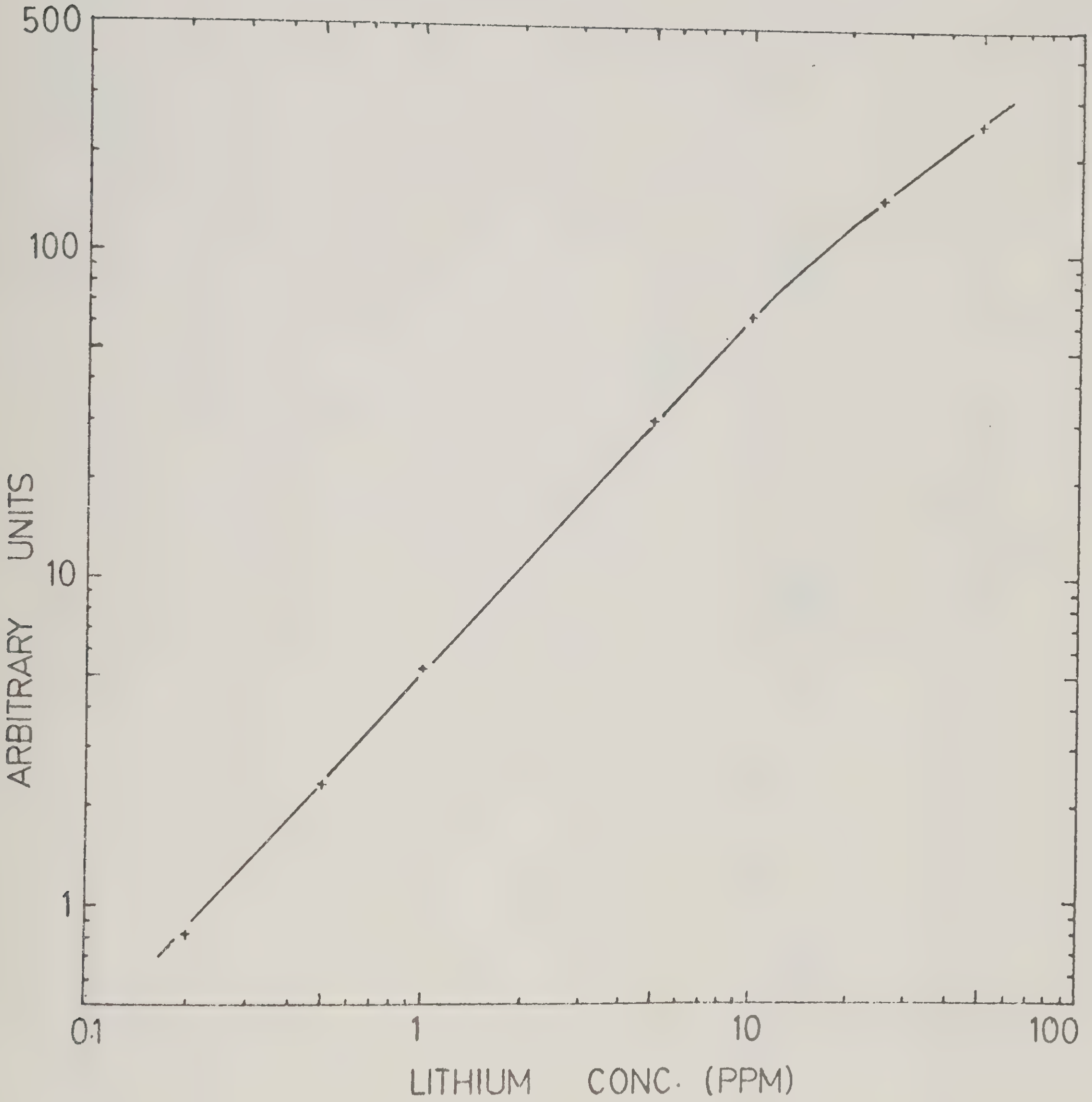

Figure 46. Analytical curve for lithium flame emmission.

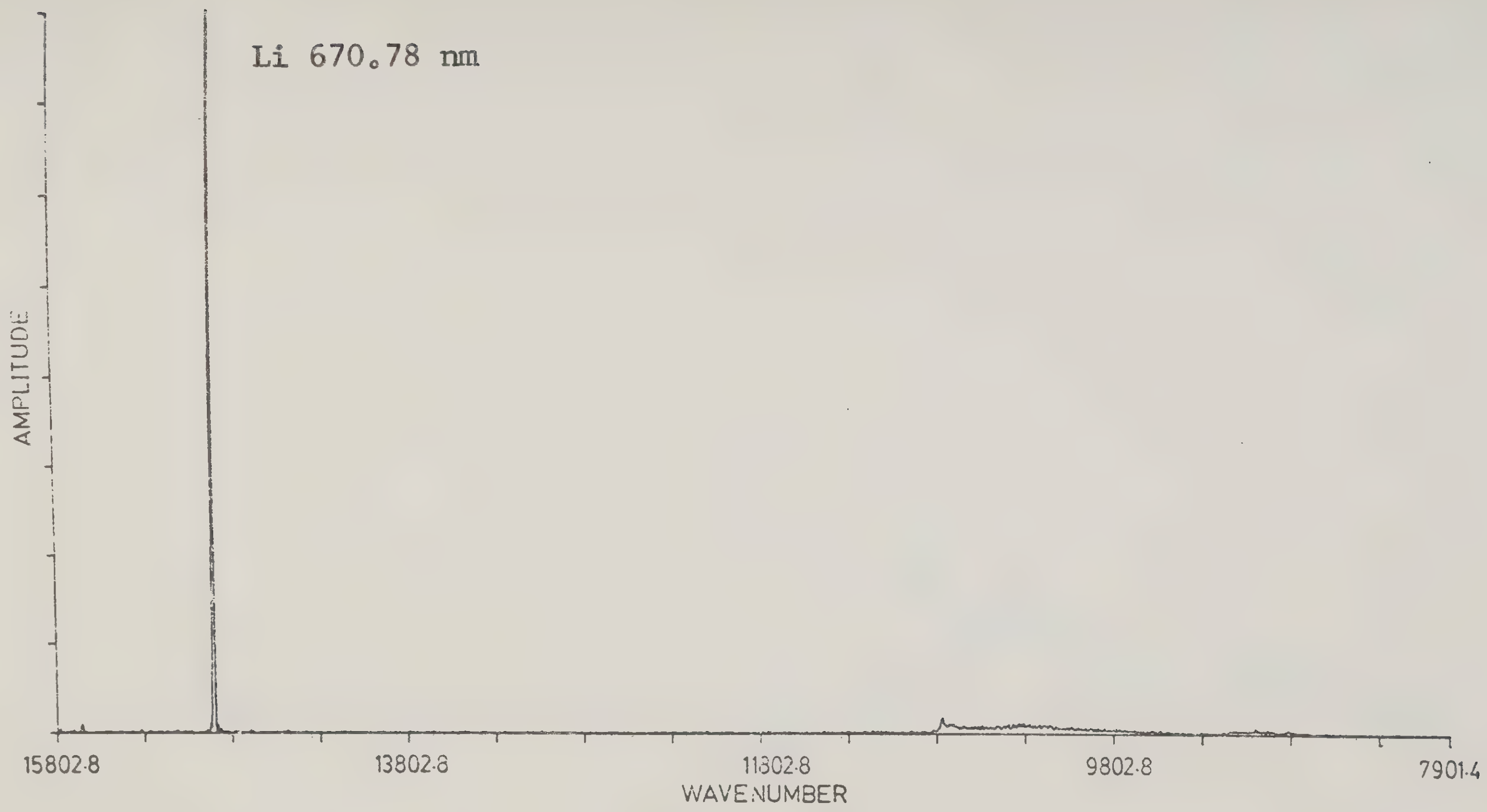

Figure 47. Spectrum of a 5 ppm lithium solution.

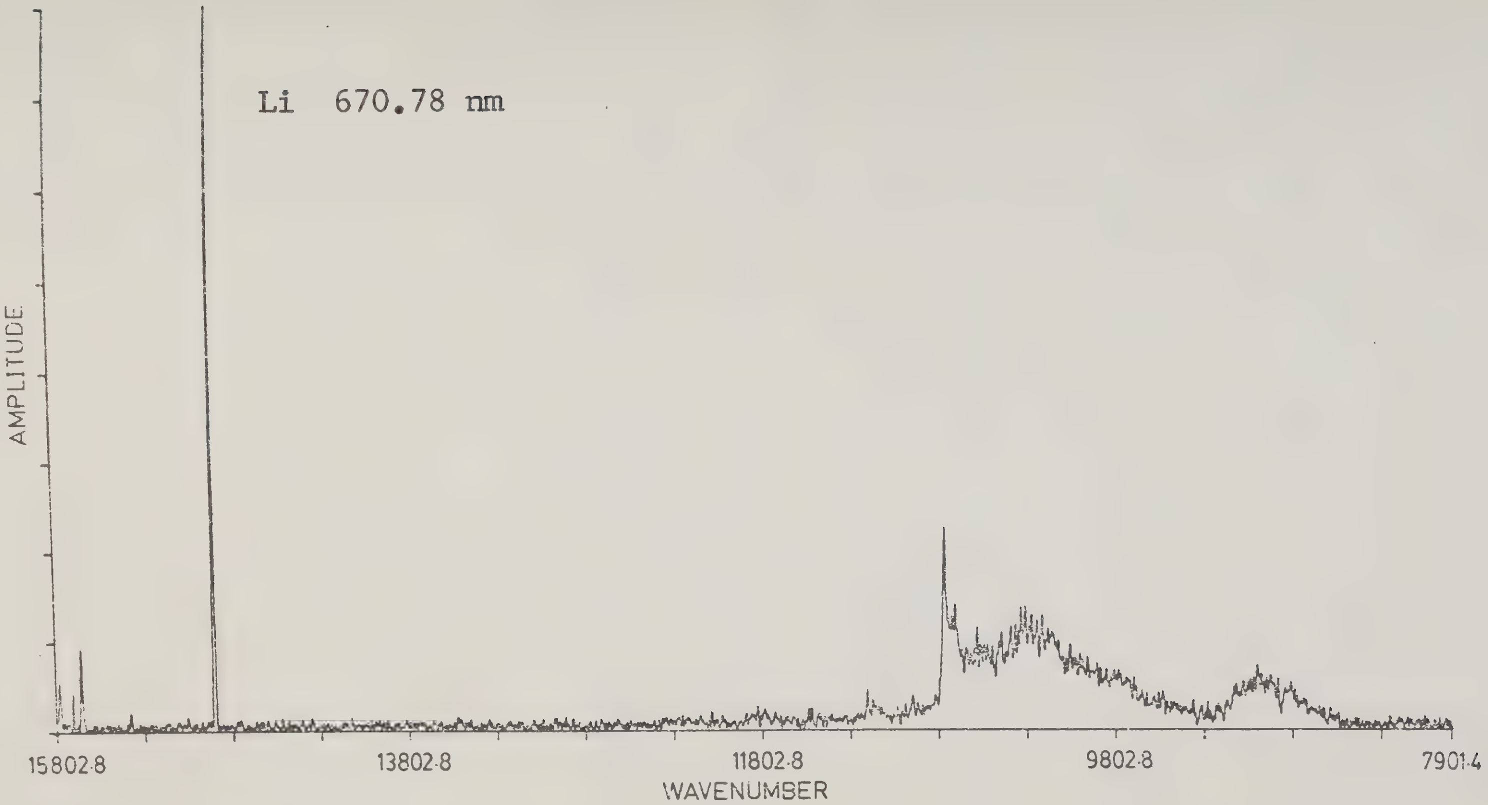

Figure 48. Spectrum of a 0.5 ppm lithium solution.

lithium respectively. The interferograms were double-sided and were each the average of 50 scans. Gaussian apodization was applied to the 4096 point interferograms (0.6328 um sampling interval). The absolute peak amplitude was calculated from the scaling factor needed to scale the spectrum from 0 to 4096 on the vertical axis. The band spectra around 10800 to 9800 cm^{-1} are due to water bands around 960 nm (72). The amplitudes of these bands remain relatively constant. The bands in the 5 ppm Li spectrum appear smaller because both spectra have been scaled between 0 and 4096, but, the Li peak is ten times larger for the 5 ppm spectrum than for the 0.5 ppm spectrum.

To extend the measurement of spectra to shorter wavelengths, studies were carried out in the visible region. The atomic spectra of most elements lie in the visible region of the spectrum.

B. Measurements in the Visible Spectral Region

Measurements made in the visible spectral region used a photomultiplier tube (1P28) as the detector. The negative high DC voltage for the PMT was supplied by a Heath EU-701-30 power supply module and was set for 400 to 500 V. The dynode chain for the PMT was mounted inside the PMT housing. The housing has an adaptor piece which fits into the detector mount of the interferometer. Different size apertures could be placed on the adaptor piece. Most of the spectra were taken with a 1.0 mm aperture.

Sources measured were flame emission of Ca, Sr, Ba, Na, Li and hollow cathode lamps (HCL) of several elements. All the spectra are from double-sided interferograms apodized with a Gaussian function (FAC=2.5). The direct sampling rate (0.6328 um) was used and 4096 points were acquired.

Fifty scans were averaged. This number was chosen as a compromise between improved S/N ratio with more scans and shorter time of data acquisition with fewer scans. To test the S/N ratio improvement with more scans, the baseline noise of Na spectra was measured for interferograms of 1, 10, and 100 scans. The increase in the S/N ratio (decrease in noise with the signal constant) roughly follows the square root

of the increase in the number of scans.

1) Atomic Flame Emission

The flame emission spectra of Li, Na, Ba, Sr, and Ca is shown in Figure 49. The concentrations were: Ba 800 ppm, Sr 100, Na 1, Li 10, and Ca 100. The flame used was the same air/acetylene flame used for near-IR measurements. No attempt was made to optimize the flame conditions. Measurements using a nitrous oxide/ acetylene flame would give better emission signals for many elements including Ca, Ba and Sr. Another excellent source for emission is the inductively coupled plasma. This is a very good source for simultaneous multielement analysis.

The barium peak is overlapped by a CaOH band centered at about 555 nm. Again, the spectral lines are all aliased. The labelled axis is for region (9-12) which includes the lines of Na, Ba, Sr, and Ca. The Li line is in region (5-8). The interferogram is shown in Figure 50 (the middle 3000 points are plotted). Note that since the Na doublet dominates the spectrum in terms of peak amplitudes, the interferogram has the general shape of the Na interferogram (a beat pattern from the summation of two cosine waves of slightly differing frequencies). The interferogram is fairly symmetrical. The symmetry is very dependent on the proper alignment of the Michelson mirror. The literature and measured

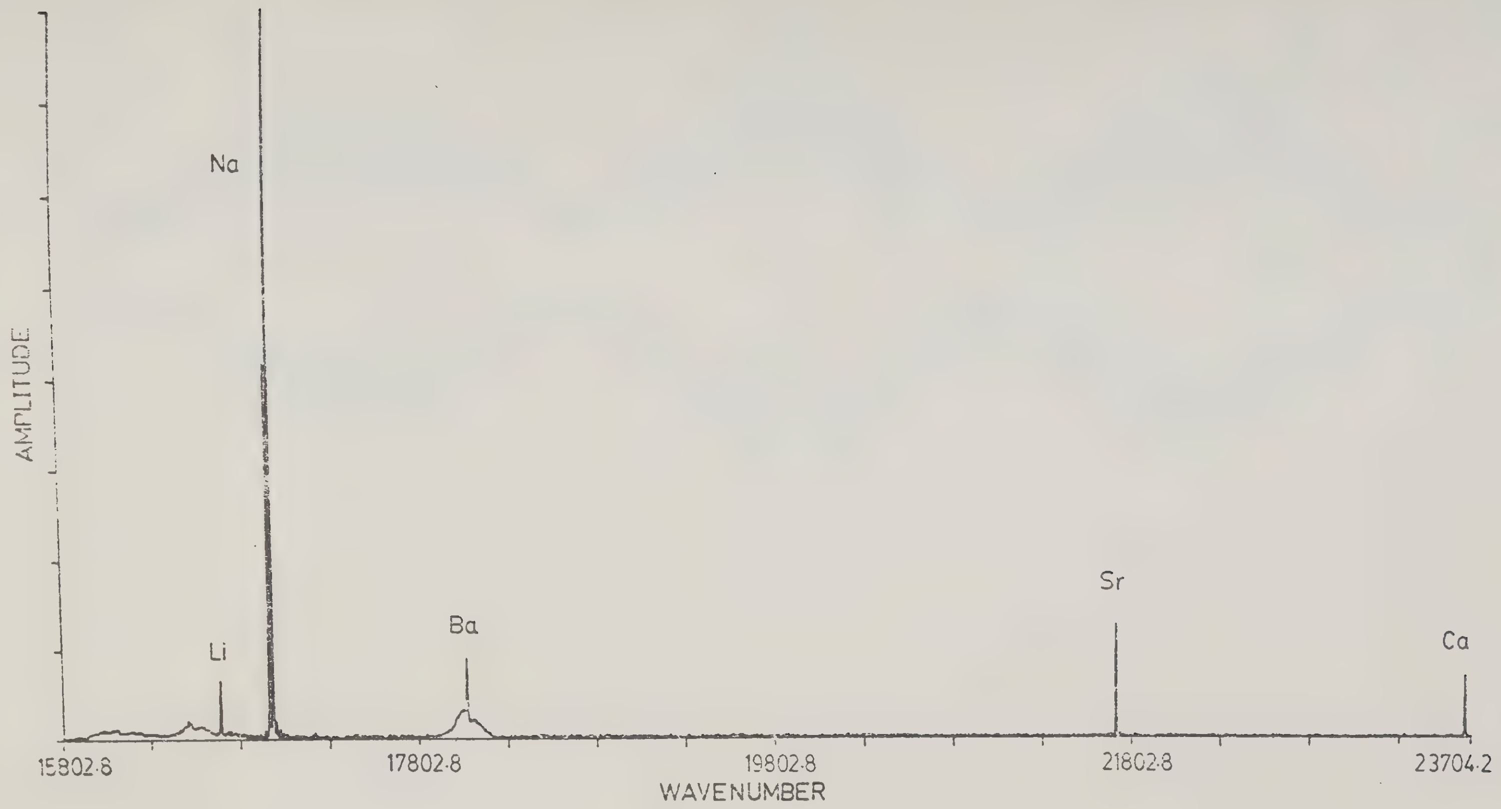

Figure 49. Flame emission spectrum of a multielement solution of lithium, sodium, barium, strontium, and calcium.

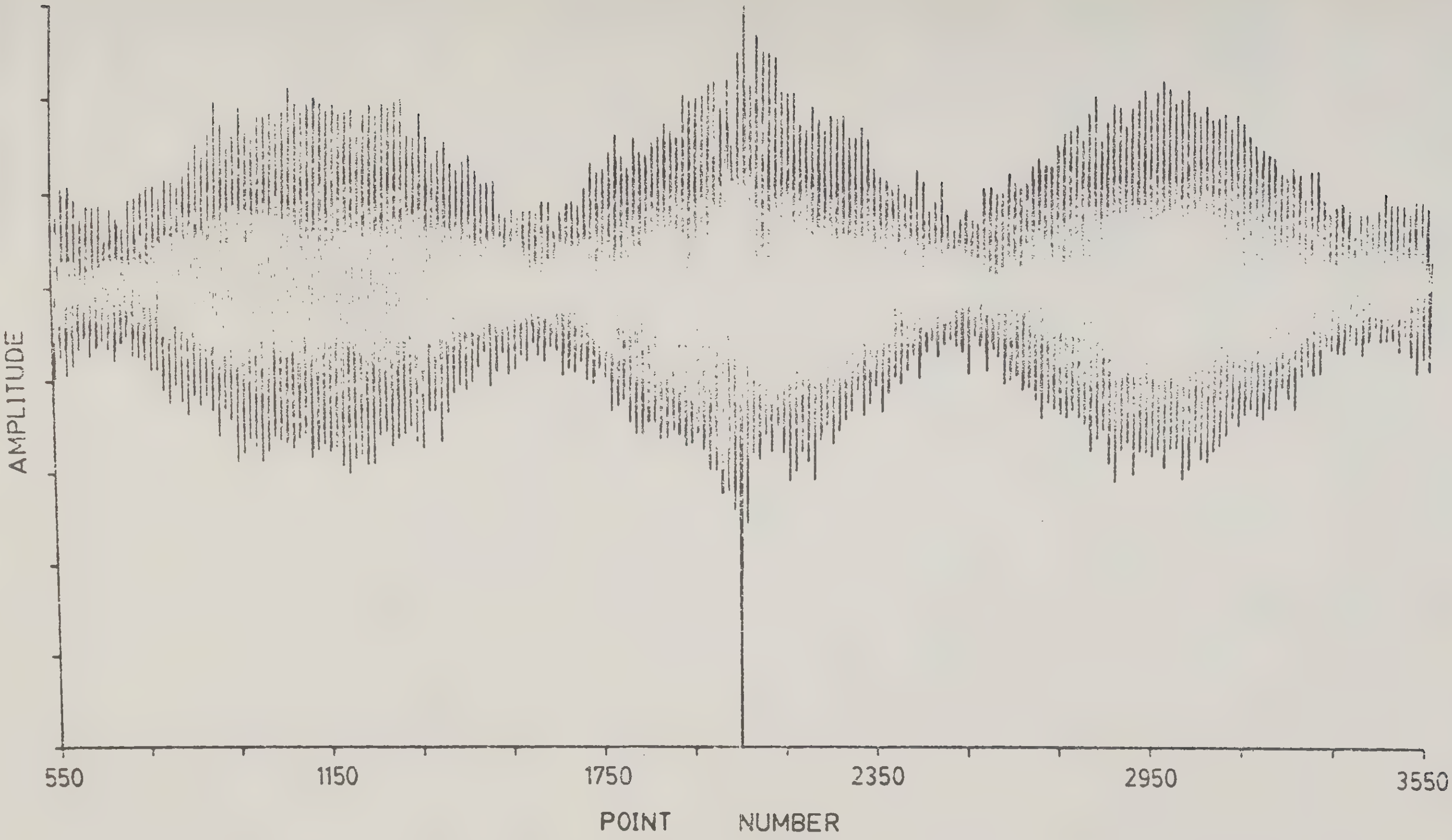

Figure 50. Digitized interferogram which produced the spectrum in Figure 49.

wavelengths are tabulated in Table V for comparison. Again, the agreement is quite good.

2) Hollow Cathode Lamp Spectra

The ability to measure a spectrum with a number of spectral lines was studied using hollow cathode lamps as the source. A Heath EUW-15 power supply was adjusted to give 20 to 35 ma of current (depending on the lamp used) to the hollow cathode lamps. The lamps were clamped in place such that the cathode was at the focal point of the input off-axis parabolic mirror. All the interferograms were averages of 50 scans except the multielement steel HCL interferogram which was 250 scans. Actually, 50 scans of the steel HCL produced good spectra, but 250 consecutive scans were acquired to test the signal averaging capability of the system (that is, the stability of the precise stop flag).

The spectrum of a multielement steel HCL was measured (Figure 51). The elements present in the HCL are: iron, chromium, nickel, copper, cobalt, and manganese. An optical filter (Corning filter number 7-59) with a peak %T at 370 nm and a greater than 10%T from 305 to 465 nm was used to limit the spectral bandwidth to approximately one aliasing region. Actually, the filter used allowed a portion of another aliasing region to be measured. The chromium triplet (427 nm) shown at the far right of the spectrum in Figure 51 belongs in

TABLE V

Wavelengths Calculated From the Spectrum Shown in Figure 49

Element	Literature (nm)	Experimental (nm)	Δ nm
Li	670.78	670.54	0.24
Na	589.59	589.40	0.19
	589.00	588.80	0.20
Ba	553.55	553.34	0.21
Sr	460.73	460.56	0.17
Ca	422.67	422.49	0.18

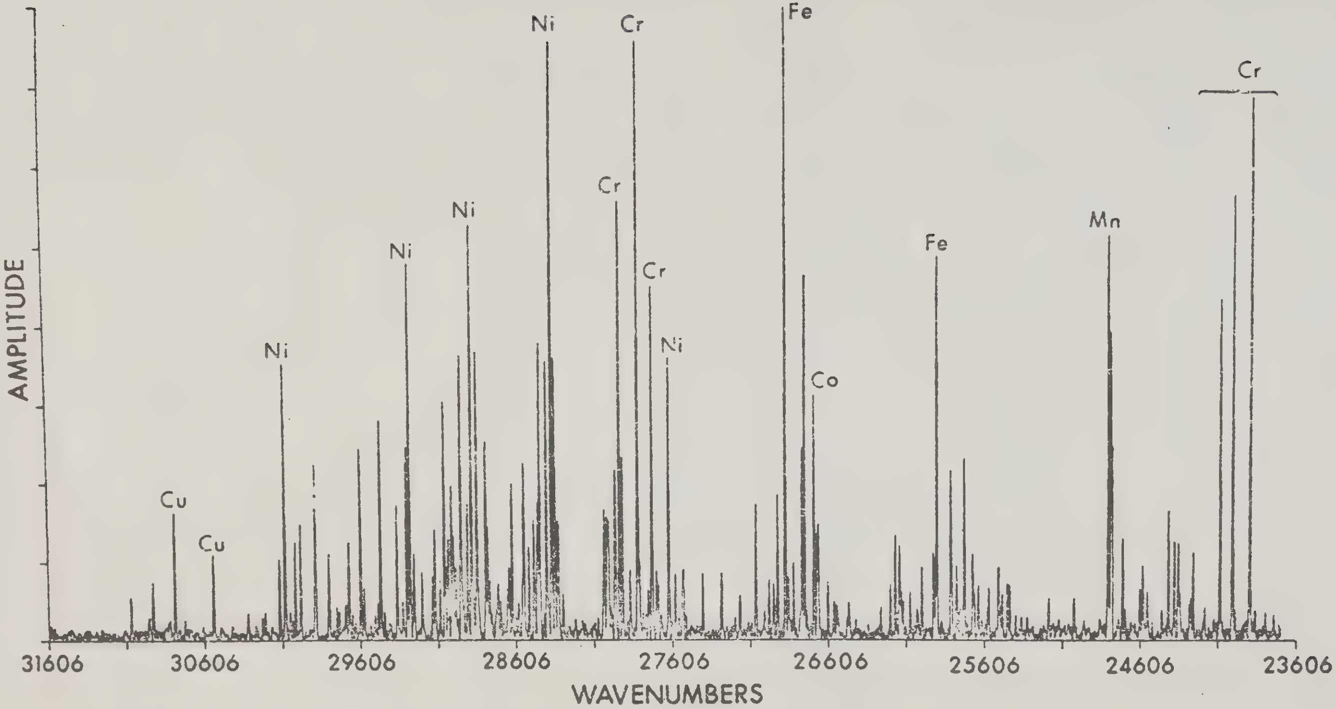

Figure 51. Spectrum of a multielement steel hollow cathode lamp.

region (9-12). The wavenumber axis shown on the spectrum is for region (13-16) which contains the remainder of the spectral lines.

The entire 4096 point spectrum is plotted for the steel HCL to emphasize the density of spectral information that is present. An important point to realize is that the entire spectrum was acquired in about 25 minutes including the Fourier transformation. If 50 scans were acquired instead of the 250 scans used for this spectrum, the time involved would only be about 6 minutes.

As a comparison, a scanning monochromator was used to measure the steel HCL spectrum. The scanning rate was set to give approximately the same resolution as in the spectrum taken with the Fourier transform spectrometer. The portion of the spectrum using the monochromator around the manganese triplet at 403 nm is shown in Figure 52. The measurement system of the Heath EU-700 Series Instrumentation for Spectroscopy was used. It consists of: EU-703-62 hollow cathode lamp power supply, a 0.35 meter monochromator, EU-701-30 PMT module, EU-20-28 log/linear current module, and a EUW-20A servo-recorder. The entrance slit width was set at 50 um, and the scan rate of the monochromator was set at 0.1 A/sec. Therefore, to measure just this 1.2 nm portion of the spectrum required 2 minutes. To cover the 305 to 465 nm range in Figure 51, the scanning

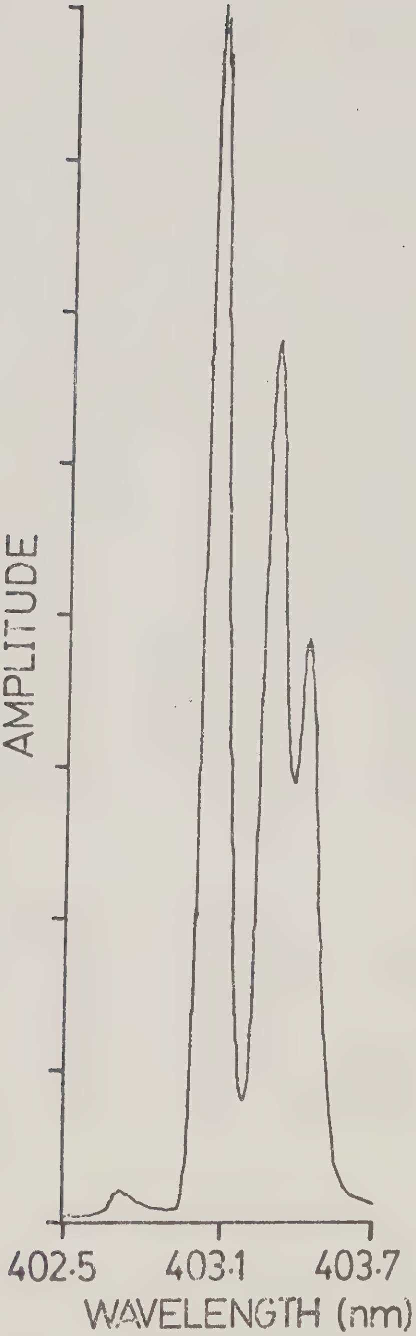

Figure 52. Spectrum of Mn 403 nm triplet using a scanning monochromator system.

monochromator would require about 260 minutes. The Heath system has a rather slow response recorder. The S/N ratio was not equalized with that in Figure 51. Even with a faster response system, the monochromator is still over an order of magnitude slower in acquiring the data. This comparison is useful to appreciate the resolution that can be achieved along with good speed of acquiring the data with the Fourier transform spectrometer.

An expanded portion of the steel spectrum measured with the Fourier spectrometer is plotted in Figure 53 showing the Mn triplet at 403 nm. The wavenumber axis is labelled for the Mn. The chromium triplet at 427 nm belongs to the next aliasing region. Expanded plots of several other portions of the steel spectrum in Figure 51 are shown in Figures 54-56. Figure 54 shows the region around the iron 371.99 nm line. Figure 55 shows the chromium triplet at 360 nm and Figure 56 shows the region around the nickel 352.45 nm line. These expanded plots show the large amount of information that is present in the entire spectrum.

Several spectral lines in Figure 51 are tabulated in Table VI. The agreement with the literature values is very good. Only a few representative lines are listed. In excess of fifty lines have been identified with the wavelength agreements in the same range as those listed in the table. Identification of the lines is

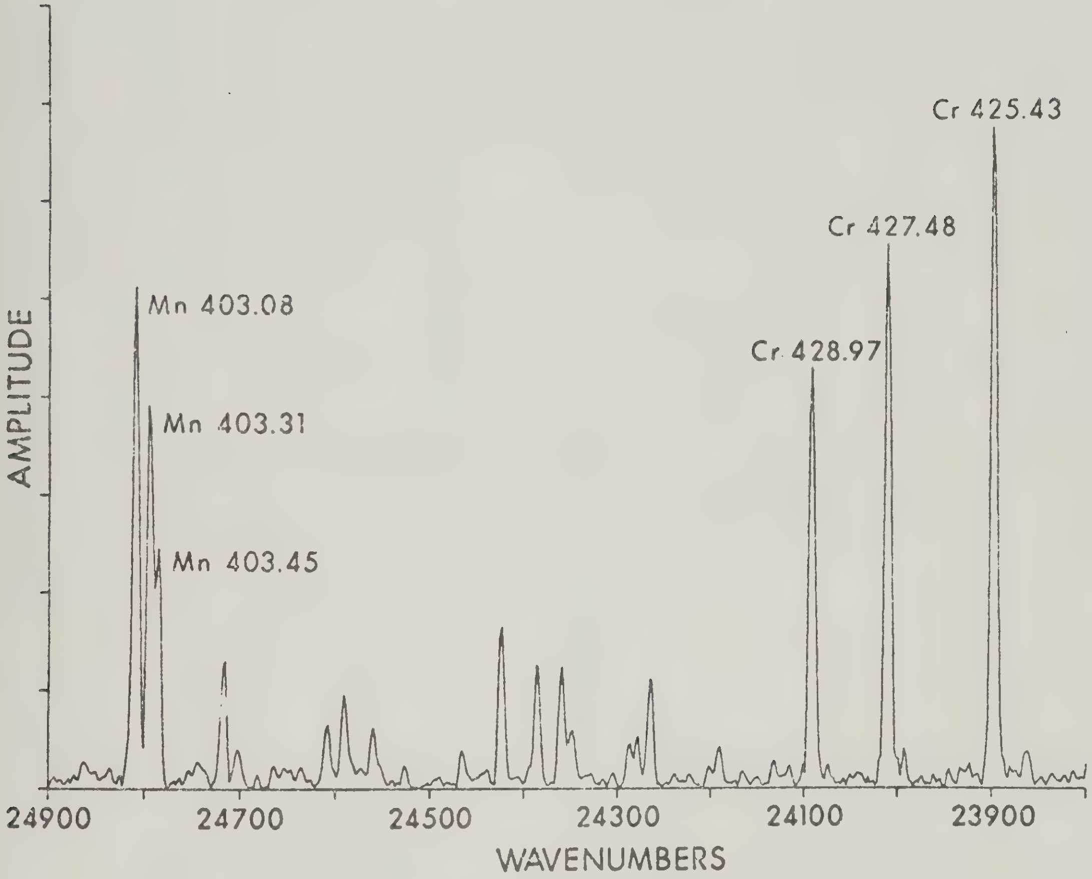

Figure 53. Expanded portion from the steel spectrum in Figure 51 showing the Mn 403 nm triplet.

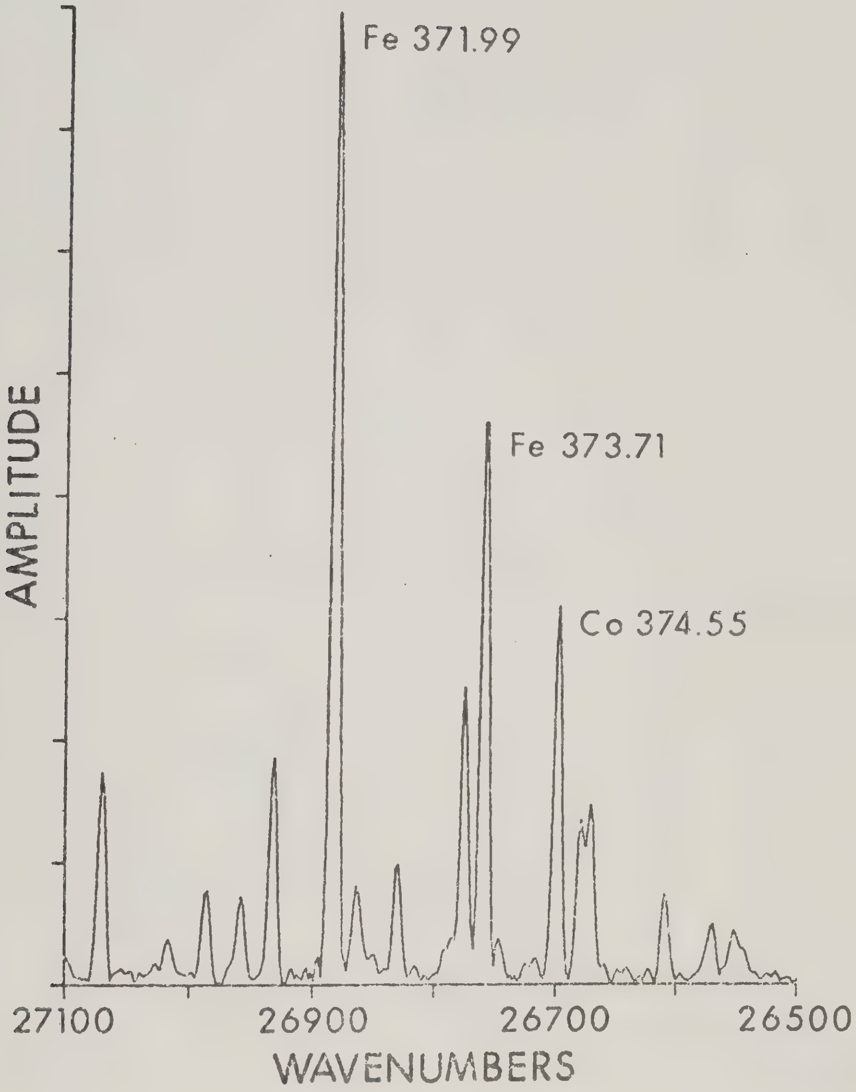

Figure 54. Expanded portion from the steel spectrum in Figure 51 in the vicinity of the Fe 372 nm line.

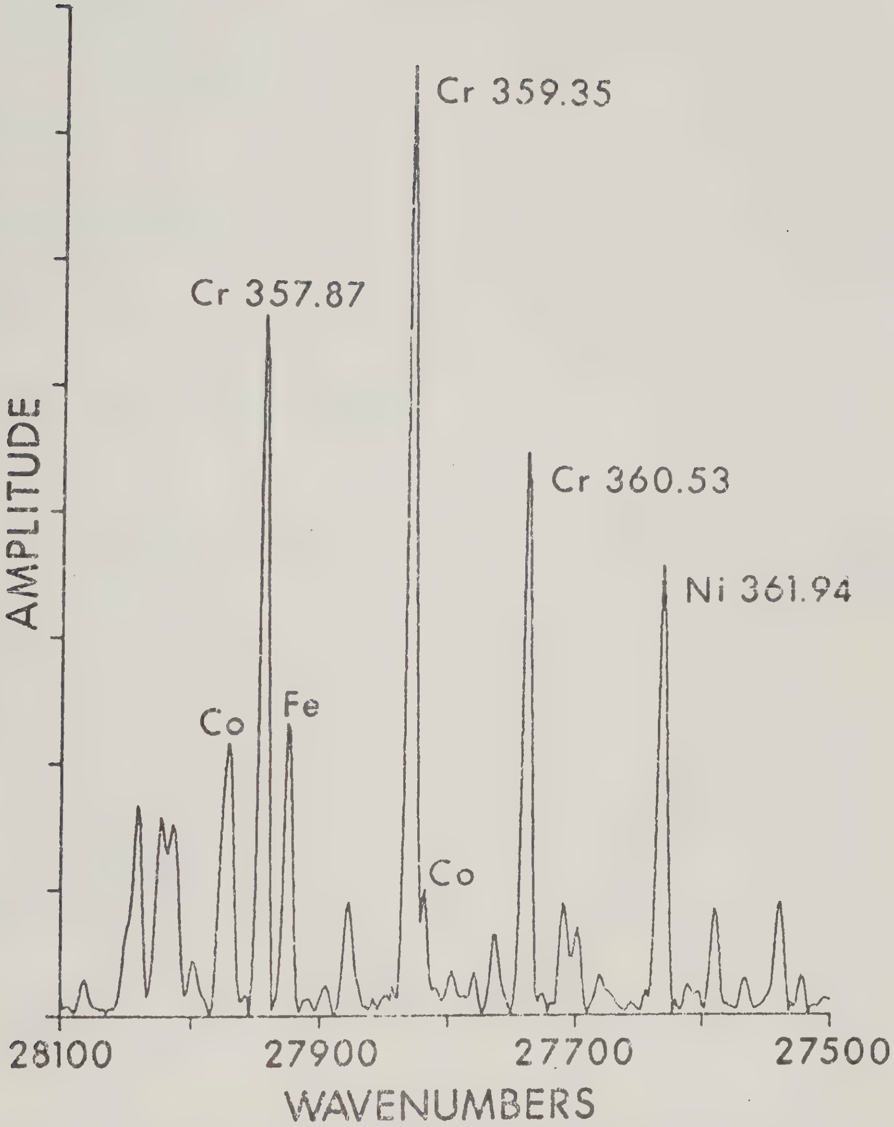

Figure 55. Expanded portion from the steel spectrum in Figure 51 in the vicinity of the Cr 360 nm triplet.

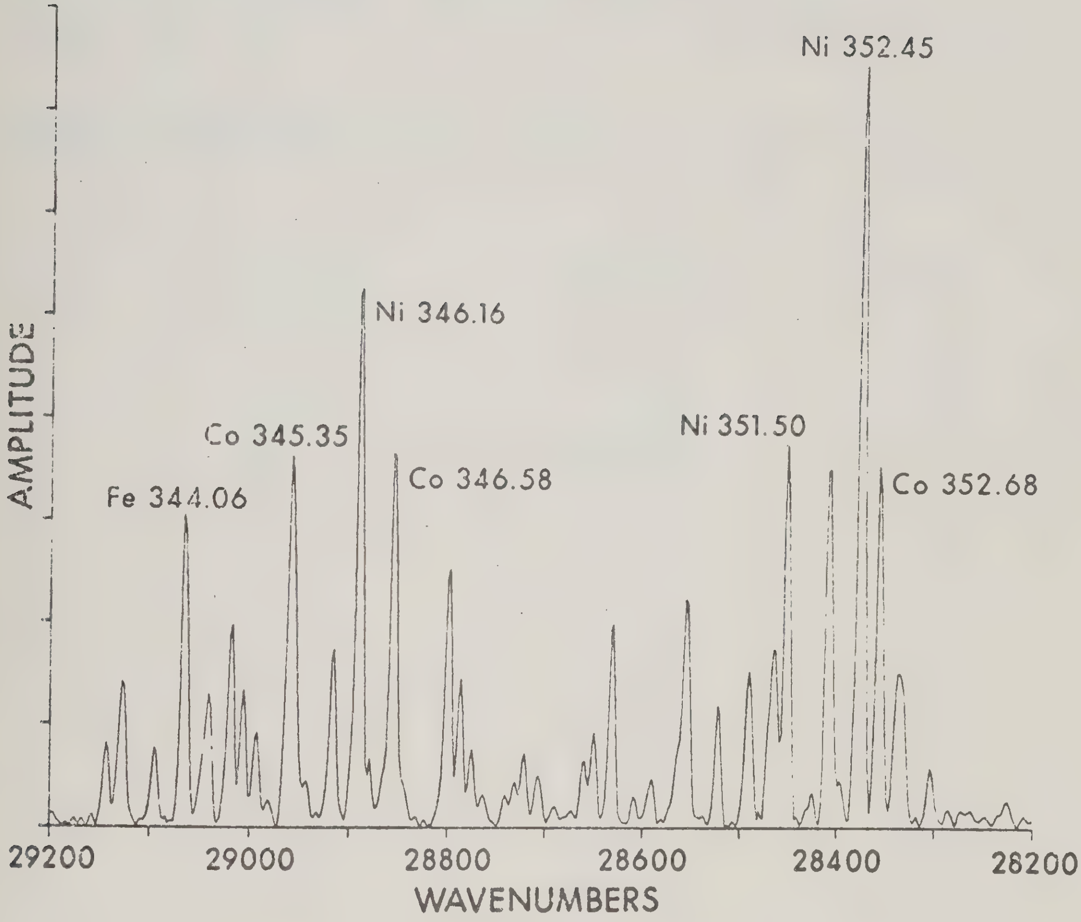

Figure 56. Expanded portion from the steel spectrum in Figure 51 in the vicinity of the Ni 352 nm line.

TABLE VI

Wavelengths Calculated From the Spectrum of the Multielement Steel HCL Shown in Figure 51

Element	Literature (nm)	Experimental (nm)	Δ nm
Mn	403.449	403.443	0.006
Mn	403.307	403.286	0.021
Mn	403.076	403.066	0.010
Co	374.550	374.548	0.002
Fe	371.994	371.968	0.026
Cr	360.532	360.505	0.027
Cr	359.348	359.331	0.017
Cr	357.868	357.842	0.026
Ni	352.454	352.440	0.014
Cu	327.396	327.372	0.024
Cu	324.754	324.726	0.028

straightforward because of the accurate wavelengths. With the Fourier transform spectrometer, the wavenumber axis is inherently accurate (depending only on the accuracy of the He-Ne laser and the accuracy of the sampling). There is no external calibration necessary.

The spectrum of other hollow cathode lamps have also been measured to further illustrate the capability of the Fourier transform spectrometer. Figure 57 shows the spectrum of a calcium, aluminum, magnesium three element HCL. The last 3000 points of the 4096 point spectrum are plotted in Figure 57(a). Again, the Corning filter 7-59 was used. The wavenumber axis is for region (13-16). The calcium 422.67 nm line belongs in another aliased region (9-12). Figure 57(b) shows an expanded portion of the spectrum. The Mg lines around 383 nm, the Ca line at 393.37 nm, and the aluminum lines around 396 nm are shown. The smaller peaks in the spectrum are due to the neon filler gas. Table VII tabulates the calculated lines from four independently measured spectra.

The spectrum of a chromium HCL is shown in Figure 58. The optical filter (7-59) was used. Only about 3000 points of the spectrum are plotted in Figure 58(a). The wavenumber axis is for region (13-16). The Cr triplet at 360 nm is expanded in Figure 58(b). The Cr 427 nm triplet at the far right in Figure 58(a) is expanded in Figure 58(c). This triplet belongs in region (9-12).

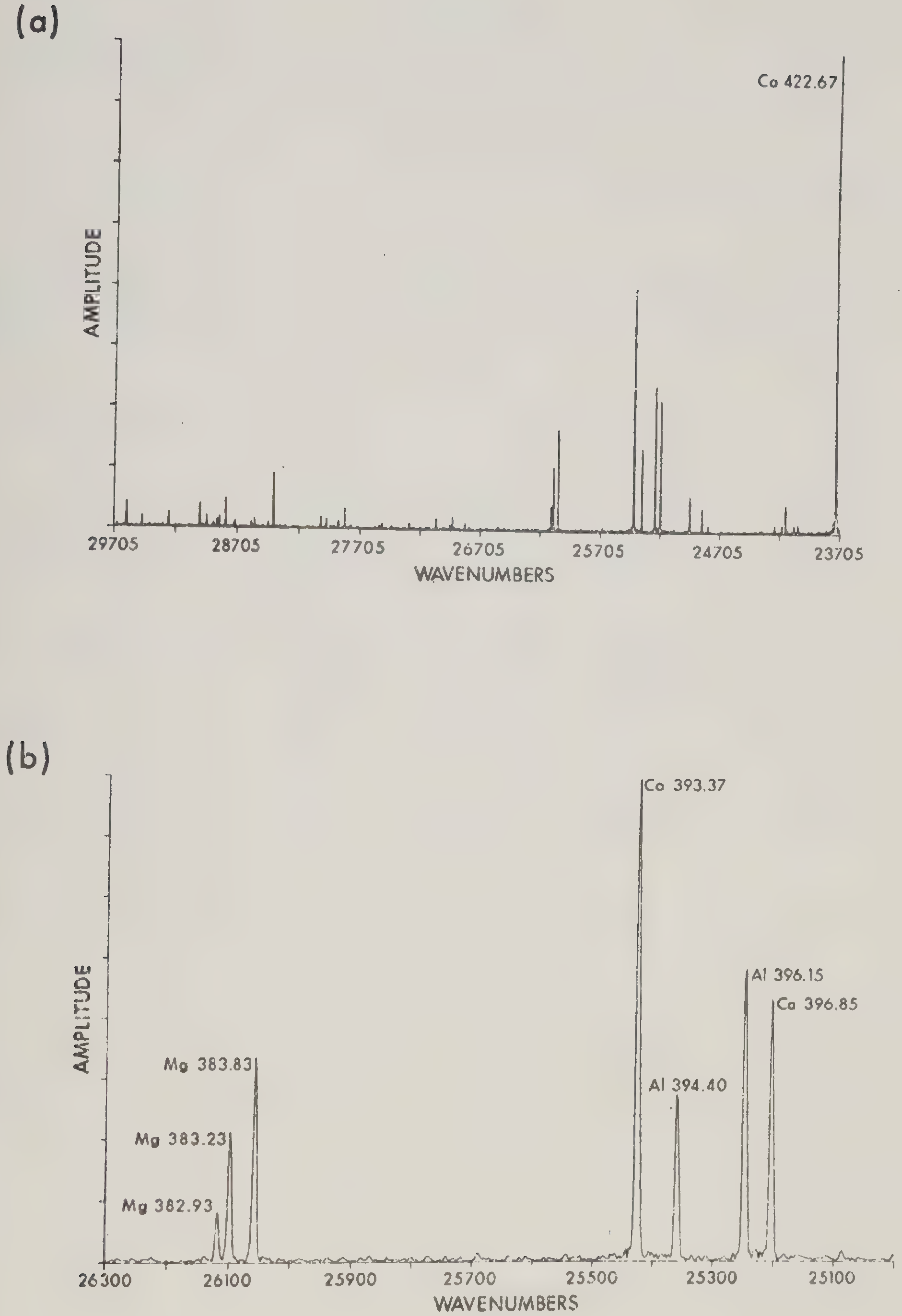

Figure 57.a) Spectrum of a Ca-Al-Mg hollow cathode lamp.
b) Expanded portion of the spectrum in a) showing some magnesium, calcium, and aluminum lines.

TABLE VII

Wavelengths Calculated From Spectra of the Ca-Al-Mg HCL

Literature Values (nm)		Experimental Values (nm)			
		1	2	3	4
Mg	382.93	382.88	382.88	382.88	382.88
Mg	383.23	383.16	383.16	383.16	383.16
Mg	383.83	383.76	383.76	383.79	383.76
Al	394.40	394.33	394.36	394.36	394.33
Al	396.15	396.10	396.10	396.10	396.07
Ca	393.37	393.31	393.31	393.31	393.31
Ca	396.85	396.77	396.77	396.80	396.77

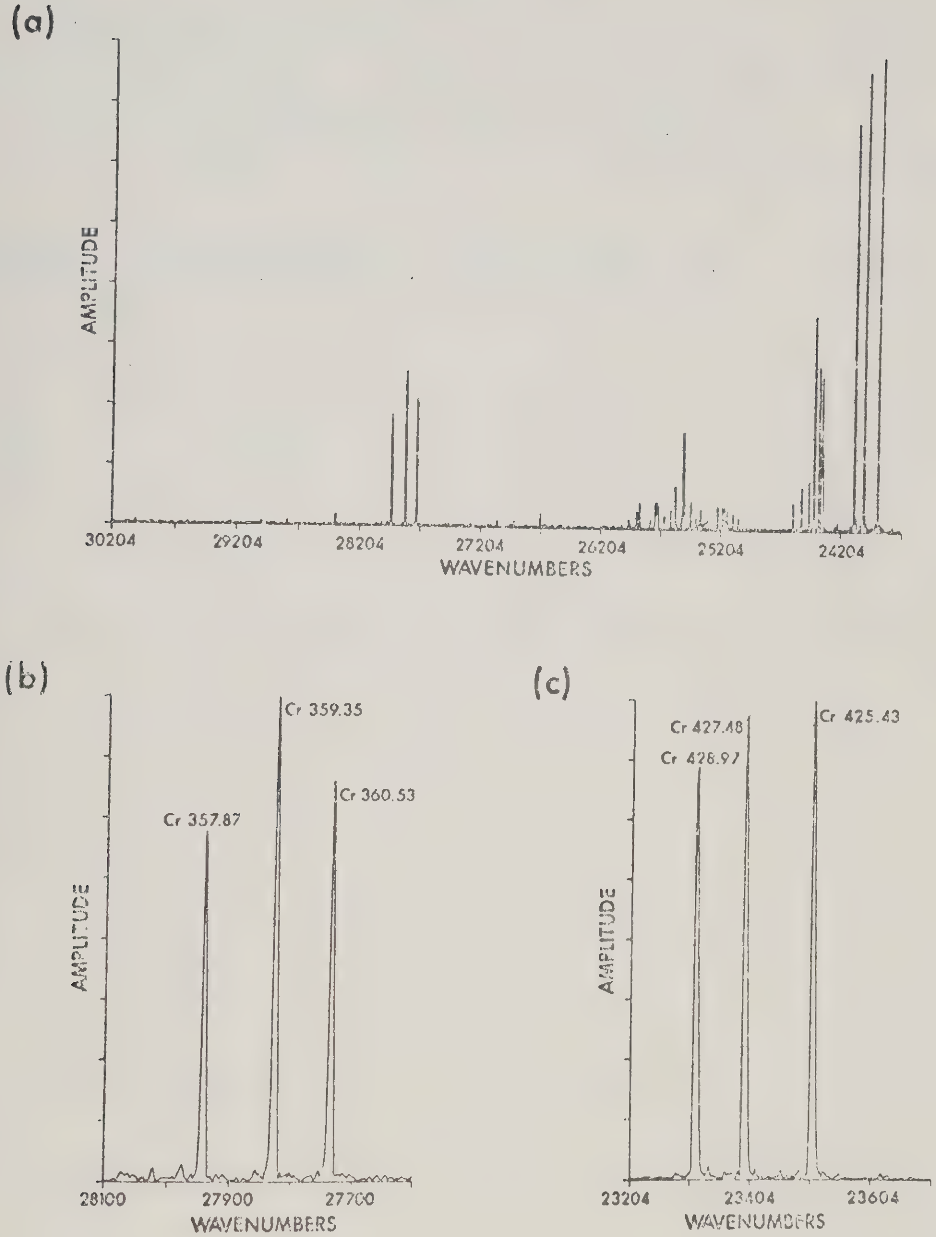

Figure 58. (a) Spectrum of a chromium hollow cathode lamp.
(b) Expanded portion around the Cr 360 nm triplet.
(c) Expanded portion around the Cr 427 nm triplet.

TABLE VIII

Wavelengths Calculated From the Spectrum of the Chromium HCL Shown in Figure 58

Element	Literature (nm)	Experimental (nm)	Δ nm
Cr	357.87	357.87	0.00
Cr	359.35	359.36	0.01
Cr	360.53	360.53	0.00
Cr	428.97	428.92	0.05
Cr	427.48	427.43	0.05
Cr	425.43	425.40	0.03

The axis is relabelled for this region in Figure 58(c). The measured wavelengths are compared with the literature values in Table VIII. The agreement is excellent.

3) Effect of Large Spectral Features on Small Peaks

One disadvantage of the Fourier spectroscopy technique is that, if one is interested in a small spectral peak, large unwanted signals may have to be measured as well. Optical filtering may help to reduce the unwanted signal, but there may be instances where the two signals are too close in wavelength to allow effective optical filtering. As the unwanted signal increases in amplitude, there may be a decrease in the S/N ratio of the small peak of interest. This effect was investigated by measuring the flame emission of a strontium/calcium solution and a strontium/sodium solution.

The flame emission of a solution of 10 ppm Sr and 1000 ppm Ca was measured (Figure 59). The Sr 460.73 nm line occurs near the 21802.8 cm^{-1} mark. The Ca 422.67 nm line at the right and the CaOH bands to the left are much larger than the Sr peak, yet, the Sr signal is still measurable. Figure 60 is an expansion of the Sr peak. Note the baseline noise in this and subsequent expanded plots of the Sr peak in this section. The noise levels will be discussed shortly.

Another example is shown in Figures 61 to 65 where the Sr concentration was kept constant at 10 ppm and the

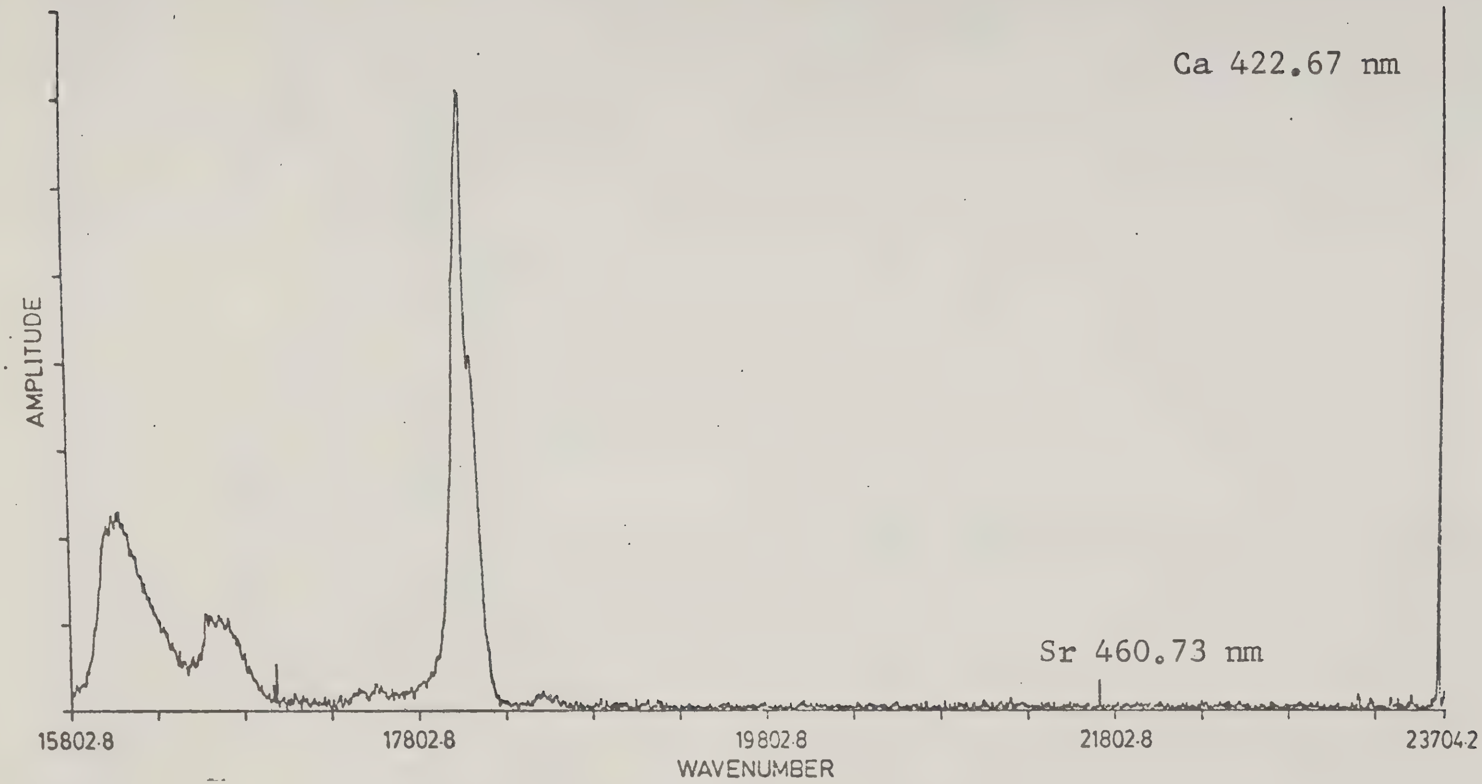

Figure 59. Flame emission spectrum of a solution of strontium (10ppm) and calcium (1000 ppm).

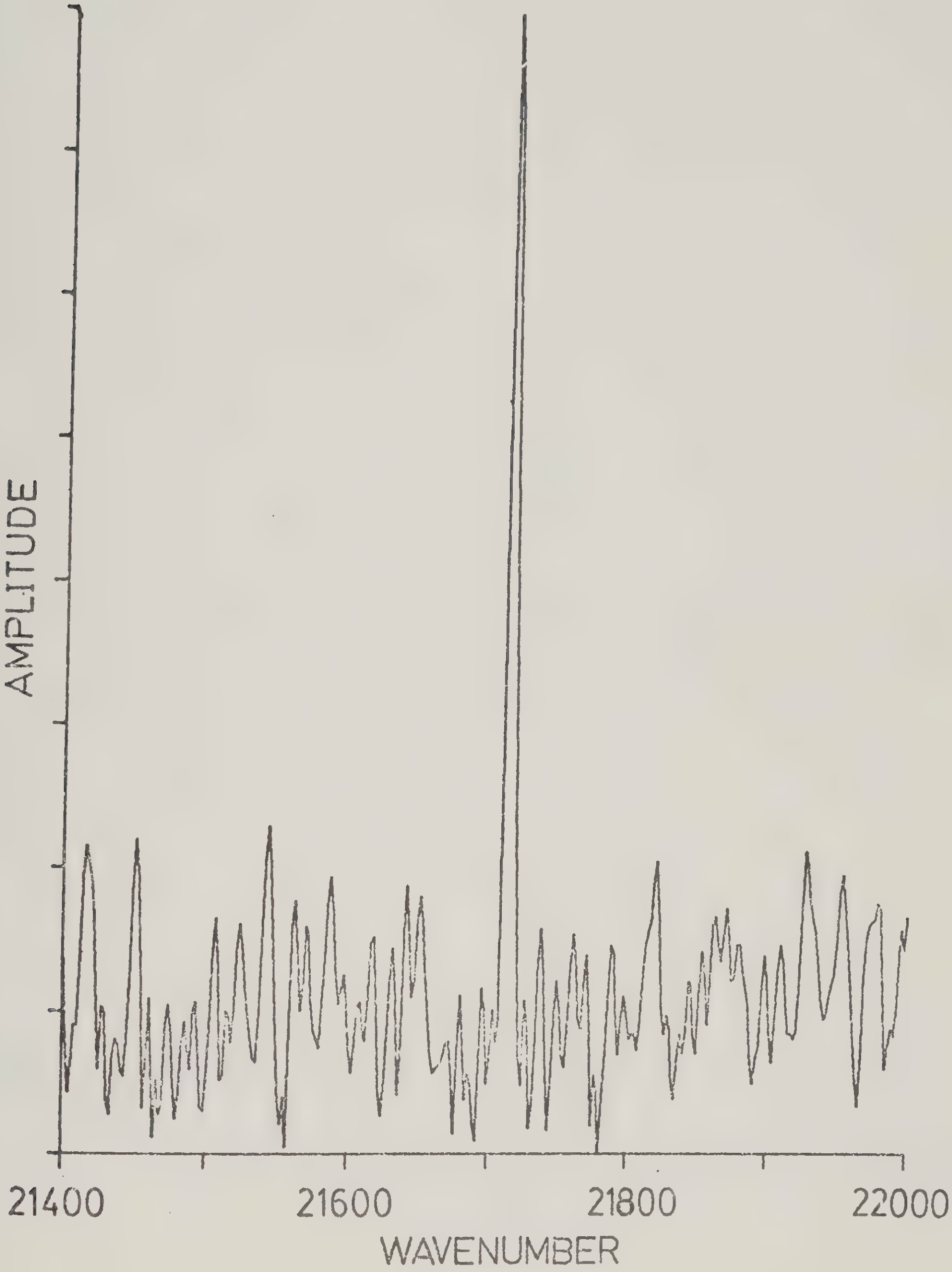

Figure 60. Expanded portion of the Sr 10/Ca 1000 ppm spectrum in Figure 59 around the Sr peak.

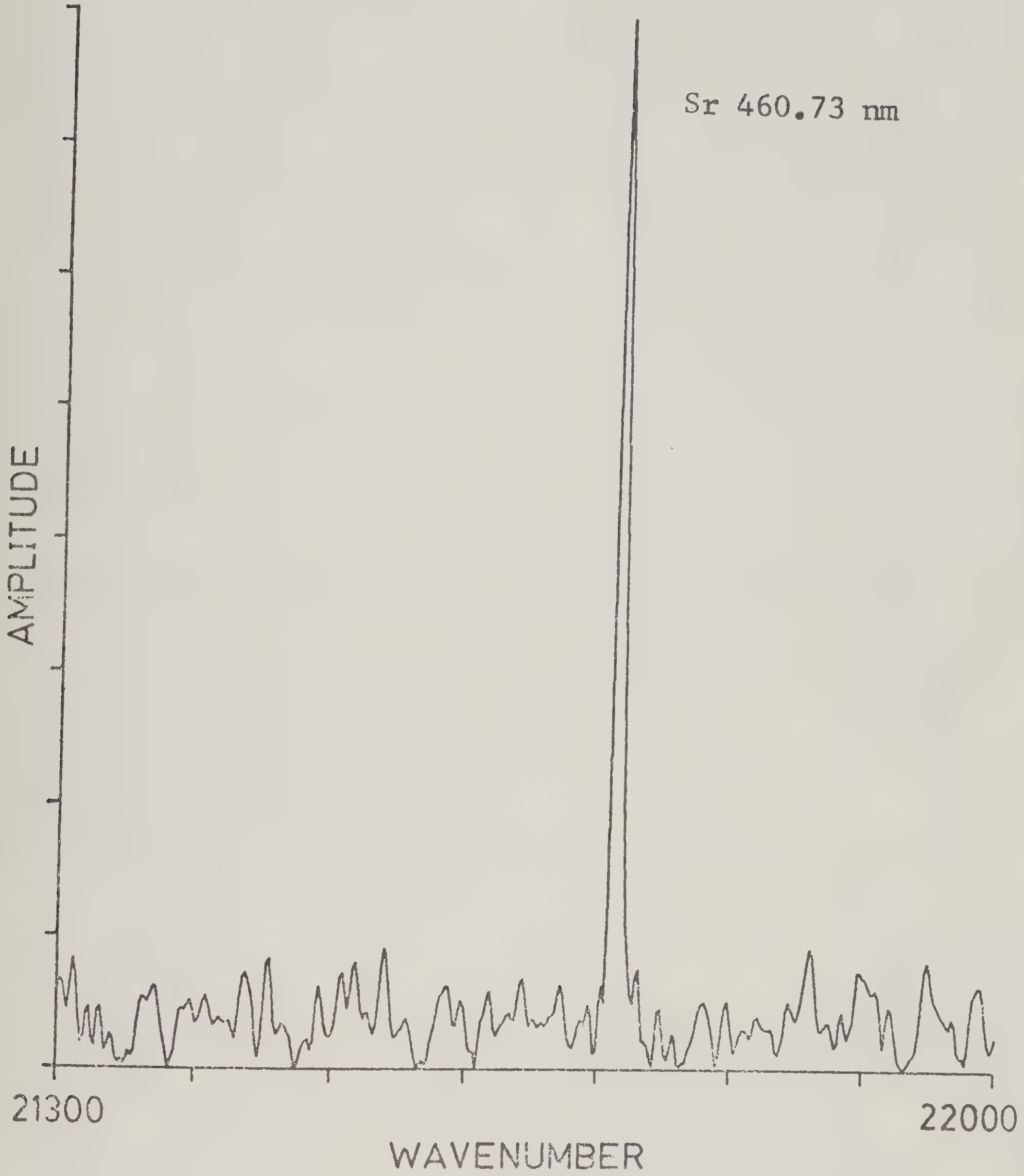

Figure 61. Flame emission spectrum of a solution of 10 ppm strontium by itself.

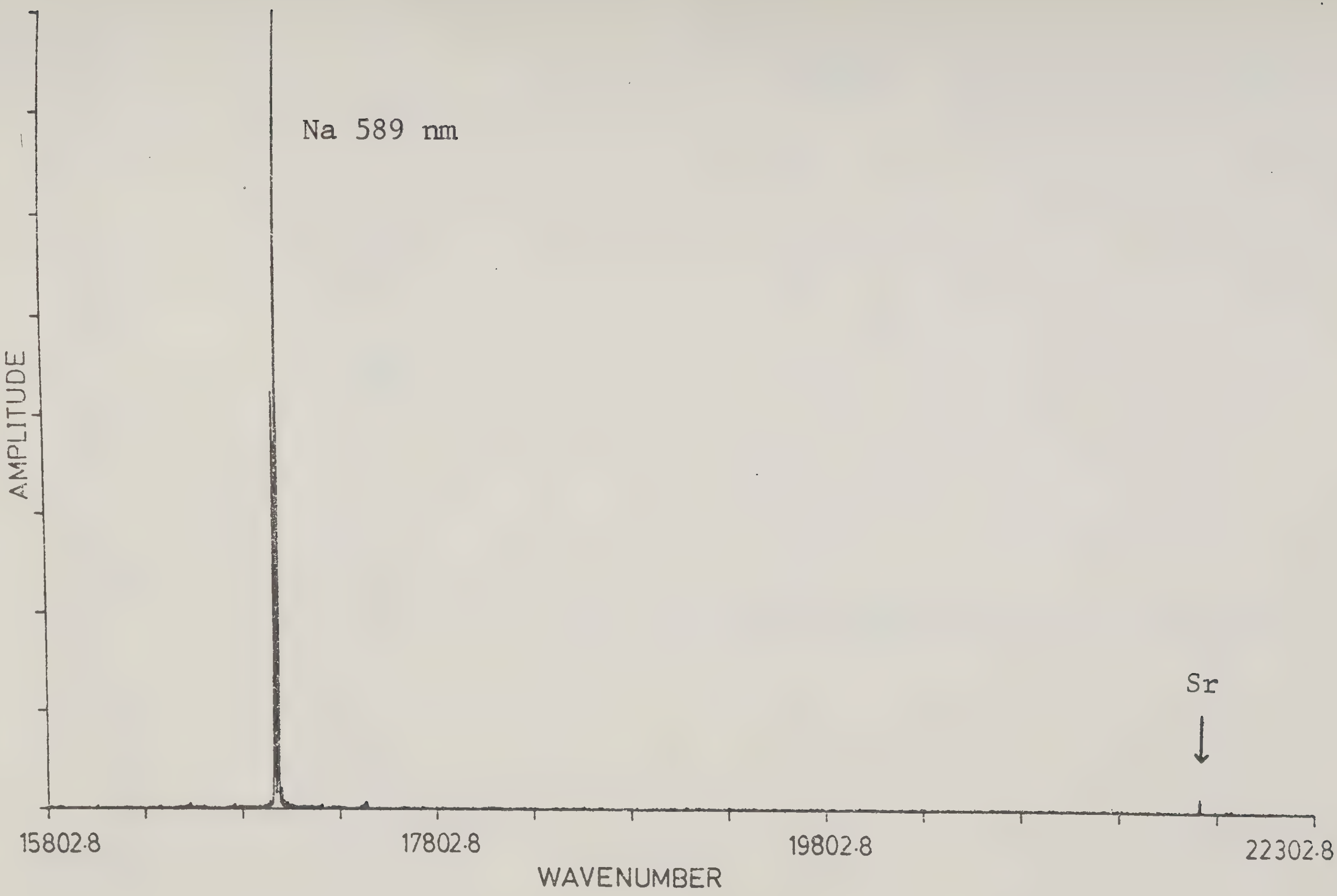

Figure 62. Flame emission spectrum of a solution of Sr (10ppm) and Na (10ppm).

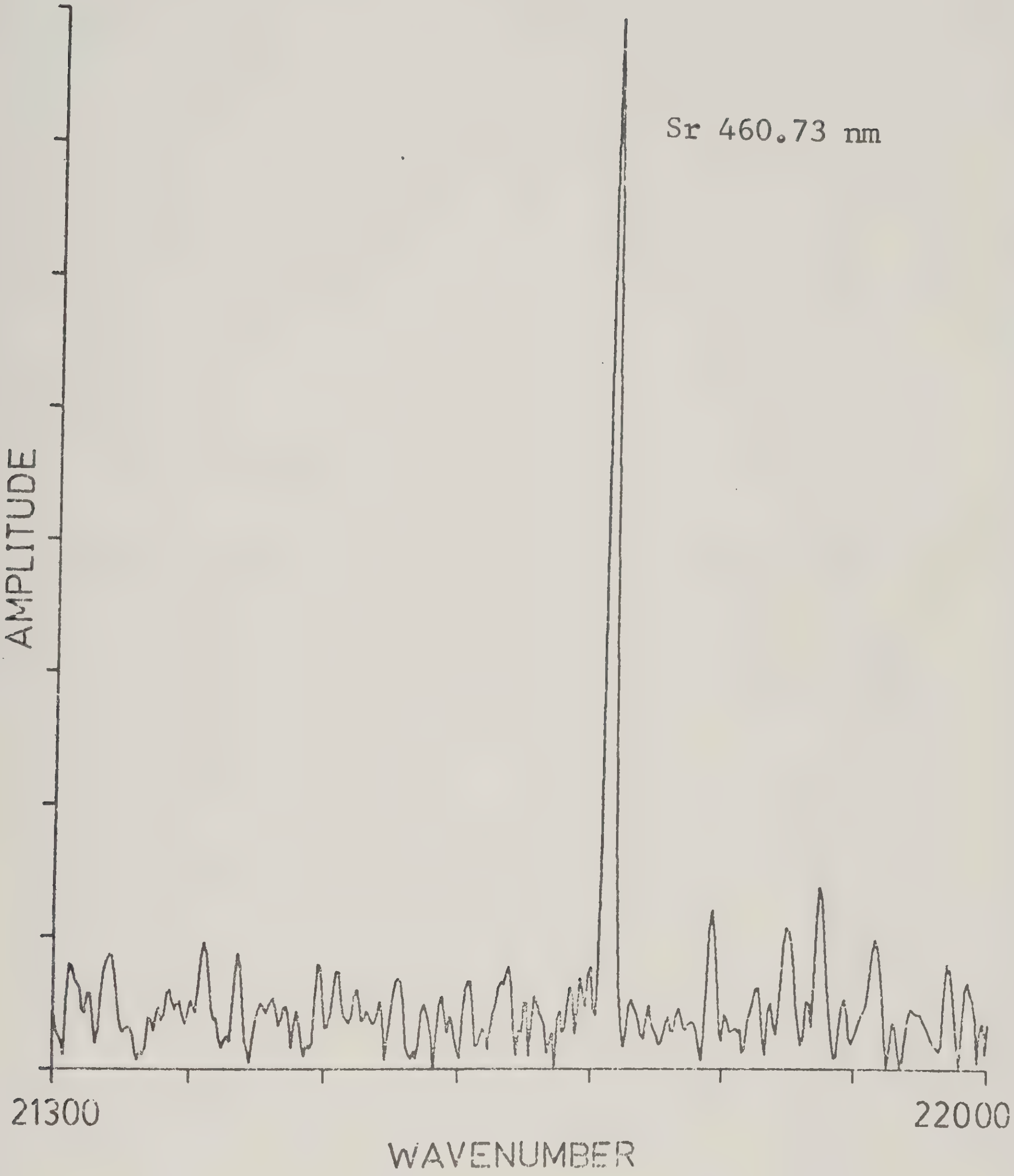

Figure 63. Expanded portion of the Sr 10/Na 10 ppm spectrum showing the Sr peak.

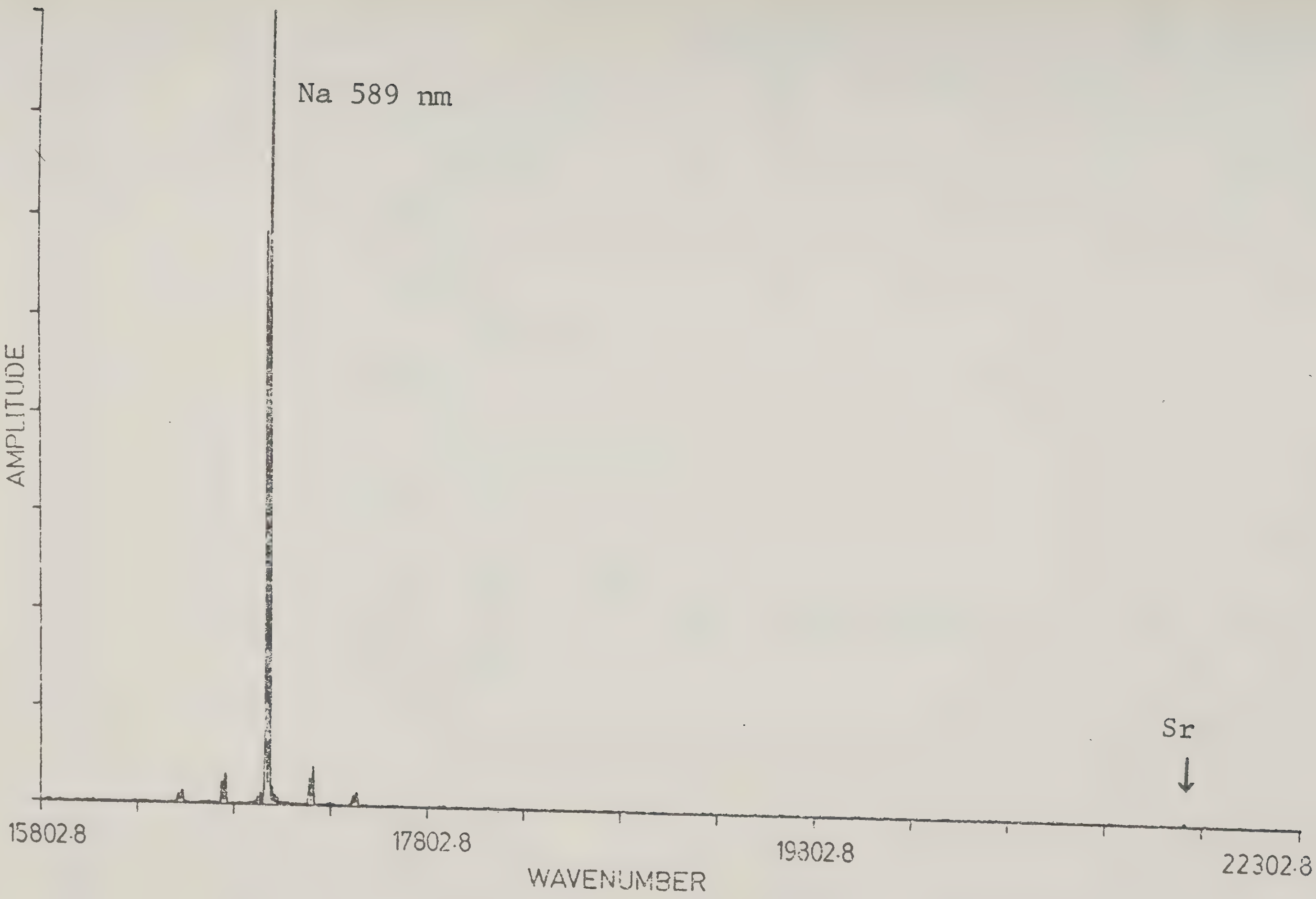

Figure 64. Flame emission spectrum of a solution of Sr (10ppm) and Na (100ppm).

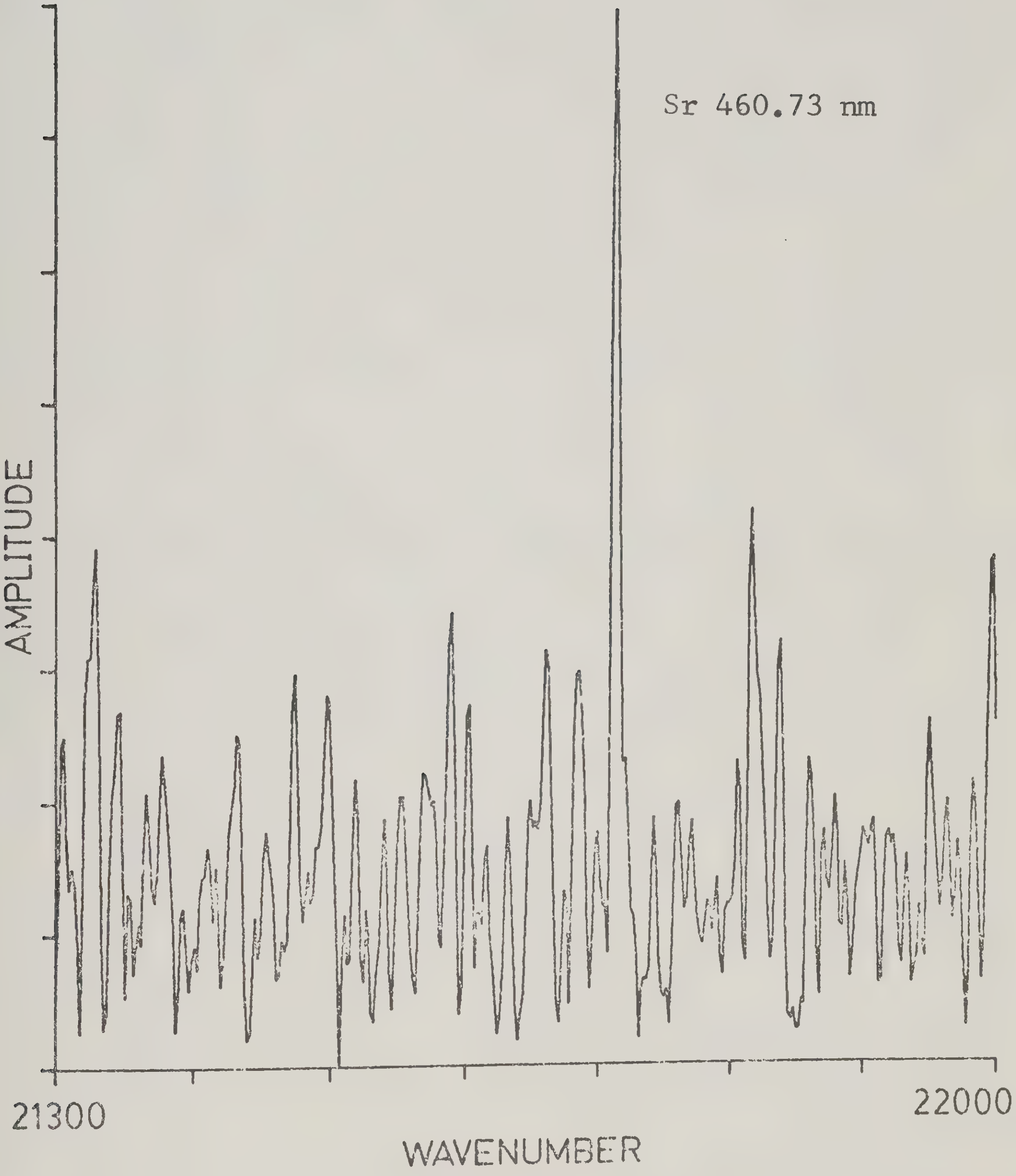

Figure 65. Expanded portion of the Sr 10/Na 100 ppm spectrum showing the Sr peak.

Na concentration was increased. In Figure 61, the spectrum was obtained with Sr by itself. Only the region around the Sr peak is plotted. Figure 62 shows the spectrum of Sr at 10 ppm and Na at 10 ppm (only the first 3370 points are plotted, the remainder of the points being continued baseline). The Sr peak is at the right and is fairly small. Figure 63 is an expansion of the region around the Sr peak. Note that the noise level has increased very slightly from Figure 61 to Figure 63. Figure 64 shows the spectrum of Sr at 10 ppm and Na at 100 ppm. The Sr peak can barely be seen. (The peaks around the Na doublet are images due to reflections off the beam-splitter substrate and compensator surfaces and are dependent on the mirror alignment.) The portion of the spectrum around the Sr peak is expanded in Figure 65. The noise level now has increased considerably.

These two examples, however, lead to differing views of the effect of large spectral features on small peaks. The Na/Sr example shows a decrease in the S/N as the large Na peaks are increased in amplitude (10 ppm Na to 100 ppm Na). This is as expected when using a signal noise limited detector such as a PMT, where the noise increases as the square root of the signal intensity (shot noise). Therefore, if much unwanted signal is present, the baseline noise increases (in Fourier spectroscopy, noise in the interferogram translates into

a noise that is distributed throughout the spectrum).

But, the Ca/Sr example seems to contradict the above view. From inspection of Figure 59, the CaOH bands are broad and intense, therefore, there must be orders of magnitude more total signal than in the Na/Sr spectra. Yet, the Sr peak is not orders of magnitude noisier than the Sr peak with just Sr present (Figure 61).

The above contradiction cannot be explained without further detailed measurements of signal and noise. There must be other factors which contribute to the baseline noise. One point to note is that, in addition to the varying flux of light as optical retardation is changed (this is the interferogram), there is a constant flux present as well. This may contribute to the noise since as the overall intensity of incoming light increases, this constant flux level also increases. The detector receives a higher overall flux, hence a greater detector noise results. Another factor is that the amplitude spectrum is calculated, thus, the baseline noise is always positive. Hence, small peaks may get buried in the positive baseline noise. Quantizing noise was considered. But measurements made with the same preamp gain did not change the results to any great extent.

The behavior of the S/N ratio in the two examples is still a mystery. The explanation may be in one of the above factors or in others, therefore, further studies

must be undertaken. Whatever the outcome and in spite of the noise contributions above, the ability to measure small peaks in the presence of large spectral features is still quite acceptable. The small Sr peak that is expanded in Figure 65 is only 0.3% of the Na peak amplitude in Figure 64.

C. Measurements in the Ultraviolet Region

The measurements made in the ultraviolet region used a solar blind photomultiplier tube (R-166). The spectral response of the PMT limits the spectral region that is measured to the aliasing region (17-20). A magnesium hollow cathode lamp was used as the source.

Figure 66(a) shows the spectrum obtained from a 512 point double-sided interferogram using a 0.6328 um sampling interval. The resolution is not good enough to resolve several of the peaks. The peak numbers refer to the lines listed in Table IX. Peak 3 is actually three lines and peak 4 is a quintet. To achieve higher resolution, the sampling interval was increased to 2.5312 um (still 512 data points). The lines are now highly aliased (Figure 66(b)). The wavenumber axis is shown for peaks 2, 3, and 4 in region 19 and for the large 285.21 nm peak which is in region 18.

The spectral region in Figure 66(b) around the peaks 1 to 4 was interpolated using the zero-filling technique (73). The result is shown in Figure 67. All the peaks are resolved and their wavelengths are listed in Table IX. The agreement with the literature values is very good.

When the new PDP-11/10 system was available, the Mg spectrum was measured again. The interferogram

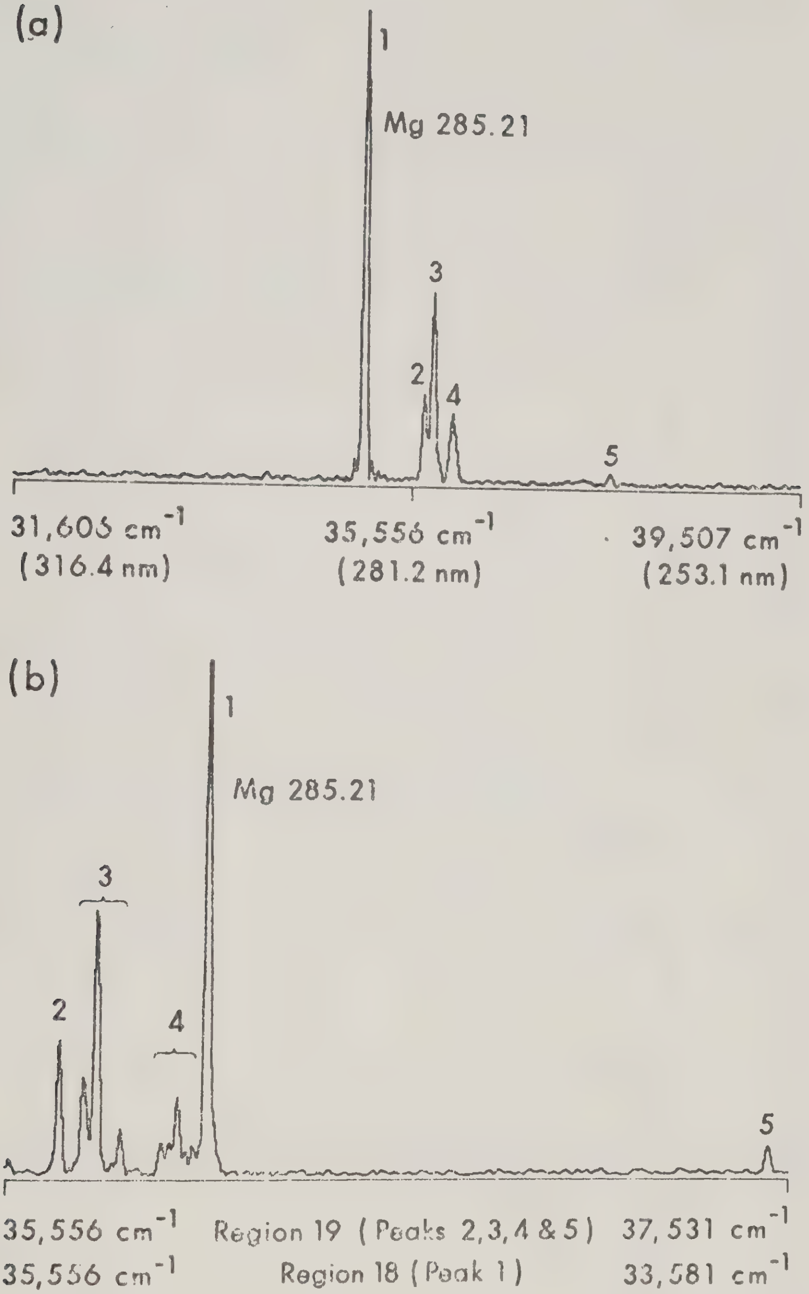

Figure 66. Spectrum of a Mg hollow cathode lamp (512 point data) (a) with a 0.6328 um sampling interval, (b) with a 2.5312 um sampling interval.

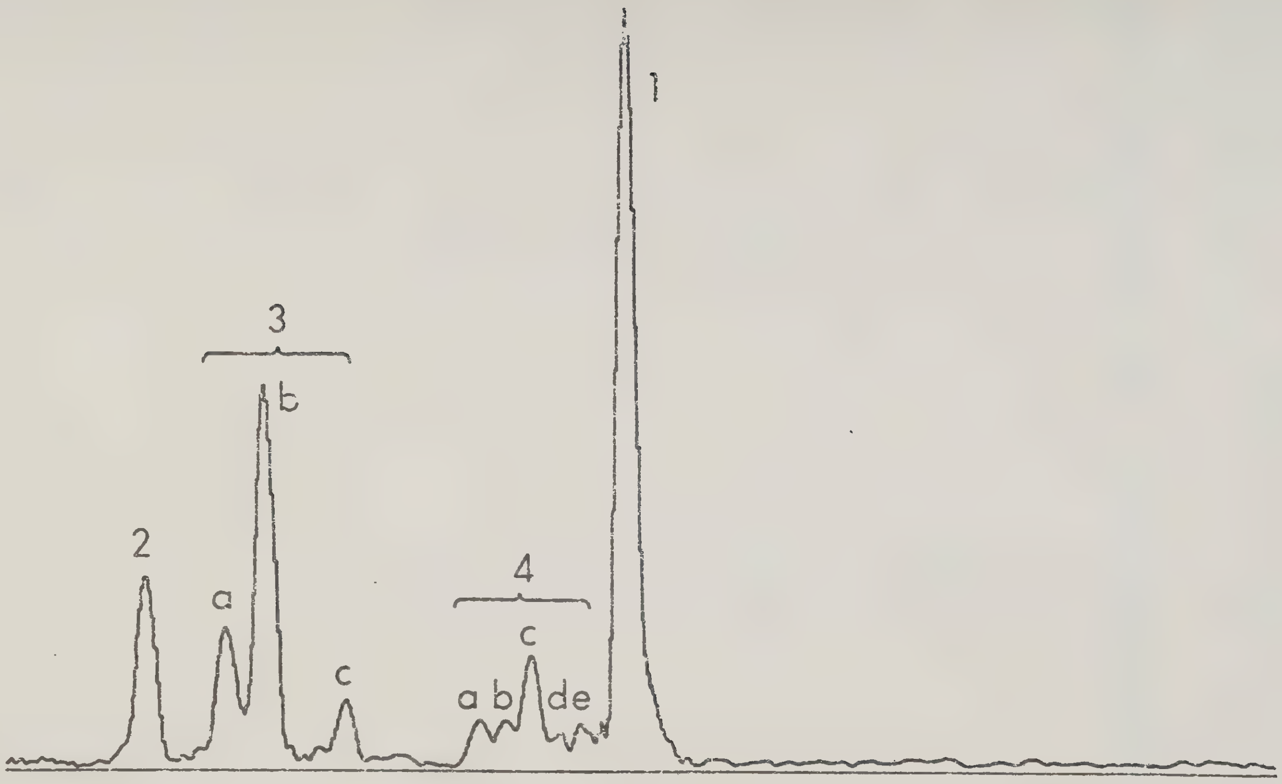

Figure 67. The spectrum of Mg in Figure 66(b) interpolated using the zero-filling technique.

TABLE IX

Wavelengths of Magnesium Spectral Lines

Shown in Figure 67

Line	Literature (nm)	Experimental (nm)	Δnm
1	285.18	285.21	0.03
2	280.26	280.27	0.01
3a	279.79	279.81	0.02
3b	279.54	279.55	0.01
3c	279.08	279.08	0.00
4a	278.28	278.30	0.02
4b	278.12	278.14	0.02
4c	277.97	277.98	0.01
4d	277.81	277.83	0.02
4e	277.69	277.67	0.02

is now 4096 points long. The resultant spectrum using the 0.6328 um sampling interval is shown in Figure 68. Only the section around peaks 2 to 4 is plotted. This spectrum can be compared with Figure 66(a) to see the increased resolution with the longer interferogram. All the peaks are resolved in Figure 68. The 285 nm line is past the left end of the plotted spectrum.

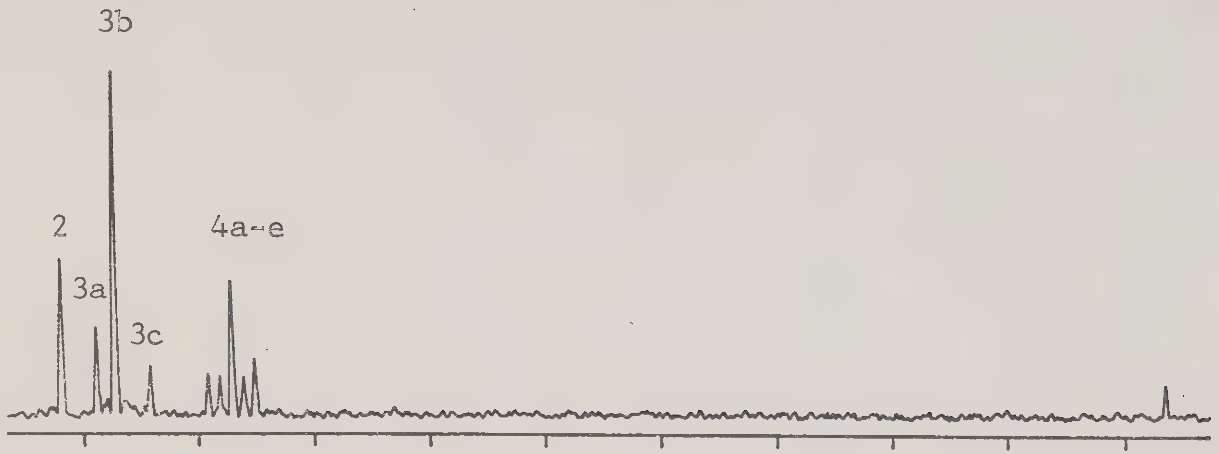

Figure 68. Spectrum of a Mg hollow cathode lamp using a 0.6328 um sampling interval (4096 point data).

D. Infrared Measurements

The Fourier transform spectrometer is also capable of infrared measurements. The modularity of the spectrometer allows the beamsplitter assembly, the source, and the detector to be easily changed for mid-IR measurements. The beamsplitter assembly uses NaCl substrate and compensator instead of quartz. Infrared studies were not done in detail. Measurements were taken to show the IR capability only.

A globar (air cooled) was used as the source. A polystyrene absorption spectrum was obtained by placing a film sample directly in front of the TGS detector in the detector assembly.

The background spectrum is shown in Figure 69(a) and the polystyrene spectrum in Figure 69(b). Only the mid-IR region of the spectrum is plotted.

The double-sided interferograms are shown in Figure 70 (background) and Figure 71 (polystyrene) to illustrate the difference in the interferograms between a broadband source and the line emission type sources presented earlier in this chapter. The middle 3000 points of the 4096 point interferograms are plotted.

Infrared measurements are the subject of a future study and are therefore only mentioned to show that the spectrometer can be used in the mid-IR.

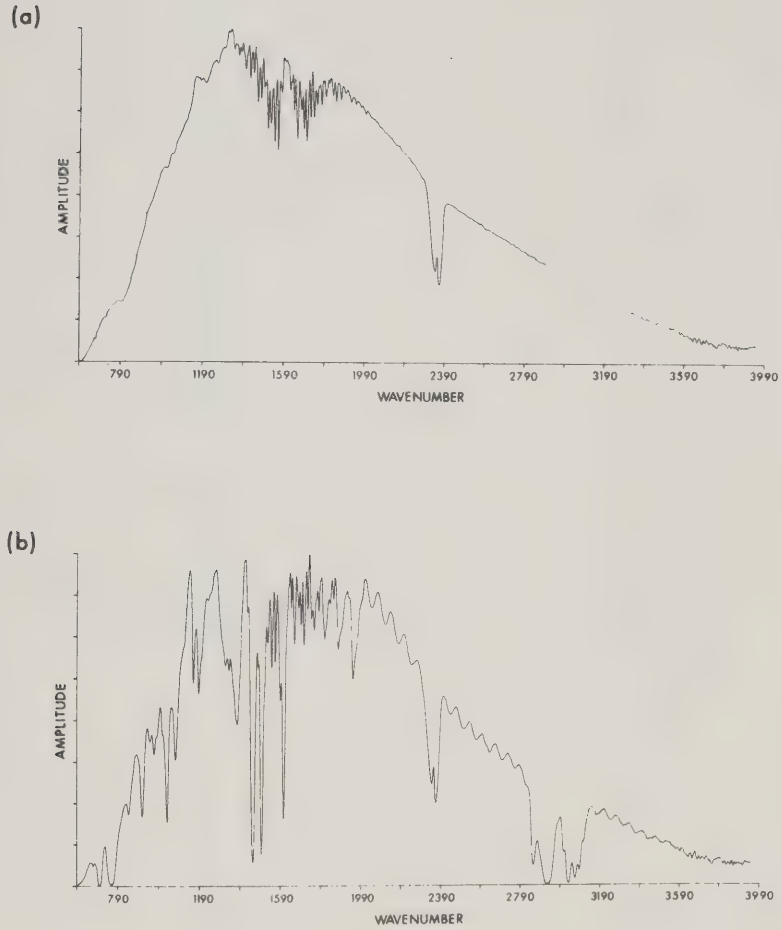

Figure 69. (a) Background spectrum with a glowbar source in the mid-IR region.
(b) Polystyrene absorption spectrum.

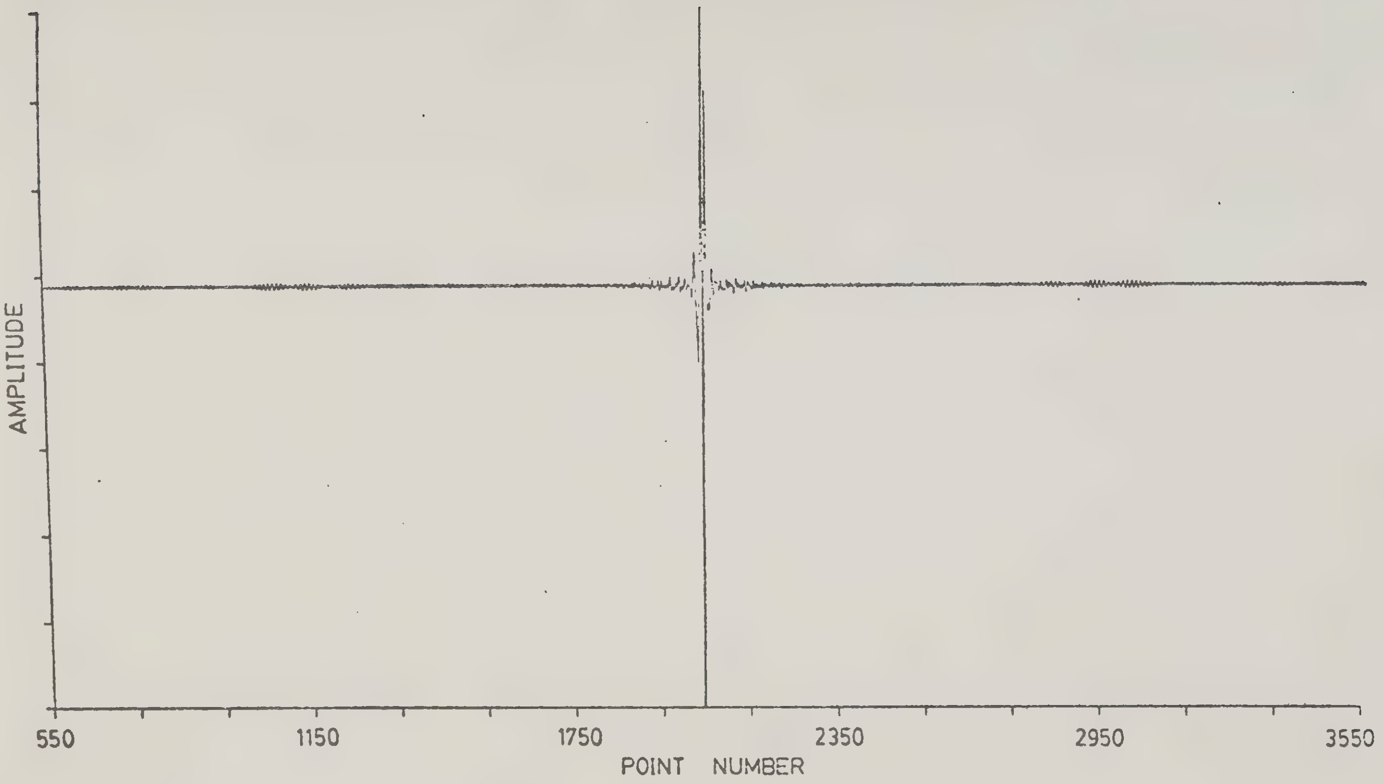

Figure 70. Digitized interferogram of the background spectrum.

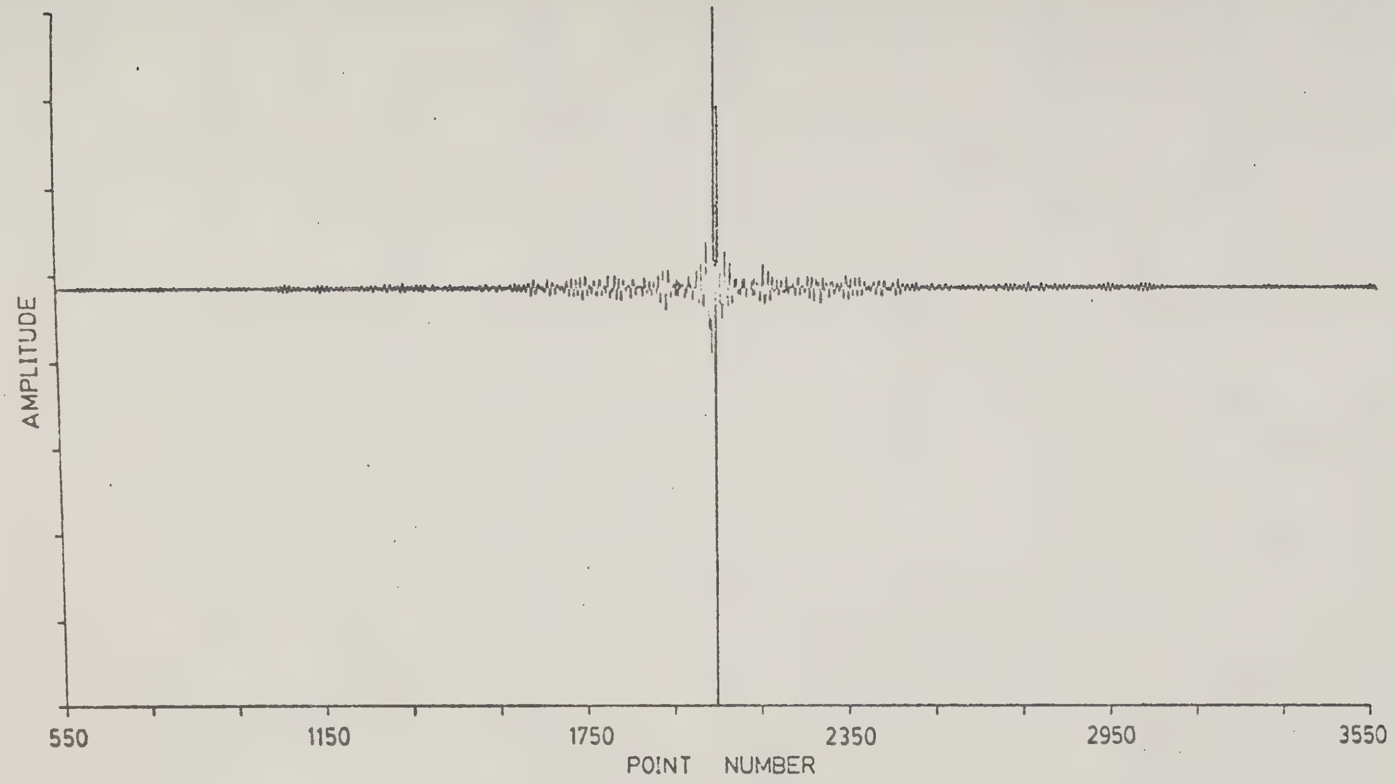

Figure 71. Digitized interferogram of the polystyrene spectrum.

CHAPTER VIII

SUMMARY

The Michelson interferometer described in Chapter VI has developed considerably from the initial design. The earlier interferometers were slow scanning using a micrometer drive. The interferogram was recorded with a digital voltmeter. The raw data was then translated onto computer cards and taken over to the computer center for the Fourier transform calculation and output plots of the processed data. The present design is fast scanning and is laser fringe referenced for digitization. The data is acquired directly and processed immediately with the minicomputer.

The interferometer is now at the stage where emphasis can be placed on experimental applications rather than on instrumental developments. This does not mean that further improvements and changes cannot take place. However, the measurements taken to this date show that the Fourier transform spectrometer is capable of producing medium resolution, high quality spectra.

To achieve this capability at shorter wavelengths than the mid-IR, several factors had to be considered. The higher spectral frequencies immediately create difficulties in the proper sampling of the interferogram. Since avoiding aliasing is not practical normally, it must

be accepted and even, perhaps, put to use.

The measurement of atomic line spectra in the UV-visible region differs from that of absorption spectra in the IR. The instrumental line shape and the means to change it for narrow emission type signals has been studied. The fundamental line shape in Fourier transform spectroscopy (sin x/x) introduces undesirable features (side lobes) in the spectrum. Therefore, apodization of the proper types must be applied to the interferogram.

Another problem with narrow emission type signals is the difficulty of phase correction. This was investigated in order to find methods of overcoming spectral distortions due to phase error. A solution was not found to correct for phase problems with single-sided interferograms. Therefore, the problem was avoided with the use of double-sided interferograms.

With a better understanding of the factors relating to atomic spectra, some measurements were undertaken. Sources that were used include flame emission and hollow cathode lamps. A wide range of wavelengths was measured extending from the ultraviolet to the near-IR spectral regions. Some of the advantages of Fourier transform spectroscopy are shown in these measurements. These include accurate wavenumber axis, wide simultaneous spectral range, speed of operation, and

good resolution in a compact system.

The performance and versatility of this Fourier transform spectrometer is proven in these measurements to be quite good. It can be concluded that the Fourier transform technique is an alternative to the standard instrumentation for atomic spectrochemical measurements. Further developments in automation, price-performance, and instrumental improvements are needed to make the technique part of the repertoire of standard instrumentation.

BIBLIOGRAPHY

1. R. M. Barnes, Anal. Chem. 46, 150R (1974).

2. J. D. Winefordner, J. J. Fitzgerald, N. Omenetto, Appl. Spectrosc. 29, 369 (1975).

3. Y. Talmi, Anal Chem. 47, 658A,697A (1975).

4. K. Busch, N. Howell, G. Morrison, Anal. Chem. 46, 575 (1974).

5. T. A. Nieman, C. G. Enke, Anal. Chem. 48, 619 (1976).

6. H. L. Felkel, Jr., H. L. Pardue, Anal. Chem. 49, 1112 (1977).

7. D. L. Wood, A. B. Dargis, D. L. Nash, Paper No. 310, Pittsburg Conference, Cleveland, Ohio, March 3-7, 1975.

8. G. Horlick, Appl. Spectros. 30,113 (1976).

9. G. Horlick, E. Codding, Appl. Spectros. 29, 167 (1975).

10. J. P. Avery, H. V. Malmstadt, Anal. Chem. 48, 1308 (1976).

11. A. Danielsson, P. Lindblom, Appl. Spectrosc. 30, 151 (1976).

12. A. G. Marshall. M. B. Comisarow, Anal. Chem. 47, 491A (1975).

13. J. A. Decker, Appl. Opt. 10, 510 (1971).

14. A. Girard, P. Jacquinot, p. 71-109, "Advanced Optical Techniques", A. C. S. Van Heel, editor (North Holland Publishing Co., Amsterdam, 1967).

15. G. A. Vanasse, H. Sakai, Vol. VI 1967, p.260ff., "Progress in Optics", E. Wolf, editor (North Holland Publishing Co., Amsterdam).

16. Y. Talmi, R. Crosmun, N. M. Larson, Anal. Chem. 48, 326 (1976).

17. J. D. Ingle, Jr., Anal. Chem. 46, 2161 (1974).

18. A. S. Filler, J. Opt. Soc. Am. 63, 589 (1973).

19. T. Hirschfeld, Appl. Spectrosc. 30, 68 (1976).

20. J. Winefordner, et al., Spectrochimica Acta 31B, 1 (1976).

21. N. M. Larson, R. Crosmun, Y. Talmi, Appl. Opt, 13, 2662 (1974).

22. F. Plankey, T. Glenn, L. Hart, J. Winefordner, Anal. Chem. 46, 1000 (1974).

23. E. G. Codding, G. Horlick, Appl. Spectrosc. 27, 85 (1973).

24. K. R. Betty, G. Horlick, Appl. Spectrosc. 30, 23 (1976).

25. G. Horlick, Anal. Chem. 44, 943 (1972).

26. G. Guelachvili, Nouv. Rev. d'Optique Appliquée, 3, 317 (1972).

27. J. Connes, H. Delouis, P. Connes, G. Guelachvili, J. P. Maillard, G. Michel, Nouv. Rev. d'Optique Appliquée 1, 3 (1970).

28. G. Guelachvili, Appl. Opt. 16, 2097 (1977).

29. G. Horlick, W. K. Yuen, Anal. Chem. 47, 775A (1975).

30. W. K. Yuen, G. Horlick, Anal. Chem. 49, 1446 (1977).

31. P. Griffiths, "Chemical Infrared Fourier Transform Spectroscopy" (Wiley-Interscience 1975).

32. R. Bell, "Introductory Fourier Transform Spectroscopy" (Academic Press, 1972).

33. G. Horlick, Appl. Spectrosc. 22, 617 (1968).

34. G. A. Vanasse, Fourier Spectroscopy: A Critical Review, CRC Critical Reviews in Solid State Sciences, Vol. 4, 1974-1975.

35. P. Griffiths, Anal. Chem. 46, 645A (1974).

36. J. Koenig, Appl. Spectrosc. 29, 293 (1975).

37. J. Kachmarsky, C. Belorgeot, A. Pluchino, K. D. Möller, Appl. Opt. 15, 708 (1976).

38. P. Connes, G. Michel, Appl. Opt. 14, 2067 (1975).

39. J. W. Brault, O. R. White, Astron. & Astrophys. 13, 169 (1971).

40. H. P. Larson, U. Fink, Appl. Opt. 14, 2085 (1975).

41. J. P. Baluteau, et al., Appl. Opt. 16, 1834 (1977).

42. A. Langlet, et al., Appl. Opt. 16, 1841 (1977).

43. "Aspen International Conference on Fourier Spectroscopy, 1970", AFCRL-71-0019, G. A. Vanasse, A. T. Stair, Jr., D. J. Baker, editors.

44. B. Liu, editor, "Digital Filters and the Fast Fourier Transform" (Halsted Press, 1975).

45. R. Bracewell, "The Fourier Transform and its Applications" (McGraw Hill, 1965).

46. P. Jacquinot, Reports on Progress in Physics, 23, 267 (1960).

47. J. Connes, Revue d'Optique 40, 231 (1961).

48. H. Sakai, G. A. Vanasse, M. L. Forman, J. Opt. Soc. Am. 58, 84 (1968).

49. J. W. Cooley, J. W. Tukey, Math. of Comput. 19, 297 (1965).

50. J. Connes, "Computing Problems in Fourier Spectroscopy" in reference 43.

51. G-AE Subcommittee on Measurement Concepts, W. T. Cochran, J. W. Cooley, et al., IEEE Transactions on Audio and Electroacoustics AU-15, 45 (1967).

52. G. Horlick, Ph.D. thesis, University of Illinois, Urbana, Illinois (1970).

53. G. Horlick, H. V. Malmstadt, Anal. Chem. 42, 1361 (1970).

54. H. V. Malmstadt, C. G. Enke, S. R. Crouch, G. Horlick, "Optimization of Electronic Measurements" (Benjamin, Menlo Park, Calif. 1974).

55. A. S. Filler, J. Opt. Soc. Am. 54, 762 (1964).

56. R. H. Norton, R. Beer, J. Opt. Soc. Am. 66, 259 (1976).

57. G. Horlick, Anal. Chem. 43 (8), 61A (1971).

58. M. L. Forman, W. H. Steel, G. A. Vanasse, J. Opt. Soc. Am. 56, 59 (1966).

59. E. V. Loewenstein, Appl. Opt. 2, 491 (1963).

60. L. Mertz, Infrared Physics 7, 17 (1967).

61. J. Kauppinen, Infrared Physics 16, 359 (1976).

62. P. R. Griffiths, Pittsburg Conference on Analytical Chemistry and Applied Spectroscopy, Cleveland, Ohio, Paper no. 440 (1977).

63. K. Tamagake, D. Setser, W. G. Fateley, Paper No. F.C.3, International Conference on Fourier Transform Infrared Spectroscopy, Columbia, South Carolina,1977.

64. "Nicolet 1080 System for FT-NMR", Nicolet Instrument Corporation, 5225 Verona Road, Madison, Wisc. 53711.

65. L. W. Chaney, L. T. Loh, M. T. Such, "A Fourier Transform Spectrometer for the Measurement of Atmospheric Thermal Radiation", Technical Report for ORA Project 05863, University of Michigan, Ann Arbour, (1967).

66. L. W. Chaney, S. R. Drayson, C. Young, Appl. Opt. 6, 347 (1967).

67. G. Horlick, K. R. Betty, Anal. Chem. 47, 363 (1975).

68. "Signetics Digital, Linear and MOS Applications", Signetics, 811 East Arques Ave., Sunnyvale, CA 94086, (1974), p. 6-1.

69. EMI Photomultiplier Tubes catalog, EMI Gencom Inc., 80 Express St., Plainview, N. Y. 11803.

70. H. Haraguchi, J. D. Winefordner, Appl. Spectrosc. 31, 195 (1977).

71. A. N. Zaidel', V. K. Prokof'ev, S. M. Raiskii, V. A. Slavnyi. E. Ya. Shreider, "Table of Spectral Lines", 3rd edition (IFI/Plenum Publishing, 1970).

72. R. W. B. Pearse, A. G. Gaydon, "The Identification of Molecular Spectra" (Chapman & Hall, London 1965).

73. G. Horlick, W. K. Yuen, Anal. Chem. 48, 1643 (1976).

APPENDIX

The computer programs listed here were used to acquire and process the interferograms. Reference should be made to Figure 43 and the general description of the programs in Chapter VI D.

The data acquisition subroutine was written in PDP-11 assembler language (MACRO). All remaining programs were written in FORTRAN IV to run on a DEC PDP-11/10 minicomputer. Commentary is sprinkled throughout the programs to make interpretation easier. A new program listing starts on a new page. The program name is given at the beginning of a new program listing.

```
C         PROGRAM NAME "DATACQ"
C         DATA ACQUISITION MAIN PROGRAM
C
C         THE DATE, SAMPLE NAME, AND NUMBER OF
C         SCANS AND POINTS ARE ENTERED BEFORE
C         THE ACTUAL DATA ACQUISITION ROUTINE
C         IS CALLED.
C
C
          DIMENSION TITLE(3), DATE(3)
          INTEGER*2 A(4105), DBLK(4)
          DATA DBLK/3RDK0,3RDAT,3RA   ,3RDAT/
          WRITE(7,500)
500       FORMAT(' ','ENTER DATE: 3A4')
          READ(5,501) DATE
501       FORMAT(3A4)
1         WRITE(7,502)
502       FORMAT(' ','INPUT SAMPLE NAME: 3A4')
          READ(5,501) TITLE
          WRITE(7,504)
504       FORMAT(' ','INPUT # SCANS,#PTS? F-FORMAT')
          READ(5,505) ANSCAN, ANP
505       FORMAT(2F9.1)
          NSCAN=INT(ANSCAN)
          NP=INT(ANP)
          A(NP+1)=NSCAN
C
C         THE MACRO ASSEMBLER LANGUAGE SUBROUTINE IS
C         CALLED TO DO THE ACTUAL DATA ACQUISITION.
C         THE SINGLE WORD TIME AVERAGED INTERFEROGRAM
C         IS STORED IN A FILE NAMED "DATA.DAT" ON THE
C         RK-05 CARTRIDGE DISK.
C
          CALL ODATA(NSCAN,NP)
C
C         THE INTERFEROGRAM IS READ OFF THE DISK
C         AND STORED IN ARRAY A.
C
          ICO=LOOKUP(0,DBLK)
          ICODE=IREADW(NP,A,0,0)
          CALL CLOSEC(0)
C
C         THE AVERAGE (DC) LEVEL IS SUBTRACTED FROM
C         THE INTERFEROGRAM.
C
          S=0.0
          DO 10 I=1,NP
10        S=S+FLOAT(A(I))
          IS=INT(S/ANP)
          DO 11 I=1,NP
11        A(I)=A(I)-IS
C
C         THE INTERFEROGRAM IS SEARCHED FOR THE MAXIMUM AND
C         MINIMUM VALUES AND THEIR POINT LOCATIONS.
C         THE DATA STORED AT THE END OF THE ARRAY A CONSISTS OF:
C         (NP+1)=NUMBER OF SCANS, (NP+2)=MAX. VALUE, (NP+3)=
C         POINT LOCATION OF THE MAX., (NP+4)=MIN. VALUE,
C         (NP+5)=POINT LOCATION OF THE MIN., (NP+6)=AMPLITUDE RANGE
C
          A(NP+2)=A(1)
          A(NP+4)=A(1)
          DO 12 I=1,NP
          IF(A(NP+2) .LE. A(I)) A(NP+2)=A(I)
          IF(A(NP+2) .LE. A(I)) A(NP+3)=I
```

```
          IF(A(NP+4) .GE. A(I)) A(NP+4)=A(I)
          IF(A(NP+4) .GE. A(I)) A(NP+5)=I
12        CONTINUE
          A(NP+6)=A(NP+2)-A(NP+4)
          WRITE(7,510) (A(NP+I), I=2,6)
510       FORMAT(' ','MAX=',I6,2X,'I=',I6//' MIN=',I6,2X,'I=',I6
     1,//' RANGE=',I6)
C
C         IF THE INTERFEROGRAM IS NOT ACCEPTABLE, CONTROL IS
C         RETURNED TO THE BEGINNING OF THIS PROGRAM.  IF IT
C         IS ACCEPTABLE, THE INTERFEROGRAM IS STORED ON THE
C         DISK AS THE FILE "FTN1.DAT".  THE FILE CONTAINS:
C         THE NUMBER OF DATA POINTS, THE DATE, THE SAMPLE NAME,
C         THE INTERFEROGRAM (IN INTEGER FORMAT), AND THE
C         INFORMATION STORED AT THE END OF THE ARRAY A AS WELL.
C
          WRITE(7,511)
511       FORMAT(' ','RETURN=1,EXIT=2: I1')
          READ(5,512) IS
512       FORMAT(I1)
          IF(IS .EQ. 1) GO TO 1
          CONTINUE
          REWIND 1
          WRITE(1) NP
          WRITE(1) (DATE(I), I=1,3)
          WRITE(1) (TITLE(I), I=1,3)
          WRITE(1) (A(I), I=1,NP+6)
          STOP
          END
```

```
;       THIS PROGRAM INTERFACES THE INTERFEROMETER TO THE
;       PDP-11/10 MINICOMPUTER.  IT IS WRITTEN IN THE
;       ASSEMBLER LANGUAGE OF THE PDP-11 CALLED "MACRO".
;       (COMMENT STATEMENTS ARE PREFACED BY A SEMICOLON)
;
;       THE HARD WORK DONE BY R. H. HALL IN WRITING THIS
;       PROGRAM IS ACKNOWLEDGED.
;
;       THIS DATA ACQUISITION PROGRAM IS CALLED AS A
;       SUBROUTINE BY THE FORTRAN PROGRAM "DATACQ".
;
                .TITLE INTERFACE TO INTERFEROMETER
                .MCALL ..V2..,.REGDEF,.FETCH,.CLOSE
                .MCALL .PRINT,.EXIT,.WRITW,.SRESET,.ENTER
                ..V2..
                .REGDEF
                .GLOBL JDIV,IJCVT,GDATA
;
                ADR=170402              ; SET ADDRESS REGISTERS
                ADSR=170400
                DSR=170410
                DOBUF=170414
                DIBUF=170412
                KBSR=177562
;
                .ASECT
                .=1000
;
        GDATA:  MOV     (R5)+,R1        ; RECEIVE DATA FROM FORTRAN
                MOV     @(R5)+,R1       ; PROGRAM (NUMBER OF SCANS
                MOV     @(R5)+,R2       ; AND NUMBER OF POINTS)
                MOV     R2,R2S
                MOV     R1,N
                MOV     #B,R0
                ADD     R2,R2
        LP1:    CLR     (R0)+           ; ZERO CORE LOCATIONS
                DEC     R2
                BNE     LP1
                MOV     #A,R0
                MOV     R2S,R2
        LP21:   CLR     (R0)+
                DEC     R2
                BNE     LP21
;
;       START THE ACTUAL ACQUISITION OF DATA
;       USING DIGITAL INPUT BUFFER AS START,CLOCK AND STOP
;
        LP4:    MOV     R2S,R2          ; SET WINDOW FOR POINTS
                ADD     #750,R2
                MOV     #A,R0           ; SET UP ARRAY A
                MOV     DIBUF,R4        ; CLEAR DIGITAL INPUT BUFFER
                MOV     R4,DIBUF
        LP2:    MOV     DIBUF,R4        ; TEST FOR START FLAG ON
                BIT     #1,R4           ; BIT 1
                BEQ     LP2
        LP3:    CLR     ADSR            ; TEST FOR CLOCK PULSE ON
                MOV     DIBUF,R4        ; BIT 3
                BIT     #10,R4
                BEQ     LP3
                INC     ADSR            ; START ADC
        LP5:    TSTB    ADSR            ; TEST FOR DONE FLAG
                BPL     LP5
                MOV     ADR,(R0)+       ; SAVE A/D BUFFER IN ARRAY A
                DEC     R2              ; CHECK FOR TOO MANY POINTS
                BEQ     LP4
```

```
                MOV     DIBUF,R4                ; CLR INPUT BUFFER
                MOV     R4,DIBUF
                BIT     #2,R4                   ; CHECK FOR STOP FLAG
                BEQ     LP3
                SUB     #750,R2                 ; CHECK FOR TOO FEW POINTS
                BGT     LP4                     ; IF THE NUMBER OF POINTS IS
;                                               ; BETWEEN N AND N+500 THE
;                                               ; SCAN IS ACCEPTED.
;
;
; DOUBLE WORD ADD ROUTINE
; TO ADD THE JUST ACQUIRED SCAN TO THE SUM OF THE PREVIOUS SCANS
;
                MOV     #B,R3                   ; START OF DOUBLE WORD ADD
                MOV     R2S,R2
        LP6:    ADD     -(R0),(R3)+
                ADC     (R3)+
                DEC     R2
                BGT     LP6
;
; LOAD LEDS WITH SCAN COUNTER TO GIVE A VISUAL INDICATION OF
; THE NUMBER OF SCANS LEFT.
;
                MOV     R1,LEDSV1               ; PUT SCANS LEFT ON LEDS
                DEC     LEDSV1
                MOV     #6,CNTLED
                CLR     LEDSV3
        LP9:    MOV     LEDSV1,LEDSV2
                BIC     #177770,LEDSV2
                MOVB    LEDSV3,LEDSV2+1
                MOV     LEDSV2,AD3
                ASR     LEDSV1
                ASR     LEDSV1
                ASR     LEDSV1
                INC     LEDSV3
                DEC     CNTLED
                BGT     LP9
                DEC     R1
                BGT     LP4                     ; IF THE NUMBER OF SCANS
;                                               ; LEFT IS NOT ZERO, THE
;                                               ; PROGRAM IS BRANCHED BACK
;                                               ; TO TAKE ANOTHER SCAN.
;
; DOUBLE WORD DIVIDE ROUTINE
; THE SUM OF THE SCANS IS A DOUBLE WORD ARRAY.
; THIS IS DIVIDED BY THE NUMBER OF SCANS TO GIVE THE
; TIME AVERAGED INTERFEROGRAM.
                MOV     R2S,R2                  ; START OF DOUBLE WORD
                MOV     #B,R3                   ; DIVIDE AND TRUNCATION
                MOV     #A,R4
        LP7:    MOV     (R3)+,AA
                MOV     (R3)+,AA+2
                MOV     R2,R2S
                MOV     R3,R3S                  ; N.B. MUST SAVE R1-R5 BEFORE
                MOV     R4,R4S                  ; ENTERING JDIV& IJCVT
                MOV     #LIST,R5
                JSR     PC,JDIV
                MOV     #LIST1,R5
                JSR     PC,IJCVT                ; THE AVERAGED INTERFEROGRAM
                MOV     R4S,R4                  ; IS CONVERTED TO A SINGLE
                MOV     R2S,R2                  ; WORD INTERFEROGRAM AND STORED
                MOV     R3S,R3                  ; BACK INTO ARRAY A.
                MOV     D,(R4)+
                DEC     R2
                BGT     LP7
;
```

```
;         WRITE ARRAY A ON DISK AS DATA.DAT FILE
;
;
                    .SRESET
                    .FETCH #CORSPC,#FPRT
                    BCS     BADFET
                    .ENTER  #AREA,10,#FPRT,#20.
                    BCS     BADENT
                    .WRITW  #AREA,#0,#A,R2S,#0
                    BCS     BADWRT
                    .CLOSE  #0
                    RTS     PC
          BADFET:   .PRINT  #FMSG
                    .EXIT
          BADENT:   .PRINT  #EMSG
                    .EXIT
          BADWRT:   .PRINT  #WMSG
                    .EXIT
          LIST:     .WORD   3
                    .WORD   AA
                    .WORD   N
                    .WORD   C
          LIST1:    .WORD   2
                    .WORD   C
                    .WORD   D
                    .EVEN
          LEDSV1:   .WORD   0
          LEDSV2:   .WORD   0
          LEDSV3:   .WORD   0
          CNTLED:   .WORD   0
          AA:       .WORD   0
                    .WORD   0
          C:        .WORD   0
                    .WORD   0
          N:        .WORD   0
                    .WORD   0
          D:        .WORD   0
          R5S:      .WORD   0
          R1S:      .WORD   0
          R2S:      .WORD   0
          R3S:      .WORD   0
          R4S:      .WORD   0
                    .EVEN
          A:        .BLKW   11000
          B:        .BLKW   20000
          FPRT:     .RAD50  /DK /
                    .RAD50  /DATA  DAT/
          AREA:     .BLKW   10
          FMSG:     .ASCIZ  /BAD FETCH/
          EMSG:     .ASCIZ  /BAD ENTER/
          WMSG:     .ASCIZ  /WRITE ERROR/
                    .EVEN
          CORSPC:   .BLKW   400.
          END:      .END    GDATA
```

```
C         PROGRAM NAME "PLTIN1"
C         THIS PROGRAM CONVERTS THE INTEGER INTERFEROGRAM
C         STORED IN "FTN1.DAT' TO A FLOATING POINT
C         INTERFEROGRAM.  FTN1.DAT IS READ FROM THE DISK:
C         THE INTERFEROGRAM IS FLOATED.  ALL THE INFORMATION
C         IS WRITTEN BACK ONTO THE DISK AS THE FILE
C         "FTN2.DAT"
C
          DIMENSION LB(4105), Y(4105), DATE(3), TITLE(3)
          REWIND 1
          READ(1) NP
          READ(1) (DATE(I), I=1,3)
          READ(1) (TITLE(I), I=1,3)
          READ(1) (LB(I), I=1,NP+6)
          DO 5 I=1,NP+6
          Y(I)=FLOAT(LB(I))
5         CONTINUE
          REWIND 2
          WRITE(2) NP
          WRITE(2) (DATE(I), I=1,3)
          WRITE(2) (TITLE(1), I=1,3)
          WRITE(2) (Y(I), I=1,NP+6)
          STOP
          END
```

```
C         PROGRAM NAME "APOD1"
C         THIS PROGRAM PERFORMS THE APODIZATION ON THE
C         INTERFEROGRAM.
C         THE INFORMATION IS READ IN FROM THE
C         FILE "FTN2.DAT" ON THE DISK.
C
          DIMENSION Y(4105),DATE(3), TITLE(3)
          REWIND 2
          READ(2) NP
          READ(2) (DATE(I), I=1,3)
          READ(2) (TITLE(I), I=1,3)
          READ(2) (Y(I), I=1,NP+6)
C
C         THE MAX. AND MIN. AND THEIR POINT LOCATIONS ARE
C         DETERMINED AGAIN TO CHECK THAT THE CORRECT
C         INTERFEROGRAM IS PRESENT.
C
          YMAX=Y(1)
          YMIN=Y(1)
          DO 10 I=1,NP
          IF(YMAX .LE. Y(I)) YMAX=Y(I)
          IF(YMAX .LE. Y(I)) IMAX=I
          IF(YMIN .GE. Y(I)) YMIN=Y(I)
          IF(YMIN .GE. Y(I)) IMIN=I
10        CONTINUE
          WRITE(7,500) YMAX,IMAX,YMIN,IMIN
500       FORMAT(' ','MAX=',F8.1,2X,'I=',I5,2X,'MIN=',F8.1,2X,'I=',I5)
C
C         THE INTERFEROGRAM DATA POINTS CAN BE LISTED
C         ON THE DECWRITER.
C
          WRITE(7,506)
506       FORMAT(' ','POINT LIST? Y:1, N:0')
          READ(5,501) N1
501       FORMAT(I1)
          IF(N1 .NE. 1) GO TO 11
          WRITE(7,502)
502       FORMAT(' ','ENTER N1,N2; 2I5')
          READ(5,503) N1,N2
503       FORMAT(4I5)
          DO 12 I=N1,N2,10
          WRITE(7,504) I, (Y(J), J=I,I+9)
504       FORMAT(' ',I4,':',10F6.0)
12        CONTINUE
C
C         THE APODIZATION FUNCTION IS CHOSEN.
C
11        WRITE(7,510)
510       FORMAT(' ','APOD. FCN; TRI:1, GAUSSIAN:2  ')
          READ(5,501) NA
          IF(NA .LT. 1 .OR. NA .GT. 2) GO TO 11
          GO TO (51,52) NA
C
C         THE BOXCAR OR TRIANGULAR APODIZATION FUNCTION
C         IS SPECIFIED BY THE FOUR VARIABLES N1-N4.
C         SEE CHAPTER IV FOR EXPLANATION.
C
51        WRITE(7,505)
505       FORMAT(' ','ENTER N1,N2,N3,N4; 4I5')
          READ(5,503) N1,N2,N3,N4
          DO 15 I=1,N1
15        Y(I)=0.0
          DO 16 I=N4,NP
16        Y(I)=0.0
          DENOM=1.0/FLOAT(N2-N1)
          DO 17 I=N1,N2
```

```
17      Y(I)=Y(I)*DENOM*FLOAT(I-N1)
        DENOM=1.0/FLOAT(N4-N3)
        DO 18 I=N3,N4
18      Y(I)=Y(I)*DENOM*FLOAT(N4-I)
        GO TO 100
C
C       THE GAUSSIAN APODIZATION IS APPLIED.
C       THE VARIABLES "FAC" AND "Z" ARE ENTERED;
C       SEE CHAPTER IV FOR EXPLANATION OF THE VARIABLES.
C
52      WRITE(7,511)
511     FORMAT(' ','GAUSSIAN APOD.; ENTER FACTOR & Z:2F8.1')
        READ(5,512) FAC, Z
512     FORMAT(2F8.1)
        DO 60 I=1,NP
        DUM=ABS(FLOAT(I)-Z)/(FLOAT(NP)-Z)
        DUM1=EXP(-FAC*DUM**2)
        Y(I)=Y(I)*DUM1
60      CONTINUE
C
C       THE APODIZED INTERFEROGRAM IS STORED ON THE
C       DISK AS THE FILE "FTN10.DAT".
C
100     CONTINUE
        REWIND 10
        WRITE(10) (Y(I), I=1,NP)
        STOP
        END
```

```
C         PROGRAM NAME "COOLF4"
C         THIS PROGRAM PERFORMS THE FAST FOURIER
C         TRANSFORM ON THE INTERFEROGRAM STORED
C         IN FILE "FIN10.DAT" ON THE DISK.  THE
C         INTERFEROGRAM IS READ INTO ARRAY X.
C
          DIMENSION X(4100),Y(4100),L(20)
          NP=4096
          REWIND 10
          READ(10)(X(I),I=1,NP)
          NPT=NP/2
          N=NP
C
C         THE ODD NUMBERED POINTS OF THE INTERFEROGRAM
C         ARE PUT INTO ARRAY X (REAL INPUT) AND THE
C         EVEN NUMBERED POINTS ARE PUT INTO ARRAY Y
C         (IMAGINARY INPUT).  THE REMAINDER OF BOTH
C         ARRAYS IS FILLED WITH ZEROES.
C
          DO 2 I=1,NPT
          X(I)=X(I*2-1)
2         Y(I)=X(I*2)
          DO 3 I=NPT+1,NP
          Y(I)=0.0
3         X(I)=0.0
          N2POW=12
          NTHPOW=2**N2POW
          N4POW=N2POW/2
          IF(N4POW)60,63,60
60        DO 61 IPASS=1,N4POW
          NXTLTH=2**(N2POW-2*IPASS)
          LENGTH=4*NXTLTH
          SCALE=6.2831853/FLOAT(LENGTH)
          DO 61 J=1,NXTLTH
          ARG=FLOAT(J-1)*SCALE
          C1=COS(ARG)
          S1=SIN(ARG)
          C2=C1*C1-S1*S1
          S2=C1*S1+C1*S1
          C3=C1*C2-S1*S2
          S3=C2*S1+S2*C1
          DO 61 ISQLOC=LENGTH,NTHPOW,LENGTH
          J1=ISQLOC-LENGTH+J
          J2=J1+NXTLTH .
          J3=J2+NXTLTH
          J4=J3+NXTLTH
          R1=X(J1)+X(J3)
          R2=X(J1)-X(J3)
          R3=X(J2)+X(J4)
          R4=X(J2)-X(J4)
          FI1=Y(J1)+Y(J3)
          FI2=Y(J1)-Y(J3)
          FI3=Y(J2)+Y(J4)
          FI4=Y(J2)-Y(J4)
          X(J1)=R1+R3
          Y(J1)=FI1+FI3
          IF(J-1)64,62,64
64        X(J3)=C1*(R2+FI4)+S1*(FI2-R4)
          Y(J3)=-S1*(R2+FI4)+C1*(FI2-R4)
          X(J2)=C2*(R1-R3)+S2*(FI1-FI3)
          Y(J2)=-S2*(R1-R3)+C2*(FI1-FI3)
          X(J4)=C3*(R2-FI4)+S3*(R4+FI2)
          Y(J4)=-S3*(R2-FI4)+C3*(R4+FI2)
          GO TO 61
62        X(J3)=R2+FI4
```

```
          Y(J3)=FI2-R4
          X(J2)=R1-R3
          Y(J2)=FI1-FI3
          X(J4)=R2-FI4
          Y(J4)=R4+FI2
61        CONTINUE
63        IF(N2POW-2*N4POW)65,66,65
65        DO 67 J=1,NTHPOW,2
          R1=X(J)+X(J+1)
          R2=X(J)-X(J+1)
          FI1=Y(J)+Y(J+1)
          FI2=Y(J)-Y(J+1)
          X(J)=R1
          Y(J)=FI1
          X(J+1)=R2
67        Y(J+1)=FI2
66        DO 68 J=1,13
          L(J)=1
          IF(J-N2POW)69,69,68
69        L(J)=2**(N2POW+1-J)
68        CONTINUE
          IJ=1
          L1=L(13)
          NTHPOW=L(12)
          ISQLOC=L(11)
          J=L(10)
          N2P1=L(9)
          N2=L(8)
          NP2MJ=L(7)
          L8=L(6)
          N2POW=L(5)
          N4POW=L(4)
          LENGTH=L(3)
          NXTLTH=L(2)
          IPASS=L(1)
          DO 601 J1=1,L1
          DO 601 J2=J1,NTHPOW,L1
          DO 601 J3=J2,ISQLOC,NTHPOW
          DO 601 J4=J3,J,ISQLOC
          DO 601 J5=J4,N2P1,J
          DO 601 J6=J5,N2,N2P1
          DO 601 J7=J6,NP2MJ,N2
          DO 601 J8=J7,L8,NP2MJ
          DO 601 J9=J8,N2POW,L8
          DO 601 J10=J9,N4POW,N2POW
          DO 601 J11=J10,LENGTH,N4POW
          DO 601 J12=J11,NXTLTH,LENGTH
          DO 601 JI=J12,IPASS,NXTLTH
          IF(IJ-JI)610,610,601
610       R=X(IJ)
          X(IJ)=X(JI)
          X(JI)=R
          FI=Y(IJ)
          Y(IJ)=Y(JI)
          Y(JI)=FI
601       IJ=IJ+1
          ARG=3.1415927/FLOAT(N)
          C1=COS(ARG)
          S1=-SIN(ARG)
          C1JX=1.
          S1JX=0.
          N2=N/2
          N2P1=N2+1
          DO 70 J=2,N2P1
          NP2MJ=N+2-J
          SORR1=X(J)+X(NP2MJ)
```

```
          SORI1=Y(J)-Y(NP2MJ)
          R=C1JX
          C1JX=C1JX*C1-S1JX*S1
          S1JX=R*S1+S1JX*C1
          SORR2=X(J)-X(NP2MJ)
          SORI2=Y(J)+Y(NP2MJ)
          SORR3=C1JX*SORR2-S1JX*SORI2
          SORI3=C1JX*SORI2+S1JX*SORR2
          Y(J)=0.5*(SORI1-SORR3)
          X(J)=0.5*(SORR1+SORI3)
          IF(J-N2P1)71,70,71
71        Y(NP2MJ)=0.5*(-SORI1-SORR3)
          X(NP2MJ)=0.5*(SORR1-SORI3)
70        CONTINUE
          X(1)=X(1)+Y(1)
          Y(1)=0.
C
C         THE AMPLITUDE SPECTRUM IS CALCULATED
C         FROM THE REAL AND IMAGINARY OUTPUTS
C         OF THE FFT.
C         THE AMPLITUDE SPECTRUM IS STORED AS
C         THE FILE "FTN12.DAT" ON THE DISK.
C
          DO 501  I=1,4096
          X(I)=SQRT(X(I)*X(I)+Y(I)*Y(I))
501       CONTINUE
          REWIND 12
          WRITE(12)(X(I),I=1,NP)
          STOP
          END
```

```
C       PROGRAM NAME 'INVT'
C       INPUT TO THIS PROGRAM IS FTN1.DAT.  OUTPUT GIVES
C       INTERFEROGRAM LISTING OR PLOT ON GRAPHICS
C       TERMINAL (MAX. 1000 PTS.).
        DIMENSION KY(4200), IB(3000), X(3), XX(3)
        REWIND 1
        READ(1) NP
        READ(1) (X(I), I=1,3)
        READ(1) (XX(I), I=1,3)
        READ(1) (KY(I), I=1,NP+6)
C
C       THE INTERFEROGRAM IS SCALED FROM 0 TO 1000.
C
        KMAX=KY(1)
        KMIN=KY(1)
        DO 10 I=1,NP
        IF(KMAX .LE. KY(I)) KMAX=KY(I)
        IF(KMIN .GE. KY(I)) KMIN=KY(I)
10      CONTINUE
        S=1000.0/FLOAT(KMAX-KMIN)
        DO 15 I=1,NP
        KY(I)=INT(FLOAT(KY(I)-KMIN)*S)
15      CONTINUE
C
C       THE INTERFEROGRAM CAN BE LISTED ON THE DECWRITER.
C
        WRITE(7,500)
500     FORMAT(' ','POINT LISTING? Y:1,N:0, N1,N2: I1,2I4')
        READ(5,600) NL,N1,N2
600     FORMAT(I1,2I4)
        IF(NL .NE. 1) GO TO 20
        DO 18 I=N1,N2,10
        WRITE(7,601) I, (KY(J), J=I,I+9)
601     FORMAT(' ',I4,':',10(1X,I5))
18      CONTINUE
C
C       THE POINTS OF THE INTERFEROGRAM TO BE DISPLAYED
C       ARE ENTERED.
C
20      WRITE(7,501)
501     FORMAT(' ','ENTER PTS. TO DISPLAY(MAX=1000): 2F10.2')
        READ(5,602) AN1,AN2
602     FORMAT(2F10.2)
        N1=AN1
        N2=AN2
        N3=N2-N1
        IF(N3 .GT. 1000) N3=1000
        NXDIF=1000.0/FLOAT(N3)
        XDIF=FLOAT(NXDIF)
        CALL INIT(IB,3000)
        CALL APNT(0.0,0.0,-1,5,-1,1)
        CALL APNT(0.0,FLOAT(KY(N1)))
        DO 50 I=N1,N2-1
        YDIF=FLOAT(KY(I+1)-KY(I))
        CALL VECT(XDIF,YDIF)
50      CONTINUE
        PAUSE 'TYPE CR TO CONTINUE'
        CALL INIT
        CALL FREE
        GO TO 20
        STOP
        END
```

```
C       PROGRAM NAME "SPUT"
C       THIS PROGRAM GIVES A LISTING OF THE AMPLITUDE SPECTRUM
C       ON THE DECWRITER AND/OR A PLOT OF THE SPECTRUM ON THE
C       GRAPHICS TERMINAL (MAX. 1000 POINTS AT A TIME).
C       INPUT FOR THIS PROGRAM IS FROM DISK FILE "FTN12.DAT".
C
        DIMENSION Y(4096), IY(2000)
        WRITE(7,500)
500     FORMAT(' ','ENTER CM-1 LIMITS OF ALIASING REGION; 2F10,2')
        READ(5,501) CM1, CM2
        NP=4096
        ANP=4095.0
        REWIND 12
        READ(12) (Y(I), I=1,NP)
C
C       THE AMPLITUDE SPECTRUM IS SCALED BETWEEN 0 AND 1000.
C
        AMAX=Y(1)
        AMIN=Y(1)
        DO 5 I=1,NP
        IF(AMAX .LE. Y(I)) AMAX=Y(I)
        IF(AMIN .GE. Y(I)) AMIN=Y(I)
5       CONTINUE
        S=1000.0/(AMAX-AMIN)
        DO 6 I=1,NP
6       Y(I)=FLOAT(INT((Y(I)-AMIN)*S))
C
C       THE AMPLITUDE SPECTRUM CAN BE LISTED AT THIS POINT.
C
        WRITE(7,505)
505     FORMAT(' ','POINT LISTING? Y:1,N:0; NL,N2:I1,2I4')
        READ(5,506) NL,N1,N2
506     FORMAT(I1,2I4)
        IF(NL .NE. 1) GO TO 10
        DO 8 I=N1,N2,5
        WRITE(7,507) I, (Y(K), K=I,I+4)
507     FORMAT(' ',I4,':',5(1X,F8,3))
8       CONTINUE
C
C       THE POINTS OF THE SPECTRUM TO BE DISPLAYED ARE ENTERED,
C       THE WAVENUMBERS OF THE PLOTTED SECTION ARE PRINTED ON THE
C       DECWRITER (THE WAVENUMBERS OF THE ALIASING REGION ARE
C       ENTERED AT THE BEGINNING OF THE PROGRAM).
C
10      WRITE(7,502)
502     FORMAT(' ','ENTER POINTS TO DISPLAY(MAX. RANGE=1000): 2F10.2')
        READ(5,501) AN1,AN2
501     FORMAT(2F10,2)
        N1=AN1
        N2=AN2
        C1=CM1+(AN1-1,0)*(CM2-CM1)/ANP
        C2=CM1+(AN2-1,0)*(CM2-CM1)/ANP
        WRITE(7,503) C1,C2
503     FORMAT(' ','N1=',F10,2,1X,'CM-1',5X,'N2=',F10,2,1X,'CM-1')
        N3=N2-N1
        IF(N3 .GT. 1000) N3=1000
        NXDIF=1000./FLOAT(N3)
        XDIF=FLOAT(NXDIF)
C
C       THE GRAPHICS DISPLAY IS DONE VIA SUBROUTINE CALLS
C       DESCRIBED IN THE PDP-11  FORTRAN/RT-11 EXTENSIONS MANUAL.
C
        CALL INIT (IY,2000)
        CALL APNT (0.0,0.0,-1,5,-1,1)
        CALL APNT (0.0,Y(N1))
```

```
      DO 20 I=N1,N2-1
      YDIF=Y(I+1)-Y(I)
      CALL VECT(XDIF,YDIF)
20    CONTINUE
      PAUSE 'TYPE CR TO CONTINUE'
      CALL INIT
      CALL FREE
      GO TO 10
      STOP
      END
```

```
C          PROGRAM NAME 'PLTIN2'
C          INTERFEROGRAM PLOTTING ROUTINE
C          FOR THE ZETA INCREMENTAL PLOTTER.
C          THE FLOATING POINT INTERFEROGRAM IS READ
C          IN OFF THE DISK FILE 'FTN2.DAT'.
C
           DIMENSION Y(4105), X(3005), DATE(3), TITLE(3)
           REWIND 2
           READ(2) NP
           READ(2) (DATE(I), I=1,3)
           READ(2) (TITLE(I), I=1,3)
           READ(2) (Y(I), I=1,NP+6)
           WRITE(7,500) Y(NP+2), Y(NP+3)
500        FORMAT(' ','MAX=',F8.1,'  IMAX=',F8.1)
           WRITE(7,501) Y(NP+4), Y(NP+5)
501        FORMAT(' ','MIN=',F8.1,'  IMIN=',F8.1)
C
C          THE INTERFEROGRAM DATA POINTS TO BE PLOTTED
C          ARE ENTERED ALONG WITH THE NUMBER OF POINTS
C          PER INCH.
C
           WRITE(7,502)
502        FORMAT(' ','ENTER PTS. TO PLOT(MAX=3000):2F8.1')
           READ(5,503) AN1, AN2
503        FORMAT(2F8.1)
           N1=AN1
           N2=AN2
           ANP=NP
           WRITE(7,504)
504        FORMAT(' ','ENTER POINTS PER INCH: F8.1')
           READ(5,503) AINC
           DO 5 I=N1,N2
           Y(I-N1+1)=Y(I)
           X(I-N1+1)=FLOAT(I)
5          CONTINUE
           NPT=N2-N1+1
           XLONG=FLOAT(NPT)/AINC
C
C          THE INTERFEROGRAM IS PLOTTED USING SUBROUTINE CALLS
C          SIMILAR TO THE CALCOMP ROUTINES FOR LARGE COMPUTERS.
C          THE SOFTWARE MANUAL FOR THE ZETA PLOTTER SHOULD BE
C          CONSULTED TO DECIPHER THE LIST OF VARIABLES IN THE
C          SUBROUTINE CALLS.
C          BESIDES THE INTERFEROGRAM, THE DATE, TITLE, NUMBER
C          OF SCANS, NUMBER OF POINTS, MAX. AND MIN. VALUES AND
C          THEIR POINT LOCATIONS ARE PRINTED AT THE TOP OF THE PLOT.
C
           X(NPT+1)=AN1
           X(NPT+2)=AINC
           Y(NPT+1)=Y(NP+4)
           Y(NPT+2)=(Y(NP+2)-Y(NP+4))/8.0
           CALL PLOTST (0.005,'IN')
           CALL PLOT (0.0,0.0,-3)
           CALL PLOT (0.5,0.0,-3)
           CALL LINE (X,Y,NPT,1,0,0)
           CALL AXIS (0.,0.,10HPT. NUMBER,-10,XLONG,0.0,X(NPT+1),X(NPT+2))
           CALL AXIS (0.,0.,9HAMPLITUDE,+9,8.0,90.0,Y(NPT+1),Y(NPT+2))
           CALL SYMBOL (2.0,9.4,0.14,DATE,0.0,12)
           CALL SYMBOL (2.0,9.2,0.14,TITLE,0.0,12)
           CALL SYMBOL (2.0,9.0,0.14,6HNSCAN:,0.0,6)
           CALL NUMBER (3.0,9.0,0.14,Y(NP+1),0.0,-1)
           CALL SYMBOL (4.0,9.0,0.14,3HNP:,0.0,3)
           CALL NUMBER (5.0,9.0,0.14,ANP,0.0,-1)
           CALL SYMBOL (2.0,8.7,0.14,5HIMAX:,0.0,5)
           CALL NUMBER (3.0,8.7,0.14,Y(NP+3),0.0,-1)
```

```
      CALL NUMBER (4.5,8.7,0.14,Y(NP+2),0.0,-1)
      CALL SYMBOL (2.0,8.5,0.14,5HIMIN;,0.0,5)
      CALL NUMBER (3.0,8.5,0.14,Y(NP+5),0.0,-1)
      CALL NUMBER (4.5,8.5,0.14,Y(NP+4),0.0,-1)
      CALL PLOT ((XLONG+1.0),0.0,+3)
      CALL PLOTND
      STOP
      END
```

```
C        PROGRAM NAME "PLTINA"
C        APODIZED INTERFEROGRAM PLOTTING ROUTINE
C        FOR THE ZETA INCREMENTAL PLOTTER.
C        THE FLOATING POINT INTERFEROGRAM IS READ
C        IN FROM THE DISK FILE "FTN10.DAT".
C
         DIMENSION Y(4105), X(3005), DATE(3), TITLE(4)
         NP=4096
         ANP=4096.0
         REWIND 10
         READ(10) (Y(I), I=1,NP)
C
C        SINCE THE DATE, TITLE, AND NUMBER OF SCANS
C        WERE NOT STORED IN FTN10.DAT, THEY MUST BE
C        ENTERED IN ORDER TO BE INCLUDED IN THE PLOT.
C
         WRITE(7,500)
500      FORMAT(' ','ENTER DATE; 3A4')
         READ(5,501) (DATE(I), I=1,3)
501      FORMAT(3A4)
         WRITE(7,502)
502      FORMAT(' ','ENTER TITLE; 4A4')
         READ(5,503) (TITLE(I), I=1,4)
503      FORMAT(4A4)
         WRITE(7,504)
504      FORMAT(' ','ENTER NO. OF SCANS; F10.2')
         READ(5,505) Y(NP+1)
505      FORMAT(2F10.2)
C
C        THE MAX. AND MIN. AND THEIR POINT LOCATIONS
C        MUST BE DETERMINED AGAIN SINCE THEY WERE NOT
C        STORED IN FTN10.DAT.
C
         Y(NP+2)=Y(1)
         Y(NP+4)=Y(1)
         DO 10 I=1,NP
         IF(Y(NP+2) .LE. Y(I)) Y(NP+2)=Y(I)
         IF(Y(NP+2) .LE. Y(I)) Y(NP+3)=FLOAT(I)
         IF(Y(NP+4) .GE. Y(I)) Y(NP+4)=Y(I)
         IF(Y(NP+4) .GE. Y(I)) Y(NP+5)=FLOAT(I)
10       CONTINUE
         WRITE(7,510) Y(NP+2), Y(NP+3)
510      FORMAT(' ','MAX=',F10.2,'    IMAX=',F10.2)
         WRITE(7,511) Y(NP+4), Y(NP+5)
511      FORMAT(' ','MIN=',F10.2,'    IMIN=',F10.2)
C
C        THE INTERFEROGRAM DATA POINTS TO BE PLOTTED
C        ARE ENTERED ALONG WITH THE NUMBER OF POINTS
C        PER INCH.
C
         WRITE(7,506)
506      FORMAT(' ','ENTER PTS. TO PLOT(MAX=3000);2F10.2')
         READ(5,505) AN1,AN2
         N1=AN1
         N2=AN2
         NPT=N2-N1+1
         WRITE(7,507)
507      FORMAT(' ','ENTER POINTS PER INCH; F10.2')
         READ(5,505) AINC
         DO 20 I=N1,N2
         Y(I-N1+1)=Y(I)
         X(I-N1+1)=FLOAT(I)
20       CONTINUE
         XLONG=FLOAT(NPT)/AINC
C
```

```
C         THE COMMENTS IN PROGRAM "PLTIN2" AT THIS POINT
C         ALSO APPLY HERE.
C
          X(NPT+1)=AN1
          X(NPT+2)=AINC
          Y(NPT+1)=Y(NP+4)
          Y(NPT+2)=(Y(NP+2)-Y(NP+4))/8.0
          CALL PLOTST (0.005,'IN')
          CALL PLOT (0.0,0.0,-3)
          CALL PLOT (0.5,0.0,-3)
          CALL LINE (X,Y,NPT,1,0,0)
          CALL PLOT (0.0,0.0,+3)
          CALL AXIS (0.,0.,10HPT. NUMBER,-10,XLONG,0.,X(NPT+1),X(NPT+2))
          CALL AXIS (0.,0.,9HAMPLITUDE,+9,8.0,90.0,Y(NPT+1),Y(NPT+2))
          CALL SYMBOL (2.0,9.4,0.14,DATE,0.0,12)
          CALL SYMBOL (2.0,9.2,0.14,TITLE,0.0,16)
          CALL SYMBOL (2.0,9.0,0.14,6HNSCAN!,0.0,6)
          CALL NUMBER (3.0,9.0,0.14,Y(NP+1),0.0,-1)
          CALL SYMBOL (4.0,9.0,0.14,3HNP!,0.0,3)
          CALL NUMBER (5.0,9.0,0.14,ANP,0.0,-1)
          CALL SYMBOL (2.0,8.7,0.14,5HIMAX!,0.0,5)
          CALL NUMBER (3.0,8.7,0.14,Y(NP+3),0.0,-1)
          CALL NUMBER (4.5,8.7,0.14,Y(NP+2),0.0,-1)
          CALL SYMBOL (2.0,8.5,0.14,5HIMIN!,0.0,5)
          CALL NUMBER (3.0,8.5,0.14,Y(NP+5),0.0,-1)
          CALL NUMBER (4.5,8.5,0.14,Y(NP+4),0.0,-1)
          CALL PLOT ((XLONG+1.0),0.0,+3)
          CALL PLOTND
          STOP
          END
```

```
C         PROGRAM NAME "PLOTSP"
C         INPUT TO PROGRAM IS FTN12:DAT
C         OUTPUT IS PLOT OF THE AMPLITUDE SPECTRUM
C         POINTS BETWEEN SPECIFIED CM-1 LIMITS
C         AMPLITUDE RANGE OF PLOTTED SECTION SCALED TO 8 INCHES
C
          DIMENSION Y(4100), X(3503)
          WRITE(7,500)
500       FORMAT(' ','ENTER CM-1 LIMITS OF ALIASING REGION; 2F10.2')
          READ(5,501) CM1, CM2
501       FORMAT(2F10.2)
          IF(CM1 .LE. CM2) GO TO 5
          CM1=-CM1
          CM2=-CM2
5         CONTINUE
          CM=ABS(CM1-CM2)
1         NP=4096
          ANP=4095.0
C
C         THE AMPLITUDE SPECTRUM IS READ FROM THE DISK FILE
C         FTN12.DAT INTO ARRAY Y.
C
          REWIND 12
          READ(12) (Y(I), I=1,NP)
C
C         THE SPECTRUM IS SCALED BETWEEN 0 AND 4096.
C
          AMAX=Y(1)
          AMIN=Y(1)
          DO 15 I=1,NP
          IF(AMAX .LE. Y(I)) AMAX=Y(I)
          IF(AMIN .GE. Y(I)) AMIN=Y(I)
15        CONTINUE
          S=4096.0/(AMAX-AMIN)
          DO 16 I=1,NP
16        Y(I)=(Y(I)-AMIN)*S
C
C         THE WAVENUMBER LIMITS TO PLOT ARE ENTERED.
C         THE CORRESPONDING POINT NUMBERS ARE PRINTED
C         ON THE DECWRITER.
C
          WRITE(7,502)
502       FORMAT(' ','ENTER CM-1 LIMITS TO PLOT; 2F10.2')
          READ(5,501) AN1, AN2
          IF(AN1 .LE. AN2) GO TO 10
          AN1=-AN1
          AN2=-AN2
10        CONTINUE
          N1=((AN1-CM1)*ANP/CM)+1.49
          N2=((AN2-CM1)*ANP/CM)+1.49
          NPT=N2-N1+1
          WRITE(7,503) N1,N2
503       FORMAT(' ','N1=',I4,5X,'N2=',I4)
          DO 20 I=N1,N2
          Y(I-N1+1)=Y(I)
          X(I-N1+1)=AN1+FLOAT(I-N1)*CM/ANP
20        CONTINUE
          WRITE(7,504)
504       FORMAT(' ','ENTER CM-1 PER INCH; F10:2')
          READ(5,501) AINC
C
C         THE SPECTRAL REGION TO BE PLOTTED IS
C         SEARCHED FOR THE MAX. AND MIN. VALUES.
C         THE PLOT IS SCALED SO THAT THE MAX. AND
C         MIN. VALUES EXTEND 8 INCHES.
```

```
C
          AMAX=Y(1)
          AMIN=Y(1)
          DO 21 I=1,NPT .
          IF(AMAX .LE. Y(I)) AMAX=Y(I)
          IF(AMIN .GE. Y(I)) AMIN=Y(I)
21        CONTINUE
          Y(NPT+1)=AMIN
          Y(NPT+2)=(AMAX-AMIN)/8.0
          X(NPT+1)=AN1
          X(NPT+2)=AINC
C
C         THE COMMENTS IN PROGRAM "PLTIN2" ABOUT THE SUBROUTINE
C         CALLS ALSO APPLY HERE.
C
          CALL PLOTST (0.005,'IN')
          CALL PLOT (0.0,0.0,-3)
          CALL PLOT (1.0,0.0,-3)
          CALL LINE (X,Y,NPT,1,0,0)
          CALL AXIS(0.,0.,'CM-1',-4,(AN2-AN1)/AINC,0.,X(NPT+1),X(NPT+2))
          CALL AXIS(0.,0.,'AMPLITUDE',+9,8.0,90.0,Y(NPT+1),Y(NPT+2))
          CALL PLOT (0.0,0.0,-3)
          CALL PLOTND
          GO TO 1
          STOP
          END
```

```
C         PROGRAM NAME "TEMP"
C         INPUT TO PROGRAM IS FTN12.DAT
C         THE ENTIRE AMPLITUDE SPECTRUM IS SCALED 0-4096.0
C         OUTPUT IS PLOT OF POINTS BETWEEN SPECIFIED CM-1 LIMITS
C         THE PLOTTED SECTION IS NOT EXPANDED TO 8 INCHES AS
C         IN THE PROGRAM "PLOTSP".  THE AMPLITUDE RANGE
C         0 TO 4096 EXTENDS TO 8 INCHES.
C
          DIMENSION Y(4100), X(3503)
          WRITE(7,500)
500       FORMAT(' ','ENTER CM-1 LIMITS OF ALIASING REGION; 2F10.2')
          READ(5,501) CM1, CM2
501       FORMAT(2F10.2)
          IF(CM1 .LE. CM2) GO TO 5
          CM1=-CM1
          CM2=-CM2
5         CONTINUE
          CM=ABS(CM1-CM2)
1         NP=4096
          ANP=4095.0
C
C         THE AMPLITUDE SPECTRUM IS READ FROM DISK FILE FTN12.DAT
C         INTO ARRAY Y AND THEN SCALED BETWEEN 0 AND 4096.
C
          REWIND 12
          READ(12) (Y(I), I=1,NP)
          AMAX=Y(1)
          AMIN=Y(1)
          DO 15 I=1,NP
          IF(AMAX .LE. Y(I)) AMAX=Y(I)
          IF(AMIN .GE. Y(I)) AMIN=Y(I)
15        CONTINUE
          S=4096.0/(AMAX-AMIN)
          DO 16 I=1,NP
16        Y(I)=(Y(I)-AMIN)*S
C
C         THE WAVENUMBER LIMITS TO PLOT ARE ENTERED.
C         THE CORRESPONDING POINT NUMBERS ARE PRINTED
C         ON THE DECWRITER.
C
          WRITE(7,502)
502       FORMAT(' ','ENTER CM-1 LIMITS TO PLOT; 2F10.2')
          READ(5,501) AN1, AN2
          IF(AN1 .LE. AN2) GO TO 10
          AN1=-AN1
          AN2=-AN2
10        CONTINUE
          N1=((AN1-CM1)*ANP/CM)+1.49
          N2=((AN2-CM1)*ANP/CM)+1.49
          NPT=N2-N1+1
          WRITE(7,503) N1,N2
503       FORMAT(' ','N1=',I4,5X,'N2=',I4)
          DO 20 I=N1,N2
          Y(I-N1+1)=Y(I)
          X(I-N1+1)=AN1+FLOAT(I-N1)*CM/ANP
20        CONTINUE
          WRITE(7,504)
504       FORMAT(' ','ENTER CM-1 PER INCH; F10.2')
          READ(5,501) AINC
          AMAX=Y(1)
          AMIN=Y(1)
          DO 21 I=1,NPT
          IF(AMAX .LE. Y(I)) AMAX=Y(I)
          IF(AMIN .GE. Y(I)) AMIN=Y(I)
```

```
21      CONTINUE
        Y(NPT+1)=0.0
        Y(NPT+2)=512.0
        X(NPT+1)=AN1
        X(NPT+2)=AINC
        CALL PLOTST (0,005,'IN')
        CALL PLOT (0.0,0.0,-3)
        CALL LINE (X,Y,NPT,1,0,0)
        CALL AXIS(0.,0.,'CM-1',-4,(AN2-AN1)/AINC,0.,X(NPT+1),X(NPT+2))
        CALL AXIS(0.,0.,'AMPLITUDE',+9,8.0,90.0,Y(NPT+1),Y(NPT+2))
        CALL PLOT (0.0,0.0,-3)
        CALL PLOTND
        GO TO 1
        STOP
        END
```

```
C       PROGRAM NAME "PKLO"
C       THIS PROGRAM GIVES A LISTING OF THE
C       AMPLITUDE SPECTRUM AND SEARCHES THE SPECTRUM
C       FOR PEAKS ABOVE A STATED THRESHOLD VALUE.
C       THE WAVELENGTH AND CM-1 ARE PRINTED OUT
C       ON THE DECWRITER.
C       THE AMPLITUDE SPECTRUM IS READ FROM THE DISK
C       FILE FTN12.DAT INTO ARRAY Y AND SCALED
C       BETWEEN 0 AND 4096.
C
        DIMENSION Y(4096), J(4096)
        REWIND 12
        READ (12) (Y(I), I=1,4096)
        NP=4096
        ANP=4095.0
        AMAX=Y(1)
        AMIN=Y(1)
        DO 5 I=1,NP
        IF(AMAX .LE. Y(I)) AMAX=Y(I)
        IF(AMIN .GE. Y(I)) AMIN=Y(I)
5       CONTINUE
        S=4096.0/(AMAX-AMIN)
        DO 6 I=1,NP
6       J(I)=(Y(I)-AMIN)*S
        S=1.0/S
C
C       A VALUE CALLED THE PK. HT. IS PRINTED.
C       THIS IS THE AMPLITUDE OF A SPECTRAL POINT RELATIVE
C       TO 4096.  FOR EXAMPLE, IF PK. HT.=2, THE SPECTRAL
C       POINT HAS AN ABSOLUTE VALUE OF 2*4096=8192.
C
        WRITE(7,510) S
510     FORMAT(' ','PK. HT.(RELATIVE TO 4096)=',F14.4)
C
C       THE SPECTRUM CAN BE LISTED ON THE DECWRITER.
C
10      WRITE(7,500)
500     FORMAT('0','PT. LISTING? & PTS. TO LIST? 1=0. I1,2I4')
        READ(5,501) NL,N1,N2
501     FORMAT(I1,2I4)
        IF(NL .NE. 1) GO TO 20
        DO 15 I=N1,N2,10
        WRITE(7,502) I, (J(K), K=I,I+9)
15      CONTINUE
502     FORMAT(' ',I4,':',10(1X,I5))
C
C       THE THRESHOLD OVER WHICH A MAXIMA IS CONSIDERED A SPECTRAL
C       LINE IS ENTERED PLUS THE POINT LIMITS TO SEARCH IS ENTERED.
C
20      WRITE(7,503)
503     FORMAT('0','ENTER PK. LOC. THRESHOLD & PTS.TO SEARCH; 3I4')
        READ(5,504) ITH,N1,N2
504     FORMAT(3I4)
        WRITE(7,505)
505     FORMAT(' ','ENTER CM-1 LIMITS OF ALIASING REGION; 2F10.2')
        READ(5,506) CM1,CM2
506     FORMAT(2F10.2)
        WRITE(7,507)
507     FORMAT(' ','POINT NUMBER   PEAK LOCATION  CM-1         NM.')
C
C       THE SPECTRUM IS SEARCHED FOR SPECTRAL LINES BY FINDING
C       A POINT THAT IS GREATER IN AMPLITUDE THAN THE PRECEDING
C       AND FOLLOWING TWO POINTS.  THIS MAXIMA MUST BE ABOVE THE
C       THRESHOLD VALUE BEFORE IT IS IDENTIFIED AS A SPECTRAL LINE.
```

```
C       THE WAVENUMBER AND WAVELENGTH IN NM OF THIS MAXIMA IS
C       PRINTED ON THE DECWRITER.
C
        DO 30 I=N1+1,N2-2
        IF(J(I) .LT. ITH) GO TO 30
        IF(J(I+1) .GE. J(I)) GO TO 30
        IF(J(I+2) .GE. J(I+1)) GO TO 30
        IF(J(I-1) .GT. J(I)) GO TO 30
        PK=FLOAT(I)
        CM=CM1+(PK-1.0)*(CM2-CM1)/ANP
        ANM=1.0E7/CM
        WRITE(7,508) PK,CM,ANM
508     FORMAT(2X,F8.1,14X,F10.2,3X,F10.4)
30      CONTINUE
        GO TO 10
        STOP
        END
```

B30210